Lawrence Berkeley Laboratory
UNIVERSITY OF CALIFORNIA

Materials & Molecular Research Division

CROSSED MOLECULAR BEAM STUDIES
OF CHEMILUMINESCENT REACTIONS

Carol Cuzens Kahler
(Ph.D. thesis)

April 1980

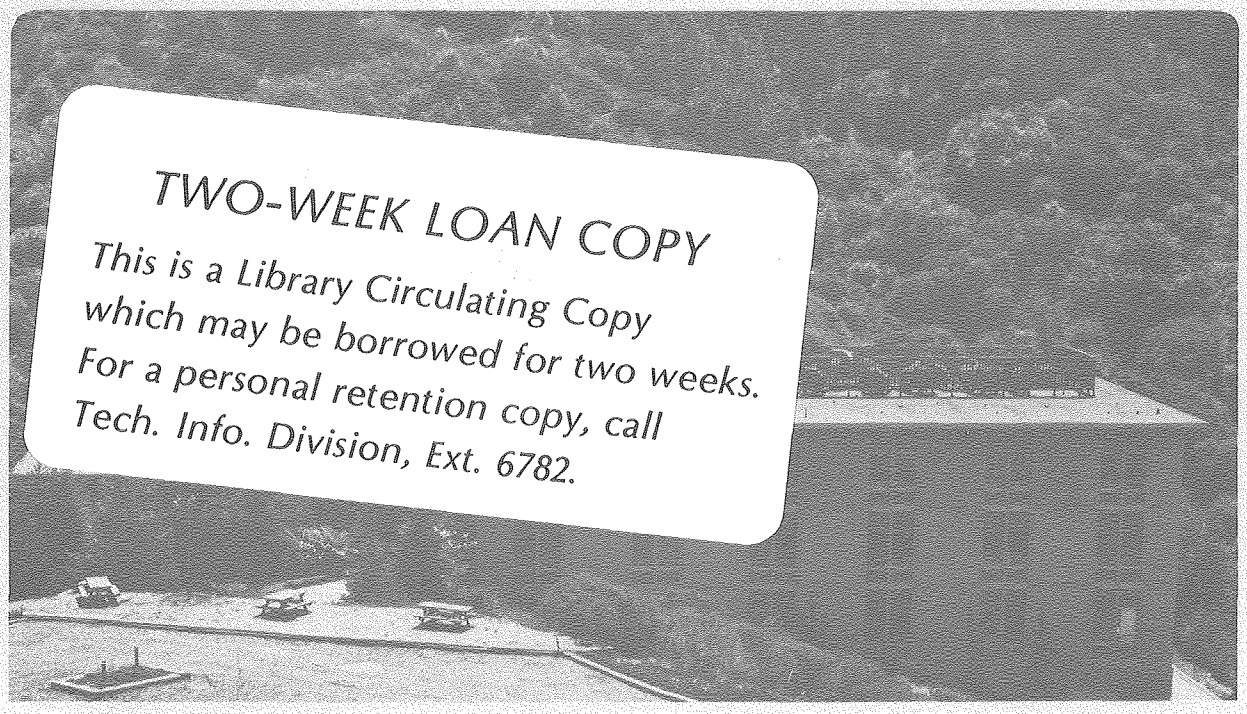

Prepared for the U.S. Department of Energy under Contract W-7405-ENG-48

DISCLAIMER

Laser enhancement of the $I_2 + F_2$ reaction was attempted, but no enhancement was seen.

Also described is a crossed molecular beam study of the chemiluminescent reaction of $NO + O_3 \rightarrow NO_2^* + O_2$. The collision energy dependence was measured using a supersonic NO beam and the cross section was found to increase with increasing collision energy. The reaction threshold was 2.1 kcal/mole. An effusive NO beam was used to study the effects of internal NO energy on chemiluminescence production. The chemiluminescence was found to increase with increasing NO temperature. This can be explained by assuming the cross section varies as $E_{rot}^{1.4}$ where E_{rot} is the average rotational energy of the NO beam. No attempt was made to calculate the dependence of the cross section on J. The chemiluminescence enhancement was not found to have the dependence on the increased $NO(^2\Pi_{3/2})$ population that had been previously suggested. Low resolution spectra of the chemiluminescence were recorded in the range of 450-800 nm as a function of collision energy. The emission curve shifted to the blue as the collision energy increased.

The chemiluminescence-laser fluorescence crossed molecular beam machine used in these experiments is also described. The machine has the capability of detecting total or dispersed light from the reaction zone and also allows use of a laser for laser induced fluorescence or excitation of the molecular beam. Calculations indicating the minimum observable reaction cross sections under certain circumstances are presented.

CROSSED MOLECULAR BEAM STUDIES OF CHEMILUMINESCENT REACTIONS

Carol Cuzens Kahler

Materials and Molecular Research Division
Lawrence Berkeley Laboratory

and

Department of Chemistry
University of California
Berkeley, California 94720

April, 1980

Abstract

The chemiluminescent bimolecular halogen-halogen reactions, $F_2 + I_2$, Br_2 and ICl, have been studied by the crossed molecular beam technique. Undispersed chemiluminescence was measured as a function of collision energy and, for $I_2 + F_2$, as a function of the two beam pressures. Although no spectra were obtained to positively identify the emitters as IF, ClF and BrF, arguments are given to support this identification. The observed reaction thresholds of 4.2 and 5.9 kcal/mole for $I_2 + F_2$ and $ICl + F_2$, respectively, are the same as the threshold energies for production of the stable trihalogens I_2F and ClIF. This coincidence of threshold energies, as well as similar high collision energy behavior, implies that the chemiluminescent reaction proceeds via a stable trihalogen intermediate. This mechanism can explain our results and the results of other workers without resorting to a symmetry forbidden four center reaction mechanism. A threshold of 11.3 kcal/mole was found for $Br_2 + F_2$, no threshold for Br_2F has been previously reported.

Finally, two computer programs used in the data analysis are described. One of the programs calculates a relative velocity distribution from time-of-flight velocity analysis data, taking beam width and velocity spread into account. The second program facilitates determination of the reaction cross section energy dependence using an assumed cross section functional form, the relative velocity distribution and experimental data.

This dissertation is dedicated to Irene Cox and to the memory of Elizabeth Andersen, my grandmothers, who always encouraged me to make my own path.

TABLE OF CONTENTS

ACKNOWLEDGEMENTS

First, of course, I want to thank Professor Yuan T. Lee for his support and guidance during my graduate career. His unending enthusiasm, patience, good humor and skill in matters both scientific and technical have made these years both intellectually profitable and very enjoyable.

I regret that I do not have the space to thank everyone who has helped me, but there are a few I do want to thank especially. Charlie Taylor and Allan Susoeff were indispensible in machining all sorts of special parts and coming up with ideas to fix the myriad of problems encountered in getting everything working at the same time. Ann Weightman, the secretary of our research group, helped in ways too numerous to list here. More than their special skills, Charlie, Allan and Ann were good friends and fascinating people. I also want to thank Diana Morris for typing this manuscript, her skill and cheerful personality made the process more enjoyable.

I wish I could thank every member of our research group individually, but, again, I lack the space. I do want to thank Scott Anderson for helpful discussions (and pre-prints) concerning the $NO + O_3$ reaction. I owe a great deal of thanks to Marta Kowalczyk, my partner in the $NO + O_3$ experiments. The experiment would have been much more difficult and much less fun to do without Marta's expertise (particularly in ozone handling) and company. The many discussions we had concerning the experiment were invaluable. I also want to thank Dr. Richard Buss for his help with technical, scientific

and computer problems, and for his friendship -- he has been instrumental in the rapid expansion of my interest in the world around me.

My family and friends have provided a great deal of moral support. My parents, my parents-in-law, and my brother have always encouraged me in my endeavors, helped me celebrate the good parts and weather the bad. My greatest debt is to my husband, Charley Kahler, without whom I might not have made it. He has encouraged me to achieve to my limits, but realized that I have limits. He offered support not just in words of encouragement (which were invaluable on the darkest days), but in action -- he spent many hours in the lab at night keeping me company, and has brought me dinner during those experiments that had no respect for time.

Finally, I would like to thank the donors to the Eric B. Abramson Memorial Fellowship, from which I received support during my first year.

This work was supported by the Division of Chemical Sciences, Office of Basic Energy Sciences, U. S. Department of Energy under contract No. W-7405-Eng-48.

I. INTRODUCTION

The study of chemiluminescent reactions is one way to work toward the ultimate goal in chemical kinetics: to be able to measure state-to-state reaction rates. In other words, we want to measure the reaction rate for reactions in specific quantum states having a specific collision energy and orientation and forming products in specific quantum states with a given relative parting translational energy and orientation. While we are a little way from obtaining such specific reaction rate constants, some experimental[1-3] and theoretical[4,5] work has been done which indicates that the disposal of the various kinds of energy does not always result in a distribution (either between or within the various degrees of freedom) corresponding to thermal equilibrium. Likewise, it has been suggested that vibrational energy, say, may be much more effective than translational energy in driving some kinds of reactions (for example, a thermoneutral reaction with the barrier in the exit channel, see references 4 and 5 for a more complete discussion), and so it is conceivable that a reaction might be made more efficient (perhaps even over a competing reaction path) if the available energy were in the proper mode instead of randomized.

The application of the crossed molecular beams technique to chemiluminescent reactions is an important step forward in the study of such reactions for three main reasons: the technique allows the study of unstable or highly reactive species; the chemiluminescence coming from a reaction is obtained under well-defined conditions

(single collision conditions with a very narrow, but variable collision energy); and the chemiluminescence comes from products whose quantum states have not been changed through collisions. These last two reasons make the molecular beam technique particularly advantageous in the continuing effort to obtain state-to-state reaction rates. This was the main reason behind the construction of the laser fluorescence-chemiluminescence crossed molecular beam machine described in Chapter II. This machine was designed to enable us to obtain more information on the disposal of energy in reaction products. The machine has one supersonic and one quasi-effusive beam source, so the collision energy is well defined. The light from the reaction zone can be collected either dispersed or as total fluorescence. The machine also allows for addition of a laser to either detect vibrationally excited ground state products through laser induced fluorescence or excite one of the reactant beams. A calculation of the minimum observable cross section for this machine, under various assumptions, is presented and indicates that the photon detection of crossed molecular beam products can be more sensitive than mass detection, although this is partly because the total cross section is observed in this machine while many mass detection machines measure the differential cross section.

This high sensitivity is required to obtain the results, described in Chapter III, from a study of the chemiluminescent reactions of F_2 with I_2, ICl and Br_2. This study was prompted by an apparent disagreement between the results of previous studies,[6-8] with two papers[7,8] supporting a four center reaction mechanism for the

reaction $I_2 + F_2 \rightarrow IF^* + IF$ and one[6] presenting evidence against a symmetry forbidden four center mechanism for this reaction. Our data suggest a bridge between the two sets of results and support the mechanism suggested in reference 6.

The light level was too low to obtain a spectrum, so a positive identification of the emitters cannot be made. Arguments are given, however, supporting our belief that the emitters are IF, ClF and BrF. The thresholds of the chemiluminescent reactions are 4.2, 5.9 and 11.3 kcal/mole for $F_2 + I_2$, ICl and Br_2, respectively. The coincidence of the thresholds for $F_2 + I_2$ and ICl with those found for the production of I_2F and ClIF from the same reactants[6] suggests a chemiluminescence mechanism going through a stable trihalogen intermediate. The proposed mechanism also explains results obtained by other workers.[7] Laser enhancement of $I_2 + F_2$ through the excitation of I_2 was attempted, but no enhancement was seen.

Chapter IV describes a study of the chemiluminescent reaction of $NO + O_3 \rightarrow NO_2^* + O_2$, which was prompted by a suggestion that $NO(^2\Pi_{3/2})$ (instead of the ground state $NO(^2\Pi_{1/2})$ was responsible for the chemiluminescence. In the first part of the study, a supersonic NO beam was used to obtain a collision energy dependence of the cross section. The reaction cross section has a threshold of 2.1 kcal/mole and has an increasingly stronger collision energy dependence as the collision energy increases. A low resolution spectrum of the chemiluminescence (450–800 nm) was found to shift to the blue as the collision energy increases. In the last part of the

study, the temperature of an effusive NO beam was changed to see how NO internal energy affects the chemiluminescence production. The chemiluminescence was found to increase with NO temperature. After the known increases due to translation and vibration are accounted for, the increase can be explained by assuming the cross section increases at least as fast as $E_{rot}^{1.4}$, where E_{rot} is the average rotational energy for the NO beam. No attempt was made to find the cross section as a function of J. The data was not found to be consistent with the previous suggestion that the cross section of $NO(^2\Pi_{3/2})$ was at least four times as large as the cross section of ground state $NO(^2\Pi_{1/2})$.[9]

Finally, in Chapter V, two computer programs used in the data analysis are described. One of the programs calculates a relative velocity distribution from the time-of-flight beam velocity data, taking beam width and velocity spread into account. The second program uses the relative velocity distribution and an assumed functional form of the reaction cross section to calculate an expected signal. By varying the parameters of the cross section function until the calculated signal fits the experimental data, the dependence of the cross section on collision energy can be obtained.

A. References

1. P. E. Charters and J. C. Polanyi, Disc. Faraday Soc., 33, 107 (1962).

2. J. G. Pruett and R. N. Zare, J. Chem. Phys., 64, 1774 (1976).

3. J. L. Kinsey, "Molecular Beam Reactions," MTP International Review of Science, Physical Chemistry Series Two, Vol. 9 (University Park Press, Baltimore, 1976).

4. J. C. Polanyi, Acct. Chem. Res., 5, 161 (1972).

5. R. D. Levine and R. B. Bernstein, Molecular Reaction Dynamics, (Oxford University Press, New York, 1974).

6. J. J. Valentini, Ph.D. Thesis, University of California, Berkeley, 1976.

7. J. W. Birks, S. D. Gabelnick and H. S. Johnston, J. Mol. Spec., 57, 23 (1975).

8. F. Engelke, J. C. Whitehead and R. N. Zare, Disc. Faraday Soc., 62, 222 (1977).

9. A. E. Redpath, M. Menzinger and T. Carrington, Chem. Phys., 27, 409 (1978).

II. DESIGN OF THE CHEMILUMINESCENCE LASER FLUORESCENCE CROSSED MOLECULAR BEAM MACHINE

A. Introduction

Crossed molecular beam experiments using mass spectrometric detection have provided detailed information on dynamics and interaction potentials for reactive, inelastic, and elastic collisions.[1] Recent improvements in techniques and the steady increase in detection sensitivity have made possible the study of crossed molecular beam and beam-gas reactions using photon detection.[2-5] The latter experiments are complimentary to the former in that the mass detection and product angular distribution provide information on branching ratios, lifetime of collision complexes, relative product translational energy, reaction thresholds and energy dependences. Photon detection, so far, has not been able to provide any angular distribution information or relative product translational energies and, therefore, we cannot determine complex lifetime or parameters of the interaction potential although reaction thresholds, energy dependences and branching ratios can be measured. The one piece of information that is directly obtained in photon detection, but can only be inferred in some cases with mass detection, is the quantum state of the products as they were formed in the reaction. In addition, photon detection can reveal events with small probability, when electronically excited species are formed, where the mass detection systems may have too much background noise.

In a crossed molecular beam machine there is a well-defined collision zone but, although we have a small spatial area for product formation, the products leave the area at approximately 5×10^4 cm/sec. Vibrationally excited products, or long lived electronic states, will have a lifetime on the order of 1 millisecond which will give the molecules time to travel 50 cm, putting most of the molecules out of the detector's viewing area. A small fraction of the molecules will still radiate in the viewing area, so, with a very sensitive detector, the reaction products will be detected. Because of the short radiative lifetime and high detector sensitivity, photon detection of crossed molecular beam products in the visible and ultraviolet parts of the spectrum is more desirable. For this reason, reactions that do not produce, electronically excited states, but give vibrationally excited ground state products, are studied through the use of laser induced fluorescence (e.g., reference 2-4).

The products of the crossed molecular beam reactions can be identified, then, by their spectrum, which is obtained either by dispersal of the chemiluminescence or by laser induced fluorescence (using a tunable laser). We can obtain information on what products are formed (although photon detection may not be applied nearly as universally as mass detection), what the branching ratio is, how the branching ratio and quantum states change with translational energy, and what the reaction threshold is. Determining what quantum states are populated (e.g., is the excess energy disposed of in electronic, vibrational, or translational degrees of freedom, is there

a population inversion) and how different forms of reactant energy (e.g., translational vs. vibrational) affect the product state distribution are important steps in gaining a better understanding of microscopic rate constants and bimolecular reaction mechanisms. The big advantage in using crossed molecular beams instead of bulk phase or flow systems is that the products undergo no collisions between the time they are formed and the time they leave the collision zone, so the measured distribution accurately reflects the branching ratio among quantum states.

The machine described in this chapter was designed to study crossed molecular beam products using both of the photon detection techniques mentioned above. Because we are working with low signals (the gas pressure in the collision zone is approximately 1×10^{-4} torr), the main factors in the machine design were to minimize background light, maximize the signal and maintain the crossed beam technique advantages of good collision energy control and single collision conditions. Single collision conditions require a low vacuum outside the beam sources, so maximization of pumping speed was important. Good collision energy control requires that at least one of the beam sources be supersonic. Several factors played a part in maximizing the signal to noise ratio — having the beam sources as close to the collision zone as possible, reducing stray light by painting surfaces black, careful selection of a high sensitivity, low background photomultiplier, etc. The next section of this chapter gives a description of the machine, Section C consists of a list of the more important

characteristics (e.g., pressure, dimensions) of the machine and the final section is a calculation of the detection limit for a reaction.

B. Design of the Machine

The machine will be described in three parts: the main chamber and beam sources; the detection system; and the additional equipment used for laser fluorescence experiments.

Schematics of the main chamber are shown in Figures 1 and 2, with the parts to be discussed labeled A-N. The chamber consists of a stainless steel 304 tube with a 1/8 inch thick wall, 11 inches outer diameter and 31.5 inches long. A supersonic beam source (A-E) fits into one end and faces a stainless steel foil (10 mil thick) cone (F) which has a 1-1/8 inch diameter hole in its peak and acts as a beam catcher, dividing the main chamber into two parts. Each part is pumped by a six inch Varian oil diffusion pump (J, J') and can be closed off from the pumps by sliding gate valves. The diffusion pump (J) under the reaction chamber has a liquid nitrogen cooled trap above it to prevent pump oil from coating the detection optics (L).[6]

The effusive[1] (or quasi-effusive) beam source (G) is shown in Figure 3. It fits into a 5.895" diameter hole on top of the machine and has no differential pumping region like the supersonic source has. The effusive beam crosses the supersonic beam at 90°. There are two other pairs of flanges in the reaction chamber that cross the machine at 70° (H,H') and 60° (J,J') relative to the long axis. These flanges are used for the detection system (H), laser baffle arms

(I,I'), and electrical feed-throughs (H'), and will be discussed later.

Because we use ion gauges (K) to monitor the chamber and source pressures, and use resistance wires to heat the beam sources, there is background radiation. For this reason, the entire reaction chamber was painted with 3M 101-C10 Nextel Velvet black paint. All other surfaces in the reaction chamber (e.g., the foil cone) were painted black, except for a few surfaces that could not be painted (e.g., the beam chopper, nozzle faces). This paint was chosen as being extremely flat black, as not having the usual requirement of a high temperature bake-out, and being semi-permanent. Application of a liquid suspension of graphite was considered, but such a coating is actually fairly shiny and is easily wiped off. The main chamber was painted before being used so that no data exist on the light reduction due to painting in the chamber. However, addition of shiny surfaces to the chamber with subsequent painting provide evidence that the paint is extremely effective in reducing scattered light. Many of the laser light baffles (to be discussed later) were black anodized, but even that is not as effective as the paint. After application of the paint, the main chamber was baked, using heating tapes, and pumped for two weeks, resulting in an ultimate reaction chamber pressure of 2.2×10^{-7} torr. One problem with the paint is that pump-down of the machine may take two days after the machine has been open to the atmosphere for several days (e.g., during alignment of the laser). While the paint showed no signs of deterioration due to the chemicals used in the beams (even after F_2), it seems that the chemicals may aggravate the problem of long pump-down time.

The effusive source (Figure 3, parts labeled A-I) was used in both experiments described later in the dissertation. The source is designed so that the nozzle (A) can be both heated and cooled with a temperature range of -140 to +130°C. This feature was used in both experiments described later — to change the internal molecular temperature in one case, and to prevent the condensation of beam molecules in the other. The heating and cooling of the stainless steel nozzle are provided by thermal conduction through a copper plating (B) on the stainless steel tube. The 1/4 inch tubing was plated with copper to slightly greater than 1/2 inch diameter and machined down to exactly 1/2 inch diameter. The machining produces a smooth and uniform surface, providing good thermal conduction to the plating from the copper heating and cooling block. The block also helped clamp (E) the nozzle in place for alignment. The copper block is hard-soldered to a stainless steel liquid nitrogen feed tube (G) which attaches to the top of the beam source housing via a confat flange and copper gasket (H). The copper block has six holes, 1/8 inch in diameter, drilled in it to hold alumina rods (F). Each rod, in turn, has four holes through which is threaded .010 inch diameter nichrome resistance heating wire which is connected to an electrical feed-through on the top of the beam source housing. The temperature is monitored using a copper constantan thermocouple (Omega Engineering) attached to the nozzle tip with a hose clamp. We found that it was necessary to add a radiation shield to prevent the resistance wire emission from reaching the photomultiplier tube. The shield consisted of two black painted aluminum foil (approximately

.010 inch thick) rings and is shown in Figure 3 (D). The nozzle tube is plated 16 inches up and is bare where the stainless steel tube is vacuum sealed against atmosphere by a 1/4 inch Cajon bore-through adapter (I). The tip of the nozzle is stainless steel and is .020 inch thick where the .015 inch diameter nozzle hole is drilled. The nozzle is aligned (and held in alignment) by a combination of the copper heating block and a three-point alignment piece attached to the beam source housing (C). The copper block holds the nozzle at its proper height above the collision zone, while the alignment piece aligns the nozzle hole with the key on the beam source housing. The nozzle can be aligned to within .001-.002 inch using either an alignment jig or, in situ, using two cathetometers (one aligned along the laser beam axis, the other along the supersonic beam axis). The flange, into which the effusive source fits, has a key, allowing removal and replacement of the source without destroying the alignment. The distance from the nozzle to the collision zone may be changed without realignment using spacers of various widths with a key on both sides.

The supersonic sources used in the two experiments will be described in detail later. They were all designed after the "standard" supersonic source.[7] The reducer (E, Figure 1 and 2) that divides the source chamber and source pump from the reaction chamber differs from others used in this research group in having more slope on the bottom and sides to increase pumping speed in the main chamber.

The optics in the detection system are sealed off from the vacuum system by a 2-1/2 inch diameter x 1/16 inch thick quartz plate (ESCO Optics grade S1-UV) pressed against an O-ring (L, Figure 2). This arrangement has the advantages of allowing lens adjustments while the machine is under vacuum as well as subjecting only the quartz plate to the diffusion pump oil vapor in the main chamber. The lens system, shown in Figure 4 (parts labeled A-L) is mounted on an Oriel 1142 optical rail (J) using two Oriel 1164 carrier (D) and one Oriel 1162 carrier (I).

In assembling the optics, the optical rail was first carefully aligned to insure that the lens axes would coincide with the axis defined by the collision center and position of the photomultiplier photocathode or spectrometer slit (i.e., the center of the flange of the optics housing). This was accomplished by aligning a He-Ne laser with the tip of the effusive source nozzle, a hole drilled in the center of a flange that fit, with a key, onto flange H' of the main chamber, and an iris mounted on the keyed flange such that its hole was on the flange axis. The detection optics holder, (M, Figure 2 and K, Figure 4) that fits into flange H opposite H', was translated in the two directions perpendicular to its axis until an iris, mounted with its hole on the optics holder axis, was centered about the He-Ne laser beam. The holder was then bolted into place and two holes were drilled through its flange and the main chamber flange. In this way, the holder could be removed and replaced, using pins through the holes, without realignment.

The optics holder has a flat stainless plate, welded in place, on which sits the optical rail. The axis of the rail was aligned so that the axis of the lenses would be on the optics holder axis. This was done by mounting an iris on an x-y translation stage and moving it along the optical rail, noting how the position of the iris had to be changed along the rail to keep the iris centered on the He-Ne laser beam. The rail was then adjusted vertically using shims and moved in a left-right direction until the iris was centered along the entire rail without adjustment. The rail was then bolted into place with 3 screws, being careful not to warp the rail by excess bolt pressure. The final slope and skew of the rail were measured so they could be accounted for when the lens holders were machined.

The lens holders (Figure 5) were made of brass and chemically blackened. Each lens holder consists of a plate that screws on to the rail carrier and has a ring machined such that the plane of the ring is perpendicular to the carrier. Each ring has a machined step into which the lens fits exactly and is held in place by another ring that screws onto the first. In spite of these efforts, the final image is offset by .175" up and .008" right of center, at a position 6" from the final lens, requiring the connection between the optics housing flange and detector to be offset accordingly.

The first lens (B, Figure 4) (Melles Griot synthetic fused silica, 75mm f.l., 50mm diameter, plano-convex) was positioned so that its distance to the collision center was equal to its focal length by making sure the size of the image of a light, placed at the collision

center, did not change with distance from the lens (i.e., the light was parallel). The holder for the second lens (C) (Melles Griot synthetic fused silica, 200m f.l., 50mm diameter plano-convex) sits on the same carrier as the first lens and focusses the parallel light from the first lens onto an iris (E) (maximum opening: .5 inch) located at its focal point. The purpose of the iris is to exclude light other than that coming from the collision center (e.g., scattered laser light, beam source heater light). The experimental signal to noise ratio will reach an optimum value as the iris opening is varied. The third lens (G) (ESCO Optics, fused silica, grade S1-UV 2 inch diameter, 2-5/8 inch f.l., plano-convex) was positioned so that its focal point was at the plane of the iris. At this point it was found that the light could not be made to come out excactly parallel, so the position of the third lens was optimized for the least light divergence. The fourth lens (H) (ESCO Optics, fused silica, grade S1-UV, 1 inch diameter, 6 inches f.l., cylindrical) was placed on the same carrier as the third lens and served to focus the light into the rectangular photocathode of the RCA C31034 photomultiplier. If the spectrometer (Jobin Yvon HRP .6 meter) is to be used, lens 4 should be replaced by another ESCO lens, same as the first except with a 5 inch f.l., which will match the spectrometer f number of 4.9 better.

The acceptance angle at the collision zone end of the optics asembly is .32 steradians. The first two lenses are made of synthetic fused quartz and have the transmission function shown in Figure 6.[8] The other lenses and windows have extended transmission (to 160nm)

in the UV, but the curve is, otherwise, the same. This gives the detection system a total efficiency of 1.7 percent at 5000Å with respect to the light emitted into 4π radians at the collision center. Light collection could, of course, be doubled by addition of a mirror opposite the quartz plate.

The lens system is covered by a black anodized tube (N, Figure 2 and L, Figure 4). This tube, which connects to the optics holder via a key, connects, again with a key, either to a flange that bolts to the PMT housing or to a flange having a tube extending to the slits on the spectrometer. The photomultiplier (RCA C31034) is housed in a dry ice cooled housing (Pacific Precision Model 3378). The tube manufacturer does not recommend dry ice cooling of the C31034 when the tube is in an ordinary teflon socket (9). For this reason, we had the housing manufacturer drill out the teflon socket to insure that the voltage divider pins would be insulated from each other but still loose in the teflon socket so that when the teflon contracted on cooling, the pins would not be stressed causing tube breakage. GE RTV 108 was used to seal the tube base to the teflon socket to prevent moisture condensation on the pins during cooling. Our tube operated very well under these conditions and had a dark count of 25 cps at dry ice temperatures, with a 1700V bias. The output of the photomultiplier tube (Figure 7) went first into an amplifier-discriminator (Pacific Precision Model AD4) then into a gating circuit (either an LBL 13X3050 Gate and Timer Module or an Ortec Model 9320) triggered by a chopper (D, Figures 1 and 2) on the supersonic beam source (Bulova type L40

150 HZ tuning fork). The electrical feedthrough for the chopper is on flange H'. The gating circuit directed the output into a dual channel scaler (Whittaker Model 1535 or Ortec Model 9315) where one channel collected signal with the chopper blocking the beam, the other channel collected signal when the chopper was clear of the beam resulting in automatic background subtraction.

The spectrometer can be used in a variety of ways. It has an exit slit as well as a photographic exit allowing use of a camera, photomultiplier or optical multichannel analyzer (PAR OMA I Model 1205A with 1205KD detector) as a detector. The spectrometer has been modified to couple to either a cooled or uncooled PAR OMA. For the work described here, the spectrometer was used only with the camera and the photomultiplier. The spectrometer has a maximum dispersion of 8Å/mm which, combined with the 500 channels, 25μ wide, on the OMA, gives a resolution of .20Å/chan. The photographic grating has 1800 grvs/mm, is blazed at 500nm, with a peak efficiency of 65 percent. The estimated efficiency of the spectrometer is .3 percent, at 500nm, based on .6 percent transmission of the light radiant on the entrance slit (experimental value). The spectrometer was aligned on laser light scattered from a wire placed in the collision center. The collision center, in this case, was defined by the intersection of the supersonic beam axis (determined using a cathetometer) and the aligned laser beam. The image of the scattered light was centered on the entrance slit and the two focussing mirrors in the spectrometer; this assured that the optical axis of the spectromter was the same as the

optical axis of the lenses. The image of the wire was then focussed on the entrance slit by adjusting the position of the spectrometer, and the entire process repeated until both alignment criteria were met.

The laser baffle arms are patterned after those designed by Zare et al.,[2] Figure 8. They are constructed of stainless steel 304 tube, 35 inches long, 2.5 inch outer diameter and 1/8 inch thick. Inside each tube are four baffles (C), as shown in Figure 8, constructed of .032" thick anodized aluminum, held in place by a pair of stainless steel flanges (D) machined to just fit inside the baffle arm tubes. The baffles are separated by black anodized aluminum spacer rings (E), each ring having 1/4" diameter holes drilled in the side to increase pumping speed in the arms. The baffle flanges are painted black, which was found to significantly decrease the scattered laser light. The baffle arms are sealed against atmosphere by quartz plates (ESCO Optics, S1-UV, 1-1/2 inch diameter x 1/8 inch thick) glued, using Dow Corning 3145 RTV, onto 1 inch diameter Pyrex tubing (the inside of which was painted black), which was cut at the Brewster angle of 55° for 6000Å light and held by Cajon fittings (A). One of the windows has a Wood's horn blown into the glass tube just below it. While this window was designed to be the exit window, there is sufficient back scattered and multiply reflected light at the entrance window that the Wood's horn was found to be of more help on the entrance than exit arm.

Because the baffle arms are so long, alignment of the laser is a critical procedure. After several alignment attempts, the following procedure was found satisfactory.

1) Without the baffle arms in place, cross hairs were put on flanges I,I' of the main chamber and the laser beam (in the experiments discussed later, a Spectra Physics Model 171 Ar^+ laser was used) was aligned, using two mirrors in Burleigh mounts to direct the beam (Figure 9), so that it hit the center of both cross hairs. A 1000mm f.l., 2 inch diameter lens after the Burleigh mounts reduced the scattered light considerably by focussing the laser beam near (but not at) the collision center. A cathetometer was aligned with the cross hairs, looking down the beam axis, and used (with an index card to block the laser!) to make sure the beam was well centered. It is important that this alignment be carried out carefully because once the baffle arms are in place, it is much harder to see how the laser beam is misaligned.

2) The laser beam was blocked and the baffle arm closest to the laser was bolted on to the machine, but the Brewster angle window was left out. The baffle arms are sufficiently heavy that a piece of channel iron was clamped on to the main chamber support stand and threaded rods attached to the channel iron to support and position the arms from underneath and the side. The arm was positioned using the threaded rods so that all four baffle holes had their axes on the cathetometer axis. The Brewster angle window was added, the index card removed from the laser path and final positioning of the arm was performed, looking for minimum laser spot distortion and scattered laser light.

3) The procedure was performed, as above, for the second baffle arm.

4) Clamps (B, Figure 8) were made to attach to the Cajon fittings that hold the Brewster angle windows in place. These clamps held a piece of aluminum about an inch in front of the Brewster angle windows to which cross hairs were attached such that the aligned laser beam hit the center of the cross hairs on both the entrance and exit arms. The positions of the cross hairs were then scratched into the aluminum. Every time the laser was turned on and peaked for maximum power, the position of the beam changed slightly. The scattered light seen by the photomultiplier is very sensitive to the position of the laser and so, by putting the cross hairs in place, the laser could be realigned with the machine under vacuum. The cross hairs could then be removed to run an experiment. This method was found to be very satisfactory. The laser could be realigned day after day, getting basically the same scattered light count as when the laser was initially aligned, approximately 800 cnts/sec at .1 watt dye laser power, 6000Å.

There was enough light split off at the entrance Brewster angle window to be sent through a Heath EU 700 spectrometer for both wavelength (if the associated dye laser, Spectra Physics Model 375, is used) and power monitoring (Figure 9). The laser power drifted substantially over the first one-half to one hour after turning it on, most likely due to thermal changes in the optics.

C. Chemiluminescence Machine Characteristics

Pressure	
Ultimate Main chamber pressure (with paint, after baking)	2.2×10^{-7} torr
Main chamber pressure with 1 torr I_2 beam from secondary source	8.0×10^{-5} torr
Main chamber pressure with a 600 torr He supersonic beam	6.6×10^{-5} torr
Optics	
Fraction of light collected at first lens	.025
Wavelength range of optics	.2-4μ
Maximum transmission of optics	.65
Offset of optics image at focal point of last lens	.175inch (.444 cm) up + .088 inch (.224 cm) right of center.
Typical Beam Source dimensions	
Effusive - Quasi Effusive Source	
Diameter of Nozzle	.015 inch (.038 cm)
Distance to collision zone (no skimmer or spacer)	.200 inch (.508 cm)
Temperature range	-140 to +130°C
Supersonic Source	
Diameter of nozzle	.003 inch (.008 cm)
Nozzle-skimmer distance	.229 inch (.582 cm)
Nozzle-collision zone distance (assuming chopper is on this source)	2.68 inch (6.81 cm)
Angular spread (30 mil skimmer)	7.5°
Scattered laser light from a .1 Watt dye laser	800 cnts/sec.

D. Detection Limit Calculation

The limit of detection is normally defined by a signal to noise ratio of 2.[10] In the case of a chemiluminescent reaction, the noise sources and approximate contributions are:

1) Photomultiplier dark count (≈25 cnts/sec).
2) Radiation from beam source heaters (for the $I_2 + F_2$ experiment discussed later, there was a negligible contribution from the F_2 source while the I_2 heater contributed ≈300 cnts/sec).
3) Statistical noise which is equal to the square root of the total count rate.

The requirement placed on the signal, then, is that $S/(25 + 300 + \sqrt{S + 2B}) = 2$. The statistical noise is represented by $\sqrt{S + 2B}$ because the signal is the difference between two counts (two channels of a dual channel scalar in our case), one count has signal (S) + background (B), the other has only background (B). The total number of counts is then S + 2B and the fluctuation is $\sqrt{S + 2B}$. If S = B then S = 744.5 cnts/sec for a signal to noise ratio of 2.

If total (undispersed) chemiluminescence is being measured then the light loss sources are:

1) Photomultiplier Quantum Efficiency (.17 at 5000Å).
2) Loss through photomultiplier housing windows (.80 at 5000Å).
3) Lens Efficiency (.65 at 5000Å).
4) Fraction of light collected by optics (.025).

There is no need to correct for the counting time lost in going through the gating circuit because all the count sources are subject to the same restrictions. The quantities quoted for noise sources 1 and 2 are, however, corrected for the gating system counting time loss. We require a signal coming out of the photomultiplier of 744.5 cnts/ sec, which means 744.5/(.17 x .80 x .65 x .025) = 33687 emission events/sec are required in the collision zone viewed by the photomultiplier.

If the chemiluminescence is dispersed, then there is additional loss on the spectrometer slit and optics of .003 at 5000Å. The stray light rejection in the spectrometer is on the order of 1×10^{-5}, so no additional noise sources need to be considered. This additional loss, however, means that we will require 1.12×10^{8} emission events/spectral width x sec.

The next step of the calculation is a correction for the loss of light due to emitters leaving the area seen by the photomultiplier and requires that assumptions be made about the velocity and lifetime of the emitter. Using the size of the rectangular photocathode of the RCA C31034 and accounting for the magnification of the lenses used, the collision area seen by the photomultiplier is .092cm x .266cm x .892 cm. The light emitted along the axis of the optics will be defocussed to a certain extent, but not cut off, so it is assumed that virtually all the light emitted along this axis will be detected. The molecular beams fill this area fairly uniformly--the supersonic beam will be ≃.892cm in diameter at this point and the quasi-effusive beam

will be much larger. If the emitter has a lifetime of 1μsec, and a velocity of 1×10^5 cm/sec, then it will travel 0.1 cm, on the average, before emitting. Therefore, while there will be some variation in number density, there will be an approximate steady state of emitters in the area (as opposed to a net flux out of the area following product formation). If the emitter has a longer lifetime, say 100μsec, then it will travel an average of 10cm before emitting and this loss must be accounted for. So, for 1μsec lifetime, 3.4×10^5 emitters/sec are required in the collision zone, but for a 100μsec lifetime $3.4 \times 10^5/1-e^{-x/v\tau}$ emitters/sec must be formed where x is the distance traveled, v is the velocity and τ is the lifetime. Assuming the emitters travel with the center of mass velocity vector (as in $I_2 + F_2$), x = .141cm, on the average. If $v = 1 \times 10^5$ cm/sec, then $e^{-x/v\tau} = .986$ and 2.4×10^7 emitters must be formed in the collision zone per second. If a spectrometer is used then 1.2×10^8 emitters/spectral width x sec for 1μsec lifetime or 8.0×10^9 emitters/spectral width x sec for 100μsec lifetime.

Using the dimensions of the collision region, the final results for required emitters/cc x sec are:

	Lifetime	
	1μsec	100μsec
Total chemiluminescence	1.56×10^7	1.10×10^9
Dispersed chemiluminescence (per spectral width seen by the photomultiplier)	5.13×10^9	3.66×10^{11}

There is one assumption in the calculation above that is highly variable; the ratio of signal to background. The data for $I_2 + F_2$ had a ratio varying from .07 to .80. The background light is a result of reactions taking place in the chamber but not as a direct result of the molecular beams crossing. A lower background light would be obtained with lower background pressure and probably with better spatial definition of the quasi-effusive source.

The calculation above is not meant to represent the absolute detection limit achievable with this machine. While the 25cps of noise from the photomultiplier is unavoidable, the heater background of 300cps could certainly be reduced. This calculation serves the purpose of pointing out areas of concern in planning an experiment and designing equipment rather than indicating a limit beyond which an experiment is impossible.

If beam source number densities of 1×10^{12} molecules/cc for the supersonic source and 5×10^{10} molecules/cc for the effusive source are assumed along with a relative velocity of 1×10^{5} cm/sec, then the numbers above can be converted into minimum reaction cross sections using

$$I\left(\frac{\text{molecules}}{\text{sec}}\right) = N_1 N_2 \, v_{rel} \sigma$$

where I is the signal, N_1, N_2, are the number densities of the beams, v_{rel} is the relative velocity and σ is the cross section. The results are, in Å^2:

	Lifetime	
	1μsec	100μsec
Total chemiluminescence	3×10^{-5}	2.2×10^{-3}
Dispersed chemiluminescence	1.0×10^{-2}	7.3×10^{-1}

Similar calculations can be done for laser-induced fluorescence experiments. The noise sources are (assuming the reactant molecules do not absorb the laser light):

1) Photomultiplier dark count (25cps)
2) background laser light (800cps at .1 watt CW)
3) Statistical noise

In this case the background light due to photon emission of background molecules will undoubtedly be fairly high, although no data has been obtained from which a reasonable estimate may be made. Assuming S = B again, means that S = 1796.85 cnts/sec will be required. There will be the same losses as before (no spectrometer will be used—a spectrum is obtained by tuning the dye laser), so 8.13×10^5 emissions/sec will be necessary.

The collision zone is now defined not only by the beam sources but also by the size of the laser beam, which has a diameter of approximately .318cm. This is still large enough compared to the area seen by the photomultiplier to assume a steady state for the case of an emitter with a 1μsec lifetime. One problem that must be considered is that since the laser induced fluorescence technique is designed to produce a spectrum that will indicate relative probabilities of product quantum state formation, saturation of a transition must be

avoided. The number of transitions per cc per second is given by $N(v")p(v',v")BF$ where $p(v',v")$ is the energy density at the required frequency, $N(v")$ is the number density of the molecules in v", F is the Franck-Condon factor and B is the Einstein B coefficient for the electronic transition.[11] For a lifetime of 1μsec, $B = 3.3 \times 10^7$ $cm^2/erg\ sec$ at 5500Å. Using a .1 watt laser at 5500Å, there will be 3.3×10^{-5} erg/cc, but the fraction of molecules able to absorb in the laser line width is approximately 7×10^{-3} so the effective energy density is 2.33×10^{-7} erg/cc. We need 8.13×10^5 transitions/sec which means

$$N(v") = 8.13 \times 10^5 / (2.33 \times 10^7 \times 3.3 \times 10^7 \times .01) = 1.05 \times 10^7$$

molecules in the collision zone assuming a Franck-Condon Factor of .01 (a fairly strong transition). This number represents the steady state product molecule concentration necessary to provide the minimum number of transitions per second. With the molecules moving at 1.0×10^5 cm/sec, they will require about 1.5 lifetimes to move out of the photomultiplier viewing area. Therefore, the steady state concentration of molecules should be increased by 1.5 to 1.5×10^7 molecules/collision zone to ensure single excitation only. The size of the collision zone is $.092 \times .266 \times .414 = .010\ cm^3$ so we will need 1.48×10^9 molecules/cc in a given vibrational level for detection, which corresponds to a cross section of 3×10^{-3} $Å^2$.

Detection sensitivity would be improved if a pulsed laser were used and the photomultiplier could be gated such that it misses the scattered light but observes the product fluorescence. This technique would be particularly advantageous for longer lived molecules.

References

(1) M.A.D. Fluendy and K. P. Lawley, Chemical Applications of Molecular Beam Scattering (Chapman and Hall, London, 1973).

(2) J. G. Pruett and R. N. Zare, J. Chem. Phys., 64 1744 (1976).

(3) R. N. Zare and P. J. Dagdigian, Science, 185, 739 (1974).

(4) J. A. Silver, W. L. Dimpfl, J. H. Brophy, J. L. Kinsey, J. Chem. Phys., 65, 1811 (1976).

(5) A. E. Redpath, M. Menzinger and T. Carrington, Chem. Phys., 27, 409 (1978).

(6) R. L. Kroes, Appl. Optics, 12, 2075 (1973).

(7) J. B. Anderson, R. P. Andres and J. B. Fenn, Adv. in Chem. Phys. X, Chap. 8 (Wiley Interscience, New York, 1966).

(8) Optics Guide 1975, Melles Griot Co., 1770 Kettering St., Irvine, Ca. 92714.

(9) C31034 Photodetector Data Sheet, RCA, 1974.

(10) J. D. Winefordner, M. L. Parsons, J. M. Mansfield and W. J. McCarthy, Anal. Chem., 39, 436 (1967).

(11) G. Herzberg, Molecular Spectra and Molecular Structure Vol. I, (Van Nostrand Reinhold Co., New York, 1950).

Figure Captions

Fig. 1. Side view assembly cross-section of the laser fluorescence-chemiluminescence crossed molecular beam machine. The labeled parts are: (A) supersonic source nozzle; (B) skimmer; (C) beam flag; (D) tuning fork chopper; (E) source reducer (differential pumping wall), a spacer is shown between the reducer and the main chamber flange—this prevents the tuning fork from hitting the secondary beam source; (F) beam catcher; (G) secondary source (see Figure 3); (H) flange for electrical feedthroughs; (I) flanges to connect to the laser baffle arms; (J) and (J') flanges leading to the gate valves and oil diffusion pumps; (K) Cajon fittings for ionization gauges.

Fig. 2. Top view assembly cross section of the machine. Parts A-J are the same as listed for Figure 1. The other parts are: (H) flange for the optics detection system holder; (L) quartz plate sealing the optics system from the machine vacuum; (M) optics detection holder (see Figure 4); (N) anodized optics cover tube. The X marks the collision zone.

Fig. 3. Side view cross section of the secondary beam source. The labeled parts are: (A) stainless steel nozzle, hole diameter is .015 inch; (B) copper plating on the nozzle tube for thermal conduction; (C) alignment piece (screws into the source flange); (D) black painted radiation shield; (E) clamp part of the copper heating and cooling block, holds the

nozzle in place; (F) holes in the copper block in which fit alumina rods containing nichrome heating wire; (G) liquid nitrogen feed tube that is hard soldered to the copper block; (H) conflat flange connecting the feed tube to a flange that then connects to a liquid nitrogen reservoir (this connection also holds the copper block clamp in line with the Cajon fitting that serves as the nozzle tube feedthrough); (I) Cajon fitting that seals the nozzle tube against the machine vacuum.

Fig. 4. Side view assembly cross section of the lens system. The labeled parts are: (A) quartz plate that seals the optics from the machine vacuum; (B) first lens (75mm focal length, 50mm diameter); (C) second lens (200mm f.l., 50mm diameter;) (D) optical rail lens carriers; (E) adjustable iris; (F) x-y translation stage for final positioning (optimization) of the iris; (G) third lens (2-5/8 inch f.l., 2 inch diameter); (H) fourth lens, a cylindrical lens (6 inch f.l., 1 inch diameter); (I) optics rail lens carrier; (J) optical rail; (K) optics system holder (M, Figure 2); (L) anodized optics cover tube (N, Figure 2). All the lenses are quartz, see Figure 6 for a transmission curve. Figure 5 gives a close-up of the lens holders that attach to the rail carriers (D) and (I). The cover tube attached to the optics holder via a key and also has a key on the other end.

Fig. 5. Close-up schematic of a lens holder showing the side (A), face-on (B) and top (C) views. View A shows the key in which the lens sits and the retaining ring that holds the lens in place. View (C) shows the screw holes for coupling the lens holder to the rail carrier.

Fig. 6. Transmission curve as a function of wavelength for the quartz lenses 1 and 2. The other lenses extend to 160nm in the UV, but otherwise have the same curve.

Fig. 7. Schematic of the signal processing. Beam 1 is the supersonic beam, beam 2 the quasi-effusive or effusive beam. The gate is used to correlate the signal with the chopper on beam 1, providing automatic background subtraction.

Fig. 8. Cross section of the laser baffle arm. The labeled parts are: (A) quartz Brewster angle window with Wood's horn (the inside of the glass is painted black); (B) aluminum support for alignment cross hairs (see text), this support clamps onto the Cajon fitting that seals the Brewster angle window against the atmosphere; (C) one of four aluminum baffle holes; (D) stainless steel baffle ring holder; (E) anodized aluminum baffle hole spacer; (F) retaining ring that holds the baffle rings and spacers in position in the tube.

Fig. 9. Schematic of the laser alignment mirror set-up. M1 and M2 are mirrors held in Burleigh mounts for the laser beam positioning. The 1000 mm f.l. quartz lens focusses the beam near, but not at, the collision zone. The purpose of this

lens is to reduce scattered light in the baffle arms. The cross hairs are supported by the aluminum supports (B) of Figure 8. The dashed line shows the path of laser light reflected off the Brewster angle window into a spectrometer where the laser wavelength and power can be monitored.

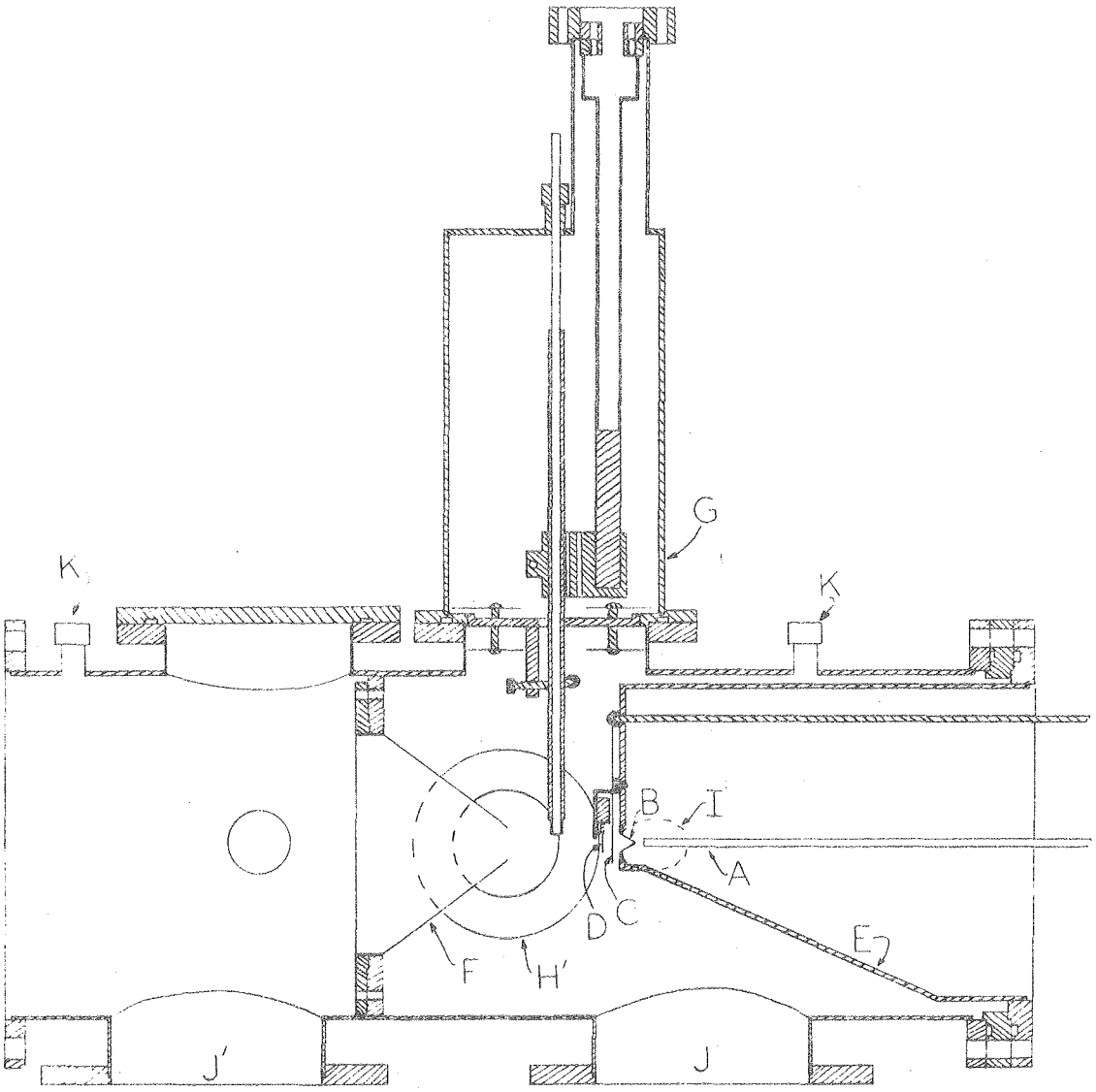

XBL 801-7847

Figure 1

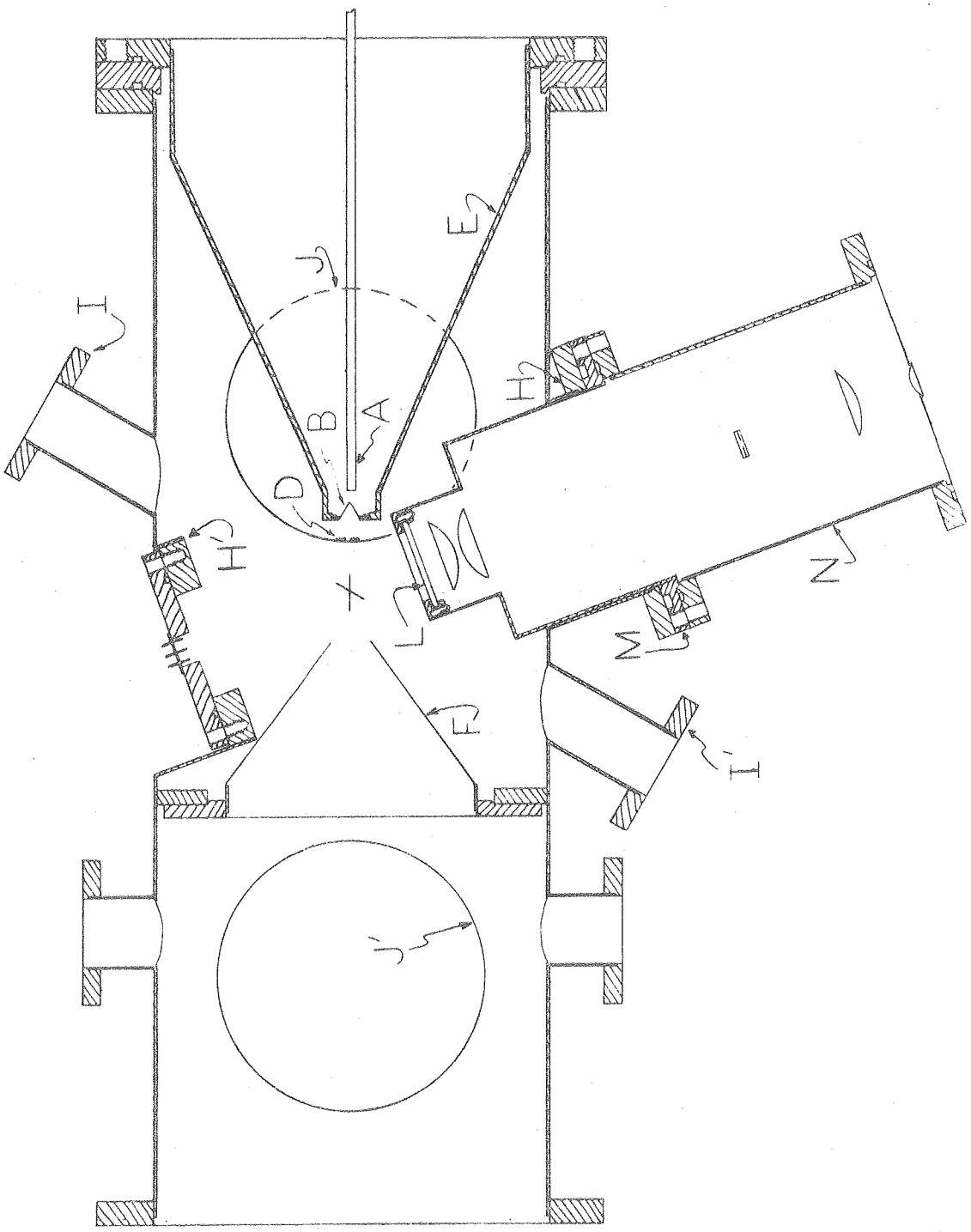

XBL 801-7849

Figure 2

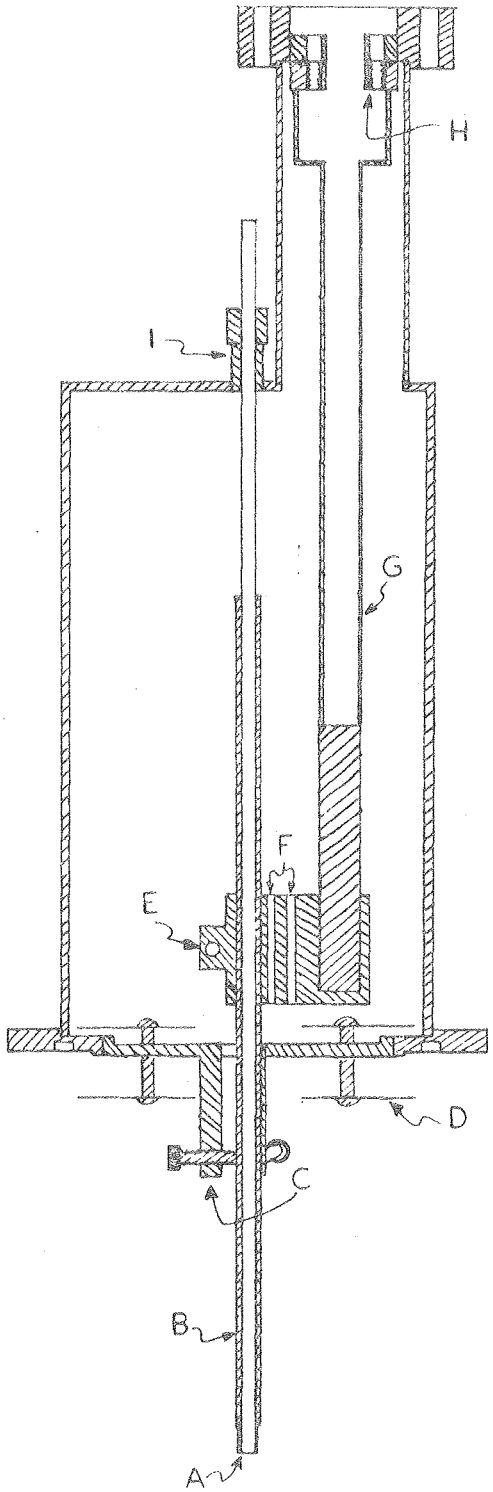

XBL 801-7848

Figure 3

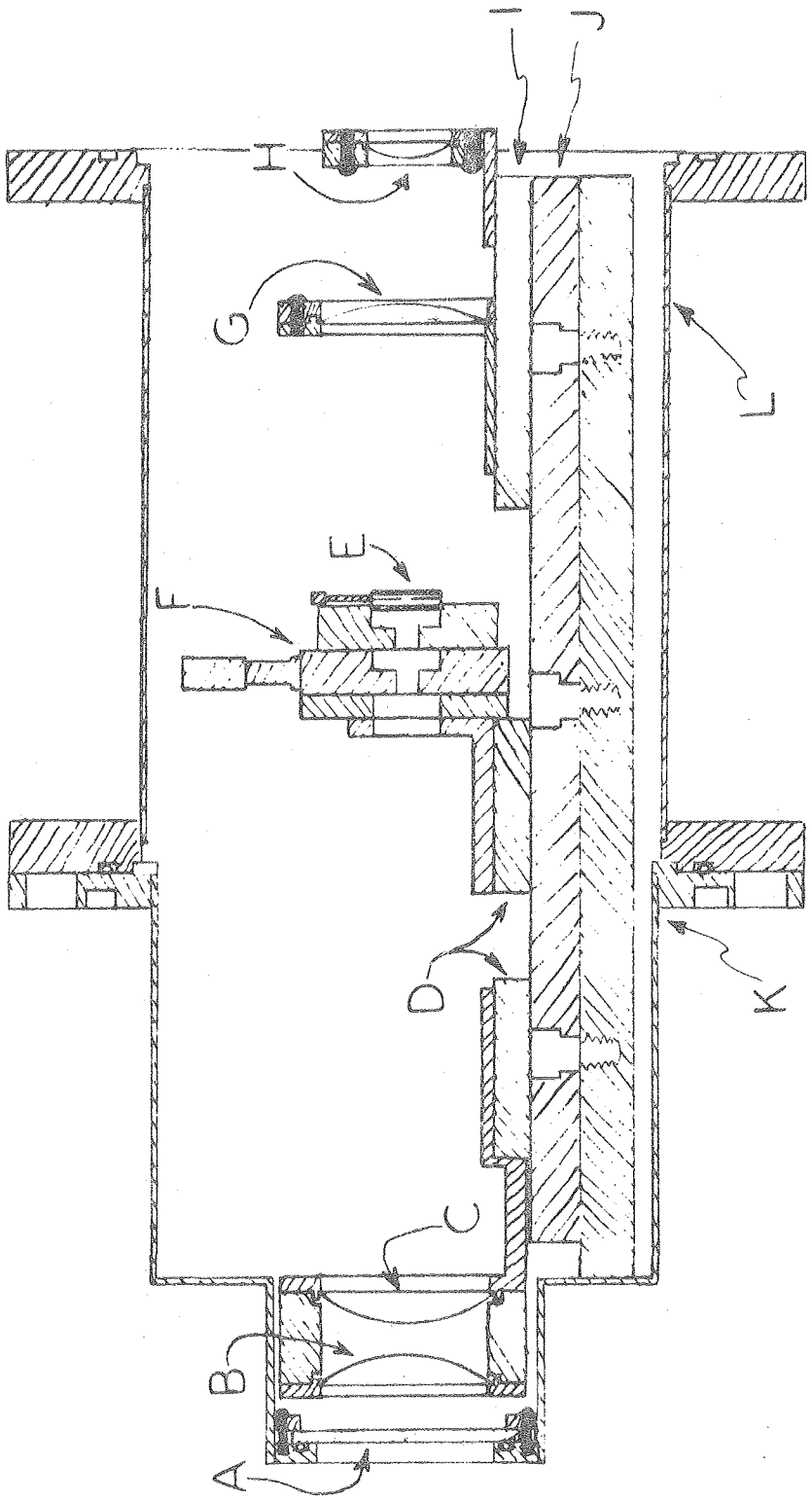

XBL 801-7852

Figure 4

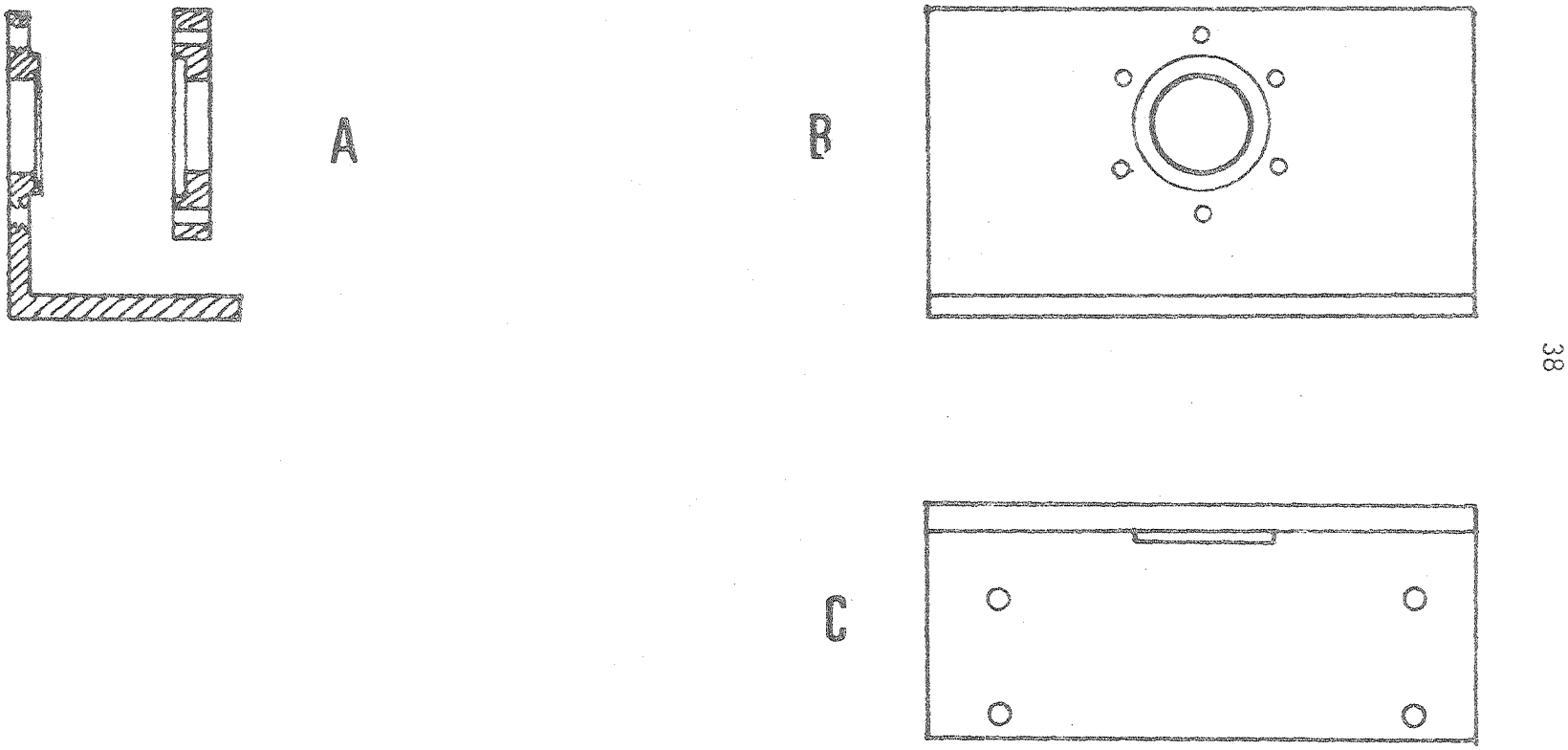

Figure 5

XBL 801-7861

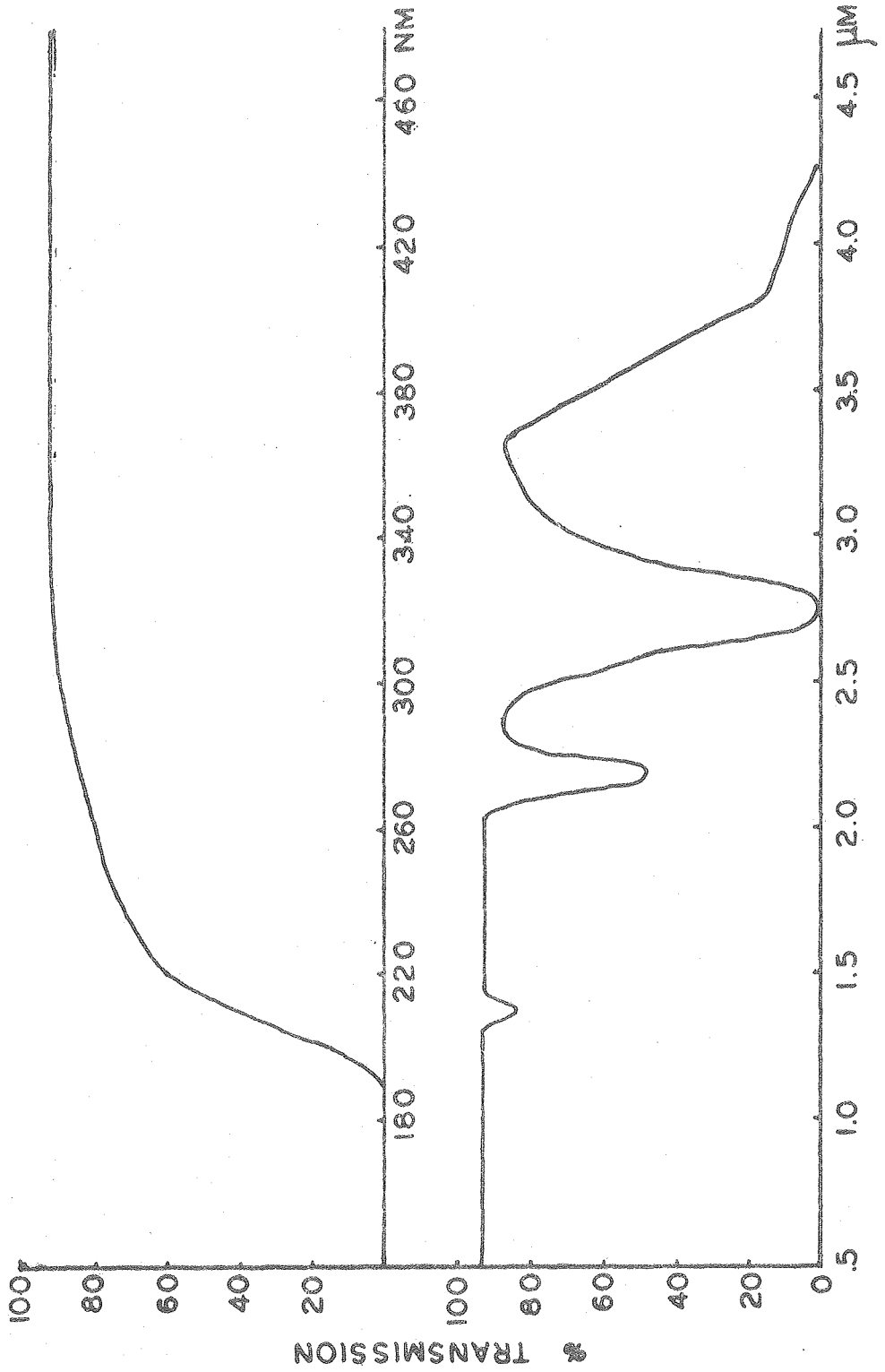

XBL 801-7867

Figure 6

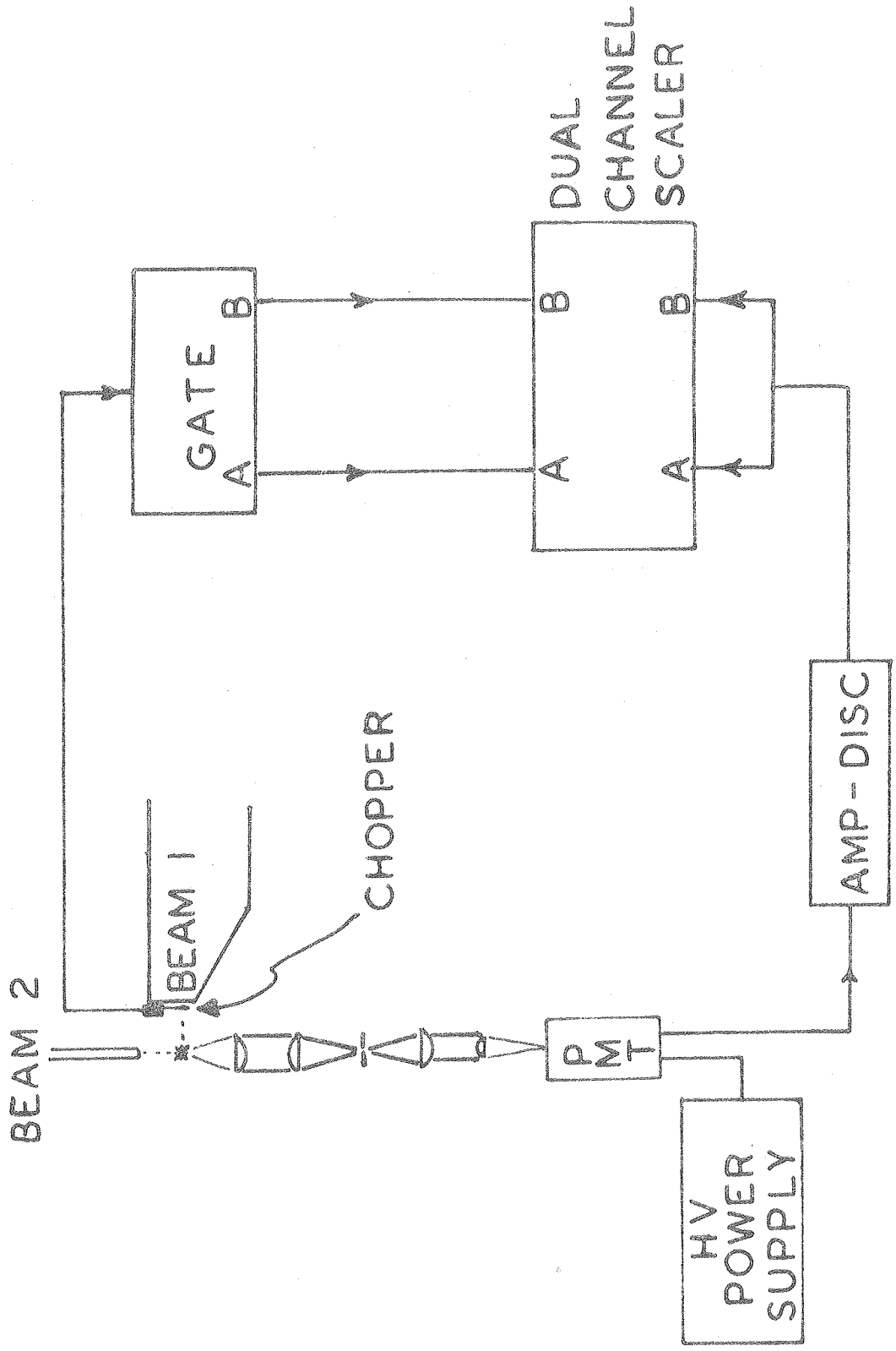

XBL 801-7859

Figure 7

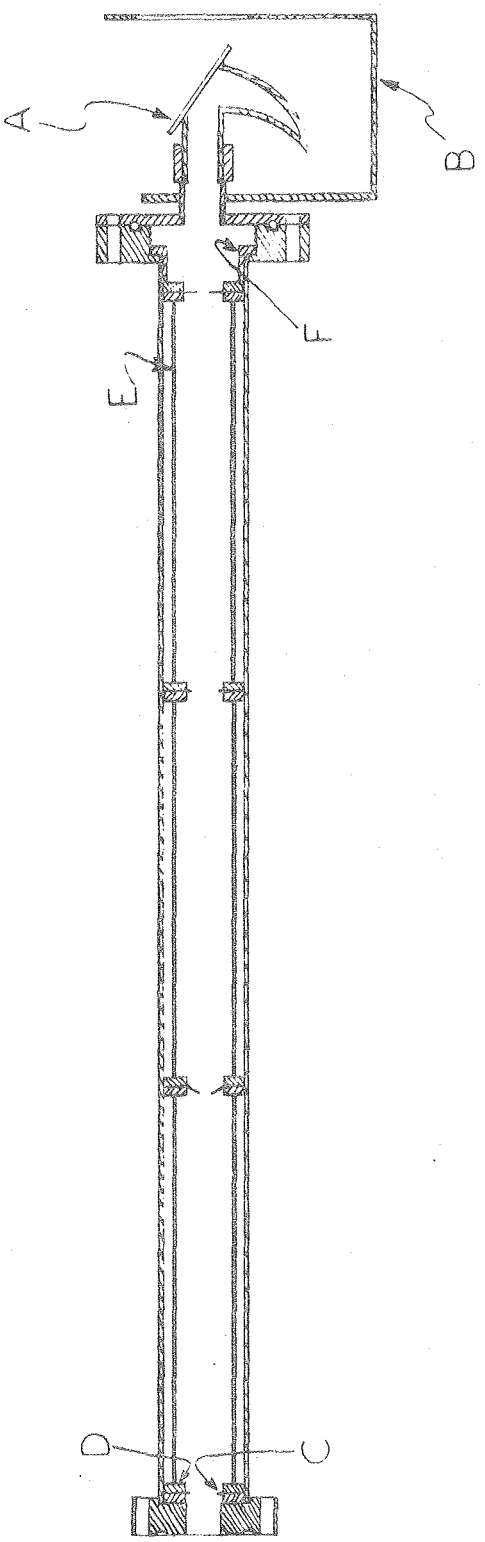

XBL 801-7851

Figure 8

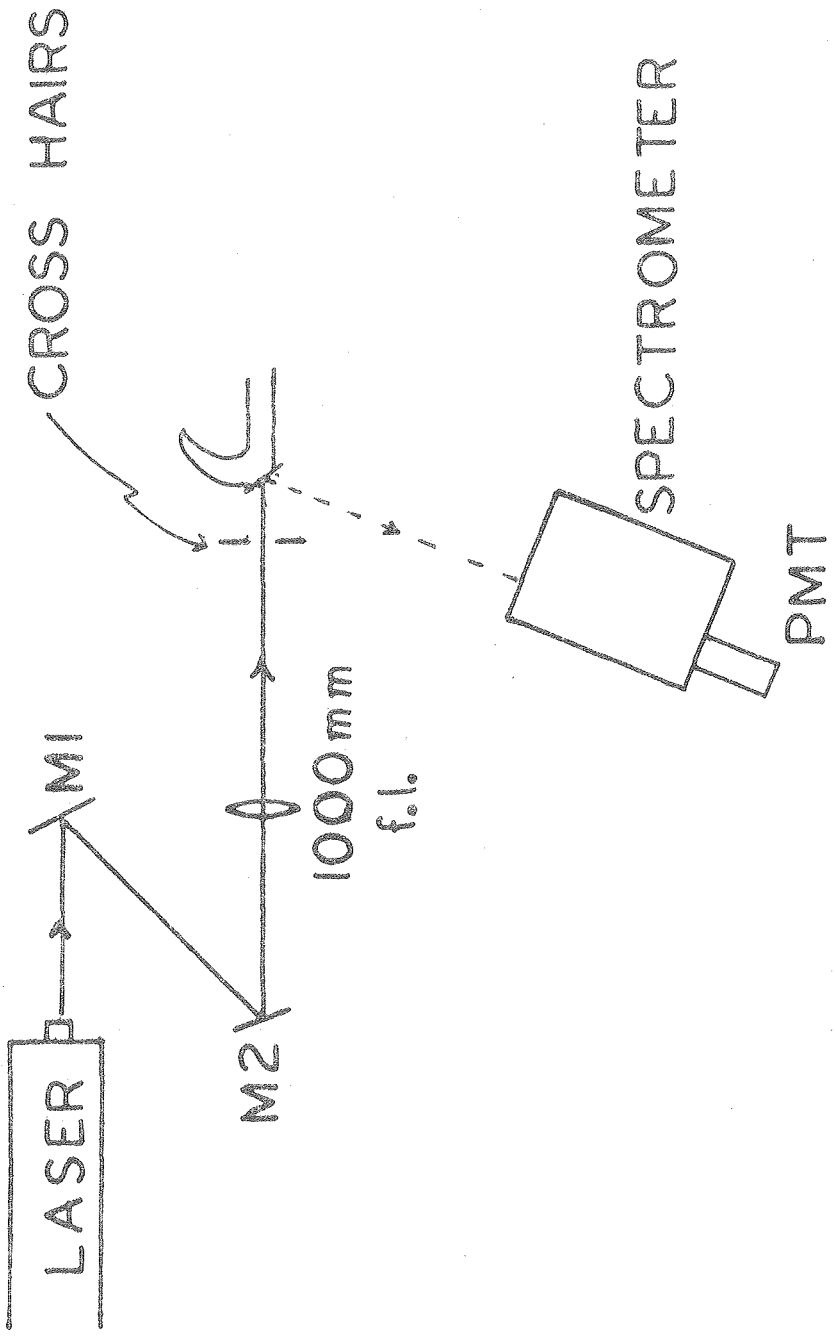

XBL 801-7858

Figure 9

III. A STUDY OF CHEMILUMINESCENT HALOGEN - HALOGEN REACTIONS

A. Introduction

It has been known for a number of years that reaction rates are not determined by energetics alone. Steric hinderance, for example, is a very important consideration in reactions involving molecules with bulky constituents. Another factor, discussed by Woodward and Hoffman,[1] is the requirement that orbital symmetry be conserved in concerted reactions. A concerted process is symmetry allowed if the occupied molecular orbitals of the reactants continually maintain their symmetry while undergoing transformation into the occupied molecular orbitals of the products. If the orbital symmetry cannot be maintained, then the reaction is symmetry forbidden and a high reaction barrier is predicted. The symmetry conservation requirement holds only for concerted reactions, reactions proceeding via a two or multi-step process are not subject to these rules.

Four center reactions provide an example of symmetry forbidden reactions. The molecular orbital diagram is shown in Figure 1 for the reaction of $I_2 + F_2 \rightarrow 2IF$. Two of the occupied molecular orbitals of the products correlate with excited product molecular orbitals, implying that four reactant electrons would have to be excited to give ground state products and that therefore this reaction should have a high barrier. This diagram assumes a C_{2V} transition state. While other transition state symmetries are possible, those that are consistent with a concerted mechanism are likewise forbidden.

Halogen-halogen reactions have been studied by several groups to test the idea of symmetry forbidden four center reactions. A crossed molecular beam study of $Br_2 + Cl_2$ showed no evidence of BrCl production up to 30 kcal/mole collision energy, in support of the forbidden four center reaction theory.[2] Another study, by Birks, Gabelnick and Johnston,[3] involved the reaction of $I_2 + F_2$ at low pressure and room temperature in a flow apparatus. The chemiluminescence from the reaction, in the 450-750mm range, was identified as $IF(B^3\Pi_{0^+} \rightarrow X\ \Sigma_0^{1+})$ and $IF(A^3\Pi_1 \rightarrow X\Sigma_0^{1+})$ and was found to be linear in I_2 pressure. A thorough investigation of the F_2 dependence was not done although it was found that the chemiluminescence increased with increasing F_2. Birks et al. offered two mechanisms as possible explanations for their results; an atom recombination or a four center reaction. Both mechanisms would be sufficiently exoergic to allow one electronically excited IF to be formed, but the four center mechanism was favored as being in better agreement with the pressure dependence results. Another crossed beam study, done by Valentini, Coggiola and Lee[4] of the reaction of F_2 with I_2, ICl and HI again provided evidence against a four center reaction mechanism. In the reaction of I_2 and F_2, a stable trihalogen, I_2F, was observed above a threshold collision energy of 4.0 kcal/mole with IF appearing above a collision energy of 6.1 kcal/mole. The IF product angular distribution did not have the backward-forward symmetry that would be expected if it were produced via a four center reaction mechanism. Similar results were obtained

for F_2 + ICl, with a threshold of 6.0 kcal/mole for ClIF and 20.1 kcal/mole for IF production. In the case of F_2 + HI, a threshold of 11 kcal/mole for HIF production was observed but the collision energies used were not sufficiently high to see IF. The conclusion reached by Valentini et al. was that there was no four center reaction occuring but that a stable trihalogen was formed and the light observed by Birks et al. was due to subsequent reaction of the trihalogen with a fluorine atom. The IF produced in the crossed beam reactions was attributed to unimolecular decomposition of the highly excited trihalogen intermediates.

In an effort to further understand the mechanism of chemiluminescence production in the halogen-halogen reactions, we have studied the reactions of F_2 with I_2, ICl and Br_2 using the crossed molecular beam method coupled with photon detection. Our results provide a connection between those of Valentini et al. and Birks et al. and suggest an explanation of the chemiluminescence at low activation energies.

B. Experimental

The reactions were studied using the chemiluminescence-laser fluorescence crossed molecular beam machine described in Chapter II. The F_2 beam was produced by a supersonic expansion using the halogen nozzle beam source described in detail in reference 5. The source consists of a resistance heated nickle nozzle with a .003 inch (.008 cm) diameter hole. The nozzle temperatures used in this experiment were between 300 and 700°K, well below the temperature at

which fluorine atom production becomes significant. The temperature was monitored using a chromel: alumel thermocouple spot welded to the tip of the nozzle. The change in nozzle temperature provided a means of fine controlling the collision energy of the reactants, the coarse control is provided by varying the seeding ratio of the fluorine in various rare gases.(6)

In mixing a heavy gas with a light gas, both types of molecules move, after the supersonic expansion, at a velocity appropriate to the mean mass of the mixture. By mixing fluorine to a few percent in helium, then, the fluorine molecules will travel much faster than they would have in a pure fluorine supersonic beam. The velocity of the heavy particles in a seeded beam is given by

$$\frac{1}{2} m_H v_H = \frac{m_H}{\bar{m}} \int_{T_B}^{T_o} \bar{C}_p dT$$

where T_o is the nozzle temperature, T_B is the temperature of the beam after expansion (which may be considered to be 0°K for many applications), $\bar{C}_p$ and $\bar{m}$ are the mean heat capacity and mass of the mixture. This equation also indicates the effect of nozzle temperature on the mean velocity of the beam.

Three gas mixtures were used in these experiments; 1 percent F_2 in He, 7 percent in He/Ar and 10 percent in Ar, to cover a collision energy range of 3 - 24 kcal/mole. These mixtures were either obtained commercially or mixed in this laboratory. The pressure behind the nozzle, approximately 600 torr, was measured using a Baratron. The

gas line to the nozzle was made entirely of stainless steel and included a needle valve and metering valve to control the pressure. The source was assembled as shown in Figures 1 and 2 of Chapter II, with a .030 inch diameter skimmer placed .229 inches in front of the nozzle and a tuning fork mounted in front of the skimmer to chop the F_2 beam. The distance from the nozzle to the collision zone was 2.69 inches.

The I_2, ICl and Br_2 beams were produced as quasi-effusive beams with Mach numbers of 3-4. These beams were run at approximately 1 torr pressure and were not seeded. The beam source used was described in Chapter II (see Figure 3). A special attachment was used on the nozzle for all three reactions, it clamped on the nozzle and supported a .070 inch diameter skimmer placed .200 inch in front of the nozzle. The skimmer provided some spatial definition for the beam and was important in narrowing the collision energy distribution for the threshold determinations (see Chapter V). The distance from the nozzle to the collision zone was .56 inch (1.42 cm). The I_2 (Mallinckrodt Analytical Reagent, resublimed crystals, 99.9 percent pure) reservoir was a round bottomed pyrex flask kept at approximately 80°C in an oil bath. The stainless steel gas lines were heated, using heating tape, to 120°C and the nozzle to 125°C to prevent I_2 condensation. The same conditions were used for Br_2 (Baker Analyzed Reagent, 99.9 percent pure) except that the bromine reservoir was kept at 0°C in an ice bath and a needle valve was used for pressure control. Because ICl decomposes above 100°C, measurements were made with both a heated and room temperature gas line and nozzle. No

difference was observed either in the chemiluminescence signal or when the ICl beam was monitored using a quadrupole mass spectrometer. The ICl (Research Organic/Inorganic Chemicals, 99.5 percent pure) reservoir was kept at 0°C in an ice bath and required no other pressure control valves.

The velocity distributions for all the beams, at different temperature and seeding ratios for F_2, were measured using the time-of-flight technique.[7] The distributions, flux and Mach numbers for the beams were obtained from the data using programs KELVIN and FLUX described in reference 5. Sample velocity flux distributions for the supersonic fluorine beam and quasi-effusive iodine beam are shown in Figures 2 and 3, respectively. The distributions of relative velocities for the beams were calculated using program CELUM described in Chapter V of this dissertation. A sample collision energy distribution, calculated from the relative velocity distribution, is given in Figure 4.

The experimental set up is shown in Figures 1 and 2 of Chapter II. The two molecular beams cross at 90° in the collision zone and the light produced in the reaction is collected and focussed onto a photomultiplier, as described, again, in Chapter II. The light from the reactions was measured using photon counting techniques, the counting period was 200 seconds with a millisecond gate width. For each gas pair, the room temperature data point was used as a normalization point and was measured first and last during each run. In no case were the two room temperature points in disagreement, within experimental error. Each data point represents the average of

approximately seven 200 second counts. The pressure in the main chamber of the machine was monitored using an ion gage and used to adjust the signal for fluctuations in I_2 pressure due to the slow response of the I_2 heater thermostat. Light from the reactions was measured as a function of collision energy; the $I_2 + F_2$ chemiluminescence was also measured as a function of F_2 pressure and I_2 pressure, the latter being changed by changing the heater setting of the reservoir. The $ICl + F_2$ data was checked for interference by any I_2 impurity in the ICl by measuring the chemiluminescence signal with the I_2 reservoir at 0°C. No signal was seen at this low I_2 pressure, so the light observed in the $ICl + F_2$ reaction was due just to ICl, not I_2. Chemiluminescence from a $Cl_2 + F_2$ reaction would not be allowed energetically. All threshold determinations are the result of two separate experiments.

An attempt was made to obtain a spectrum of the chemiluminescence observed. The spectrometer described in Chapter II was aligned with the machine and three methods were used in attempting to record the spectrum of $I_2 + F_2$, (1 percent in He), at high collision energies, the strongest of the three reactions. First, the photomultiplier was attached to the photographic exit of the spectrometer and the spectral range of 6040Å - 9180Å was scanned. The photomultiplier output was recorded using an electrometer coupled to a chart recorder. Detecting no spectrum using this method, the photomultiplier was used in a photon counting mode, again without success. Finally, a camera was attached to the photographic exit and, using Polaroid land film type 57 high speed, the film was exposed for

one hour at 5500Å and 6500Å. No spectrum was observed due to insufficient chemiluminescent yield; both the A ⇒ X and B ⇒ X transitions are in the wavelength range observed.[3] Since the $I_2 + F_2$ is the strongest reaction, no attempt was made to record the spectrum of the other two reactions.

C. Results and Analysis

In each of the three reactions studied, $F_2 + I_2$, ICl and Br_2, chemiluminescence was observed, although the intensity was too low to obtain a spectrum. Without a spectrum, positive identification of the emitting species cannot be made although the possibilities are limited; we can only be forming excited diatomics or triatomics. The photomultiplier used (RCA C31034), can detect light only in the 200-900nm range, so we were not detecting single quantum vibrational transitions of the diatomic[8] or triatomic[9,10] halogens. There is insufficient collision energy to enable electronic excitation of the reactant diatomic halogens.[8] Because both beams must be running for light to be observed, emission from hot F_2 can also be excluded. Using Valentini et al.'s value for the threshold of I_2F (F_2I was not seen) and ClIF, the formation of an electronically or highly vibrationally excited trihalogen is likewise energetically inaccessible. We are, therefore, limited to considering the formation of a highly vibrationally excited or electroncally excited diatomic in the reaction. The multiple quantum vibrational transition required to produce light in the 200-900nm range would not only be very improbable, but would also have such a long lifetime that we would be

unable to see it with our experimental arrangement. Therefore, the light must be coming from an electronically excited diatomic reaction product like IF, ClF or BrF.

The chemiluminescence of the $I_2 + F_2$ reaction was measured as a function of I_2 pressure (Figure 5) and F_2 pressure (Figure 6). The signal was linear with respect to I_2 pressure, with the counts going to zero as the I_2 pressure goes to zero. The signal was likewise linear in F_2 pressure although the line does not go through zero as the F_2 pressure goes to zero. The reason for the non-zero intercept is that the F_2 source is a supersonic source and as the pressure behind the nozzle is reduced, the source eventually undergoes a transition from supersonic flow to effusive flow.[11] In this transition region, the beam intensity in the collision zone is no longer proportional to nozzle pressure.

The linearity of the signal with respect to both I_2 and F_2 pressure, coupled with the fact that the signal is correlated with the chopped F_2 beam, means that the reaction is the result of a single bimolecular collision between I_2 and the F_2 beam. This excludes several possibilities, specifically:

1) Any mechanism that would require background F_2 or F atoms. Because the signal is correlated with the chopped F_2 beam, we know that the chemiluminescence is the result of a reaction of the beam F_2 molecules. If a reaction with background F or F_2 was also required, the chemiluminescence would have a quadratic dependence on F_2 pressure.

2) Any mechanism requiring more than one collision, this would give a higher than linear dependence on either I_2 or F_2 pressure.

3) Any mechanism involving I atoms. A reaction of F_2 with I atoms is not sufficiently exoergic to produce electronically excited IF, the exclusion of possibilities (1) and (2) above removes any atom recombination mechanism.

4) Any mechanism involving I_2 or F_2 dimers, this would give a quadratic pressure dependence on I_2 or F_2 pressures. The chemiluminescent reaction is the result of a collision between one I_2 and one F_2 molecule. A four center reaction cannot, therefore, be excluded. A pressure dependence study of the other two reactions was not made.

The chemiluminescence signal was measured as a function of collision energy for all three reactions. The velocity distributions of the three quasi-effusive beams (I_2, Br_2 and ICl) and of the supersonic fluorine beams (1 percent/He, 10 percent/Ar, 7 percent/Ar and He, each at the three nozzle temperatures) were measured and converted to relative velocity distributions using program CELUM described in Chapter V. This program takes the angular spread (and therefore the collision angle distribution) into account, as well, in calculating the relative velocity distribution. The distribution for the nozzle temperature at which data were recorded was interpolated from the distributions measured at the three temperatures. Program LUMFIT, also described in Chapter V, uses a functional form of the reaction cross section to calculate the chemiluminecence signal from

the relative velocity distribution. The cross section function is then varied until the calculated signal fits the experimental signal, within experimental error. A cross section weighted mean of the collision energy distribution can then be calculated.

In fitting the threshold data for $I_2 + F_2$, a cross section of the form $\sigma = C(1 - (E_T/E))^{.5}$ was used where E_T is the threshold energy, E is the collision energy and C is a normalization constant. The result is shown in Figure 7 where the collision energy axis represents the cross section weighted mean collision energy. E_T is 3.4 kcal/mole and is the threshold collision energy; this does not include internal energy. The amount of energy in the internal degeees of freedom can be calculated assuming thermal equilibrium. In both the supersonic and quasi-effusive molecular beams there is a certain amount of cooling in the internal degrees of freedom as well as in the translational degree of freedom. Because vibrational spacings are generally large with respect to kT over our temperature range (300-700°K), little vibration ⇏ translation energy transfer occurs and the vibrational temperature remains at the nozzle temperature. Rotational spacings are generally small and energy transfer is efficient so the rotational temperature and translational temperature are close to equal. The translational temperature, T_o, can be calculated from

$$T_o/T_n = (1 + (RM^2/2C_V))^{-1}$$

where M is the Mach number (which is calculated in program KELVIN[5]), and T_n is the nozzle temperature.[2] Table I lists

the temperatures and internal energy associated with vibration and rotation, along with the Mach numbers, for the beams used in this experiment. For the temperature corresponding to threshold in the $I_2 + F_2$ reaction, the internal energy was .8 kcal/mole so the total threshold energy was 4.2 kcal/mole.

We can make no distinction, in this experiment, between the effects of translational and internal energy. We are assuming that the three forms of energy available are equally effective in promoting the reaction, although this assumption is not necessarily true in general.[13,14] All the thresholds occurred near the room temperature end of the collision energy ranges for the various mixtures, so there should be little contribution from the supersonic beam's internal energy. Most of the internal energy comes from the quasi-effusive source and, again, may or may not contribute equally with translational energy.

The higher energy data for $I_2 + F_2$ was fit using a cross section of the form $\sigma = C\left((E/E_T) - 1\right)^A$. While the threshold cross section function is derived from scattering theory,[15] this higher energy form has no physical significance and was only used to derive a cross section weighted mean collision energy. The $I_2 + F_2$ data for the entire collision energy range studied is shown in Figure 8. The parameters used in fitting the data were $E_T = 1.0$ kcal/mole, $A = 4.95$.

The threshold cross section function was used again in the analysis of the $ICl + F_2$ data, shown in Figure 9. The threshold collision energy, E_T, is 5.1 kcal/mole, the internal energy at the

temperature corresponding to that point is .8 kcal/mole bringing the threshold energy for the reaction 5.9 kcal/mole. The $ICl + F_2$ reaction was not studied at higher energies.

The data for the $Br_2 + F_2$ reaction, shown in Figure 10, presented special problems in analysis. Looking at the $I_2 + F_2$ data in Figure 8, as the collision energy increases past approximately 5 kcal/mole the chemiluminescence starts to level off. The same phenomenon was observed by Valentini et al.[4] for I_2 F. In the case of $Br_2 + F_2$, the leveling-off and decrease in chemiluminescence with increasing collision energy occurs very shortly after the reaction threshold. The experimental points may be fit to a cross section function, as before, but the cross section weighted mean collision energy calculated from such a fit does not provide a linear translational energy scale for a graph. On the low energy side of the chemiluminescence curve, the high energy tail of the collision energy distribution is given more weight while the opposite is true of the high energy part of the chemiluminescence curve. For this reason, the translational energy scale for the $Br_2 + F_2$ data was determined in two steps. The threshold, low energy part of the curve was placed, as for the other curves, on a cross section weighted mean collision energy axis. The cross section function used was a quadratic equation with no physical significance. The threshold collision energy is 10.7 kcal/mole, the internal energy is .6 kcal/mole for a total threshold energy of 11.3 kcal/mole for $Br_2 + F_2$. The rest of the collision energy axis was taken from the high energy $I_2 + F_2$

results because I_2 + 1 percent F_2/He has a collision energy distribution almost identical to that of Br_2 + 1 percent F_2/He, which was the mixture used to obtain this data. Therefore, while the energies near the threshold of the reactions represent cross section weighted mean collision energies for the reaction of Br_2 with F_2, the rest of the energy axis does not represent the true mean energy for this reaction, although the difference is not large.

To summarize the results, light was seen in each of the three reactions and is attributed to the formation of electronically excited diatomic products, IF, ClF and BrF. The thresholds for the chemiluminescent reactions are 4.2 kcal/mole for I_2 + F_2, 5.9 kcal/mole for ICl + F_2 and 11.3 kcal/mole for Br_2 + F_2. In the case of I_2 + F_2 and Br_2 + F_2, a leveling off or actual decrease in chemiluminescence with increasing collision energy was observed.

D. Discussion

While our data on the pressure dependence of the chemiluminescence is consistent with a bimolecular reaction, the energy dependence of the light production indicates another mechanism, other than a four center reaction, may be responsible. The energetics for the three reactions are shown in Figure 11, included are the energy levels for the stable trihalogens observed by Valentini et al. In the case of I_2 + F_2, our chemiluminescence threshold of 4.2 kcal/mole agrees very well with Valentini's threshold of 4.0 kcal/mole for I_2F formation. A four center reaction of I_2 with F_2 to produce either

IF(B) + IF or IF(A) + IF, on the other hand, would either be exoergic by 6-16 kilocalories with no reaction threshold or, if the predicted barrier for the symmetry forbidden four center reaction exists, the threshold would almost certainly be higher than 4.2 kcal/mole. The reaction of I_2F with F is also exoergic enough to produce one electronically excited IF in the A or B state. Another similarity between our chemiluminescence results and Valentini's trihalogen results is the leveling off of the chemiluminescence after approximately 6 kcal/mole collision energy, which Valentini attributed to the unimolecular decomposition of I_2F. While a leveling off of the chemiluminescence might be expected for a four center reaction as well, our "threshold" for this leveling off agrees well with Valentini's for I_2F.

The agreement between our results and Valentini's suggests that the mechanism shown in Figure 12 involving the formation of the trihalogen, I_2F, and subsequent reaction of the end iodine with the departing fluorine atom may be responsible for the light we see. The pressure dependence studies restrict the chemiluminescent reaction to a single collision mechanism, so we propose that the two step reaction of $I_2 + F_2 \rightarrow I_2F + F$, $I_2F + F \rightarrow IF^* + IF$ may occur in a "single collision" between F_2 and I_2. In the vast majority of collisions occurring above threshold in the collision zone, the I_2 and F_2 would react to form I_2F and F, the products would separate and be detected by Valentini but not by us. In a few of the collisions, the I_2 and F_2 react to form I_2F but the F atom does not escape before a secondary encounter occurs giving the second step, $I_2F + F \rightarrow IF^* + IF$ and we detect the light from the IF^*. We have, then,

a branched reaction—the major branch gives I_2F and the minor branch results in electronically excited IF. This mechanism brings up several questions: why couldn't Valentini et al. see the minor branch, how does this differ from a four center reaction, does this explain the results obtained by Birks et al.[3] and does the same mechanism hold for the other reactions studied?

Using the following equation:

$$\sigma = S/(v\ N_{I_2}\ N_{F_2})$$

we can calculate, from our data, the cross section for the production of IF^* from $I_2 + F_2$. In the equation, v is the relative velocity of the products and is 1.38×10^5 cm/sec at 15 kcal/mole collision energy. S is the chemiluminescence signal, which is 1.19×10^7 at 15 kcal/mole (corrected for loss due to optics transmission, f number of the collecting optics, photomultiplier efficiency and loss of IF^* due to diffusion out of the collision zone before emission).[16] Using $N_{I_2} \cong 1.4 \times 10^{10}$ molecules/cc, we calculate a cross section, σ, of $.002\text{Å}^2$. This cross section is much smaller than the $1\text{-}2\text{Å}^2$ cross section that Valentini saw for the major reaction branch. About one in one thousand collisions results in the fluorine atom having a secondary encounter with the I_2F and producing IF^*. A $.002\text{Å}^2$ reaction cross section would have been too small for Valentini to see, especially because there was IF production from unimolecular decomposition of I_2F as well as from

fragmentation of I_2F in the detector ionizer. There are two factors that greatly enhance our detection sensitivity over that of Valentini's; photon background signal is much easier to reduce (in this case) than particle background signal and we were collecting total chemiluminescence (i.e., looking at the integrated cross section) while Valentini was looking at a differential cross section. It is not surprising, then, that Valentini did not see the symmetric IF production that would be expected for the minor reaction branch.

The factor that separates the mechanism we are proposing from a four center reaction mechanism is the stability of the trihalogen formed. As pointed out in the introduction to this chapter, the symmetry rules that forbid four center reactions require that the reaction be concerted—that the old bonds be broken at the same time as the new bonds are made. In the mechanism we propose, a stable trihalogen is formed first and, in most collisions, it is the final product. In the other collisions, the stability of the trihalogen drives the reaction to begin with, then a second reaction occurs, precluding a separation of the first reaction's products. Because we cannot measure angular distributions and the minor reaction path was too small to be seen by Valentini, we can make no estimate of the lifetime of the $I_2F...F$ complex and do not know if it lasts as long as one rotational period, although we expect it to be shorter.

The results presented here provide greater support for the suggestion[4] that the chemiluminescence seen by Birks et al. is a result of the reaction of I_2F with F. In our study of the reaction,

the light was produced from a single collision and was a low probability event. In the flow system used by Birks, many collisions will take place so the I_2F formed is not restricted to reacting with its "own" fluorine atom. Given the following elementary reactions:

$$I_2 + F_2 \xrightarrow{k_1} I_2F + F \tag{1}$$

$$I_2F + F \xrightarrow{k_2} IF^* + IF \tag{2}$$

$$IF^* \xrightarrow{k_r} IF + h\nu \tag{3}$$

$$IF^* + M \xrightarrow{k_q} IF + M \tag{4}$$

$$I_2 + F \xrightarrow{k_4} IF + I \tag{5}$$

$$I + F_2 \xrightarrow{k_5} IF + F \tag{6}$$

and assuming steady state for I and F atoms we get

$$[IF^*] = k_1[I_2]\,[F_2]/(k_r + k_Q[M]) \tag{7}$$

This is the same expression for the excited IF concentration as is obtained assuming a four center reaction and accurately describes Birk's data.

While it is impossible to make such a clear case for the reactions of ICl and Br_2 with F_2, the data we obtained is consistent with this mechanism. For ICl + F_2, we obtained a threshold of 5.9 kcal/mole while Valentini saw a threshold of 6.0 kcal/mole for ClIF production. The agreement is very good but, looking at Figure 11, a four center reaction producing IF(A) + ClF would have nearly the same endoergicity. The spectrum of ClF(A→X) has not yet been observed[8] although it is expected to be higher in energy and would not be helpful in distinguishing a four center threshold from a ClIF threshold. While Valentini observed the leveling off of ClIF production with increasing collision energy, our data does not extend to a high enough energy to check for the same effect in the chemiluminescence.

Valentini was unable to see formation of Br_2F, although that may be a detection sensitivity problem rather than an indication that Br_2F is not formed. If the mechanism works for Br_2 + F_2 as well, then the rapid leveling off and decrease of chemiluminescence indicates that Br_2F does not have as high a stability as I_2F and ClIF have. Our reaction threshold for Br_2 + F_2 was 11.3 kcal/mole. Figure 11 shows the levels for BrF(A) + BrF and BrF(B) + BrF production to be 13.8 and 16.3 kcal/mole, respectively. At first glance it would seem that we are not observing BrF^* emission, that it would be energetically inaccessible. The 13.8 kcal/mole level indicated for BrF(A) was derived from only a few A→X transitions that, most likely, did not even form a complete progression.[17,18] Recent work[19]

on the BrF(B→X) transition has provided new information on the dissociation energy for BrF that would be inconsistent with the previous assignments for the BrF(A→X) lines, making the 13.8 kcal/mole level even more suspect. Table II lists the ν_{oo} energies (in kcal/mole) for the B→X and A→X transitions of several dihalogens. The values in parentheses are uncertain. From the trends in the iodine and bromine series, it is certainly possible that the BrF(A) level could be 3 kcal/mole lower than the 13.8 kcal/mole above $Br_2 + F_2$. It would be helpful to have more spectroscopic data about both the BrF(A) and ClF(A) states.

One final question is whether the proposed mechanism is consistent with formation of IF in the $A^3\Pi_1$ and $^3\Pi_0^+$ states. In other words, do the product electronic states correlate with the reactant electronic states The first step is to determine what the electronic term symbol for the reactant I_2F is and then determine in what electronic states the I and IF fragments are formed. All three of the final product electronic states we are concerned with, IF($X^1\Sigma_0^+$, $A^3\Pi_1$, $B^3\Pi_0^+$), correlate with two ground state halogen atoms. In the case of homonuclear trihalogens, the X and A states correlate with two ground state halogen atoms, $^2P_{3/2}$, while the B state correlates with one $^2P_{1/2}$ and one $^2P_{3/2}$ halogen atom. In the heteronuclear case, however, there is an avoided curve crossing between the $B^3\Pi_0^+$ and a repulsive 0^+ state that changes the $B^3\Pi_0^+$ adiabatic correlation to two ground state halogen atoms. Therefore, either the I atom must be formed in the ground state or the IF fragment of the

I_2F reactant must be formed in the excited state. Unfortunately, we are unable to distinguish between formation of a $^2P_{1/2}$ and $^2P_{3/2}$ atom using the simple correlation rules. What we will be able to tell is whether formation of a ^2P atom and $^1\Sigma_0^+$, $^3\Pi_1$ or $^3\Pi_0^+$ IF fragment is compatible.

The trihalogens have 21 valence electrons, which puts them between the bent (≈100° bond angle) triatomic molecules with 20 electrons and the linear triatomics with 22 electrons. The geometry of 21 valence electron triatomics is not well understood. Experimental work on matrix isolated Cl_3[9] indicated a linear geometry, although subsequent work[20] suggests that the spectrum may have been due to Cl_3^-. Work on ClF_2[10] indicated a bent geometry with a bond angle of 140±19°, which was supported by the SCF calculation result of 148°.[21] The crossed molecular beam study by Valentini[4] also indicated a bent geometry for F atom abstraction in the reactions F_2 + I_2, ICl and HI. This is not conclusive evidence for a bent trihalogen product, however, because the non-linearity refers to the reactant, F-F-I-I, geometry which may not carry over into the product I_2F. If a bent I_2F geometry is assumed, then the molecular orbital configuration can be determined by analogy with the ClF_2 results.[21] The ClF_2 radical has a C_{2V} symmetry and an electron configuration of $...8a_1^2 3b_1^2 9a_1$ giving a $^2A_1$ ground electronic state. The C_{2V} symmetry of ClF_2 is consistent with the rule governing the arrangement of the atoms in a triatomic: the least electronegative atom is the middle atom. Assuming I_2F obeys this rule, it will have C_s

symmetry and an electronic configuration of $\ldots(n)a'^2(n+1)a'^2(n+2)a'$ giving a $^2A'$ ground electronic state. The C_S symmetry group has two elements, the identity and a mirror plane, the plane of the molecule in this case. The orbitals have symmetry a', symmetric, and a", antisymmetric with respect to reflection through the plane. With this criterion, we can classify the ^2P atom electronic term as having either A' (singly occupied p orbital in the molecular plane) or A" (p orbital perpendicular to the plane) symmetry. Likewise, the $^1\Sigma_0^+$ state of IF will be A'; while the $^3\Pi$ states are either A' or A". When the IF molecule and I atom unite into I_2F, they must produce an A' (ground) state. Using a direct product[22] of the I and IF state symmetries, the allowed combinations of IF and I states are:

I	IF	I_2F
$A'(^2P)$	A' $(^1\Sigma_0^+, ^3\Pi_{0,1})$	A'
$A"(^2P)$	$A"$ $(^3\Pi_{0,1})$	A'

If the I atom is formed in the A" state, with the half-occupied orbital perpendicular to the plane of the molecule, the $^3\Pi_{0,1}$ state of IF must be formed. Therefore, if there were some way of determining whether the reaction with the F atom occurred in the plane or out of the plane of the I_2F reactant (e.g., obtaining a rotation population distribution for the I_2F produced from $I_2 + F_2$) we might be able to tell if the IF fragment of I_2F was the electronically excited IF. In any case, the mechanism is consistent with excited IF formation from $I_2F(^2A')$.

When the ClF(A→X) transition is analyzed, it is likely that the reaction of ICl with F_2 could provide information on whether the newly formed ClF or the IF fragment is electronically excited. If the ClF(A→X) and IF(A→X) transition could be separated using a spectrometer, then appearance of light from only one molecule, at a collision energy high enough to allow excitation of either, would answer the question. If IF + ClF(A) lies at least 1 kcal/mole above ClIF + F, then we know that IF(A) is formed, but in the absence of any information on ClF(A) we can draw no conclusions about which half of the F-X-Y-F is formed in an electronically excited state.

E. A Study of Laser Enhancement of IF^* Production

Another study of the $I_2 + F_2$ reaction, that was not mentioned in the introduction to this chapter, was made by Engelke, Whitehead and Zare in 1976.[23] The reaction was studied using the crossed molecular beams method, but an Ar^+ laser (514nm line) was used to excite the I_2 beam to see if the additional energy (55.6 kcal/mole) and I_2 electron configuration change would affect IF^* production. The I_2 transition excited was ($X^1\Sigma_g^+$, v"=0→$B^3\Pi_{0u}^+$, v'=43, P(B) and R(15)) (24) and corresponds to the transition of one electron from a π^* to a σ^* orbital. Refering back to Figure 1, such a transition should not have much effect on the forbidden nature of a four center reaction mechanism for this system. An enhancement of $IF^*(A,B)$ production was, in fact, found to correlate with the laser excitation. The chemiluminescence was linear with respect to F_2 pressure and

laser power (the I_2 fluorescence was also linear with respect to laser power so the chemiluminescence is linear with respect to I_2^*). A cross section of 10-50Å^2 was estimated by Engelke et al. for the production of IF^* from $I_2^* + F_2$ at a collision energy of .96 kcal/mole (calculated from the most probable velocities of the two effusive beams). No emission was seen for the reaction of I_2^* with ClF and ClF_3. Engelke et al. attributed the IF^* production to a four center reaction but some doubt was cast on their results by their inability to observe IF* emission in a repeat of the experiment.[25]

An attempt to repeat this experiment was also made in this laboratory using essentially the same experimental set-up as described earlier in this chapter. An Ar+ laser was aligned (see Chapter II) to excite I_2 molecules from the effusive source in the collision zone. The I_2 source was moved .37 inches back from the collision zone to help reduce scattered laser light. In the first attempts to repeat the experiment, the Ar+ (514nm) laser was run at 0.1 watt (Engelke et al. used 1-3 watt) to keep down the scattered light. A mixture of 10 percent F_2/Ar, 300°K, was crossed with the I_2 beam, and light was collected, undispersed, from the collision zone. The fraction of I_2 excited was estimated to be $\simeq 1 \times 10^{-5}$. A signal that correlated with the chopper on the F_2 beam was observed but it corresponded to quenching, not chemiluminescence, and could also be seen, at approximately the same magnitude, using a beam of pure Ar, in place of the F_2, at the same stagnation pressure. The F_2 beam was then run as a pure F_2 beam, at the same stagnation pressure, and

again a signal corresponding to quenching was seen, although of smaller magnitude. The experiments were also tried using a 500nm cut-off filter to preferentially transmit any IF^* emission to the blue of the laser line, which is where Engelke et al. made most of their measurements. The same results were obtained both with and without the filter.

The quenching data was analyzed to obtain the quenching cross sections for I_2^* by F_2 and Ar. The equation used for the calculation is

$$\sigma = \Delta I_2^*/(I_2^* \times M \times L \times 2.0)$$

where M is the number density of F_2 and Ar, L is length of the path traveled by I_2^* through the quenching gas and the factor of 2.0 is to account for the increase in the collision rate relative to random motion at room temperature. A value for L was determined by considering the distance the I_2^* could travel, on the average, in one lifetime. Assuming a velocity of 2.2×10^4 cm/sec and a lifetime of 2.9×10^{-6} sec,[26] $L = 6.4 \times 10^{-2}$ cm. The fluxes of the Ar and F_2 beams were measured using an ion gage and converted to number densities to obtain 2.8×10^{12} molecules/cc for Ar and 1.2×10^{12} molecules/cc for F_2. The F_2 value has an approximate uncertainty of $\pm .5 \times 10^{12}$ because the filament of the ion gage was noticeably degraded during the flux measurement. With values of $\Delta I_2^*/I_2^*$ of $1.1 \pm .3 \times 10^{-3}$ for F_2 and $1.7 \pm .3 \times 10^{-3}$ for Ar, we get the following values for the quenching cross sections:

F_2: $\sigma = 72.6\text{Å}^2 \pm 18.5$ (± 35.8 including estimated error in F_2 flux determination)

Ar: $\sigma = 47.4\text{Å}^2 \pm 8.4$

The literature value for the Ar quenching cross section is 5.11Å^2,[27] no value had been measured previously for F_2. It is not clear why the cross section we obtained for Ar is so much higher than the literature value. The most likely source of error in the absolute value of the Ar cross section is in the flux value measured; the ion gage was not checked for calibration against N_2. The number density of Ar relative to F_2 should still be reliable, which gives an F_2 quenching cross section of 7.8Å^2 relative to an Ar cross section of 5.11Å^2.

Attempts to repeat Engelke et al.'s experiment by collecting total fluorescence would clearly not work due to the large degree of quenching occurring. The second, and last, attempt to repeat the experiment was performed using a spectrometer (see Chapter II) to disperse the chemiluminescence and a laser power of 3.0 watts. The output from the photomultiplier (RCA C31034), mounted on the spectrometer, went through an electrometer to a chart recorder and, first, the spectrum of I_2^* ($B \rightarrow X$) was recorded. The pure F_2 beam then was turned on, and two possibilities were checked for: the appearance of IF^* lines and the quenching of I_2^* lines. Engelke[23] found that 1 in 5 quenched I_2^* molecules formed IF^*, although a value of 1×10^{-3} sec was used as the IF^*

lifetime which is at least 100 times too long. It is hard to estimate, without knowing their detector geometry, how this would affect the .20 photon yield quoted. We could observe quenching of the I_2 lines (v'=43→v" progression), although the extent of quenching varied from line to line. One of the more strongly quenched transitions, the transition closest to the exciting line (v'=43→v"=1), dropped in height 0.45×10^{-9} amps, which means that the IF^* lines should have been observed, to the blue of 514nm, on the 3×10^{-10} scale. We saw no IF^* lines in this region and conclude that no laser enhancement, at least to the extent reported by Engelke et al. occurs.

If the experimental conditions used by Engelke et al. were not truly single collision conditions, then it is conceivable that their results are due to the same mechanism proposed to explain the results of Birks et al. That is, that I_2F could be formed on the first collision then react to form IF^* in a second collision. Exciting the I_2 molecules to the v'=43 level of the B state increases the number of $I(^2P_{3/2})$ atoms formed through predissociation[28] which would then liberate more F atoms via $I + F_2 \rightarrow IF + F$. It is the increase in F atoms that would increase IF^* production via $I_2F + F \rightarrow IF^* + IF$ unless the reaction $F + I_2 \rightarrow IF + I$ was much faster. The signal detected by Engelke et al. was not directly correlated to either beam through use of a chopper, so the light observed could be due to such background reactions. Although Engelke et al. reported no IF emission when a 90 percent thermally dissociated I_2 beam was

used,[28] it is possible that the $I_2 + F_2 \rightarrow I_2F + F$ step could not produce sufficient I_2F. Other routes to I_2F production are improbable events requiring termolecular recombination.

Using the following elementary reactions:

$$I_2 + F_2 \xrightarrow{k_1} I_2F + F \qquad 1$$

$$F + I_2F \xrightarrow{k_2} IF^* + IF \qquad 2$$

$$IF^* \xrightarrow{k_3} IF + h\nu \qquad 3$$

$$IF^* + M \xrightarrow{k_4} IF + M \qquad 4$$

$$I_2 + h\nu \xrightarrow{k_5} I_2^* \qquad 5$$

$$I_2^* \xrightarrow{k_6} I_2 + h\nu \qquad 6$$

$$I_2^* + M \xrightarrow{k_7} 2I + M \qquad 7$$

$$I_2^* + M \xrightarrow{k_8} I_2 + M \qquad 8$$

$$I + F_2 \xrightarrow{k_9} IF + F \qquad 9$$

$$F + I_2 \xrightarrow{k_{10}} IF + I \qquad 10$$

and assuming steady state for I and F atoms, we obtain

$$(IF^*) = \Big(k_1(I_2)(F_2) + k_7(I_2^*)(M)\Big)\Big(k_3 + k_4(M)\Big)$$

which is linear with respect to F_2 and I_2^* concentrations.

Another possiblity is that the production of I_2F is enhanced by vibrational excitation of I_2:

$$I_2 \xrightarrow{h\nu_1} I_2^*$$

$$I_2^* \xrightarrow{h\nu_2} I_2^{\not\ddagger}$$

$$I_2^{\not\ddagger} + F_2 \rightarrow I_2F + F$$

The overall dependence on I_2^* and F_2 would be the same. Engelke et al. varied the distance from the point of excitation of the I_2 beam to the collision center to make sure that it was not $I_2^{\not\ddagger}$ reacting. They reasoned that if $I_2^{\not\ddagger}$ was responsible for the enhancement then the chemiluminescence would be independent of the distance from the laser beam to the collision zone but if I_2^* was

responsible then the chemiluminescence would decrease. They did see a decrease, although it is not as large a decrease as would be expected from the lifetime of I_2^*. So, it is possible that $I_2^{\neq}$ was reacting under single collision conditions, following the mechanism suggested to account for the chemiluminescence we saw, and has a shorter lifetime than Engelke et al. expected; or the conditions may not be single collision and may follow the mechanism suggested for Birks et al.'s results. The decrease would then be due to a decrease of I_2F available in the photomultiplier viewing area.

F. Summary

The chemiluminescent reactions of F_2 with I_2, ICl and Br_2 have been studied using the chemiluminescence-laser fluorescence crossed molecular beam machine. The pressure dependence of the $I_2 + F_2$ reaction was measured and indicated that the reaction is the result of a single collision between the beam molecules, and that the light is emitted by the product dihalogen, IF. The collision energy dependences for all three reactions were measured and the thresholds for $I_2 + F_2$ (4.2 kcal/mole) and $ICl + F_2$ (5.9 kcal/mole) were found to agree well with the thresholds for I_2F and ClIF production. Based on these data, a mechanism for the chemiluminescent reaction was proposed. This mechanism involves a two step process: formation of the stable trihalogen and subsequent reaction of the trihalogen with a fluorine atom to produce an electronically escited

dihalogen. A threshold of 11.3 kcal/mole was found for $Br_2 + F_2$ and, assuming the same mechanism is followed, this would also be the threshold for Br_2F formation which has not been previously reported.

Laser enhancement of the $I_2 + F_2$ reaction via electronic excitation of I_2 was attempted, but no enhancement was seen.

References

1. R. B. Woodward and R. Hoffman, The Conservation of Orbital Symmetry (Verlag Chemie Academic Press, Weinheim, 1970).
2. D. L. King, D. A. Dixon and D. R. Herschbach, Fara. Disc. Chem. Soc., 55, 375 (1973).
3. J. W. Birks, S. D. Gabelnick and H. S. Johnston, J. Mol. Spec., 57, 23 (1975).
4. J. J. Valentini, M. J. Coggiola and Y. T. Lee, Disc. Faraday Soc., 62, 232 (1977).
5. J. J. Valentini, Ph.D. Thesis, University of California, Berkeley, 1976.
6. N. Abauf, J. B. Anderson, R. P. Andres, J. B. Fenn and D. G. H. Marsden, Science, 155, 997 (1967).
7. Our system is very much like the one described by J. D. McDonald, P. R. LeBreton, Y. T. Lee, and D. R. Herschbach, J. Chem. Phys., 56, 769 (1972). The dimensions for our wheel are 7 inch diameter, .033 inch slits, and we used 4 μsec/channel.
8. K. P. Huber and G. Herzberg, Molecular Spectra and Molecular Structure Vol. IV (Van Nostrand Reinhold, New York, 1979).
9. L. Y. Nelson and G. C. Pimentel, J. Chem. Phys. 47, 3671 (1967).
10. G. Mamantov, E. J. Vasini, M. C. Moulton, D. G. Vicktroy and T. Maekawa, J. Chem. Phys., 54, 3419 (1971).
11. K. P. Lawley, and M. A. D. Fluendy, Chemical Applications of Molecular Beam Scattering (Chapman and Hall, London, 1973).
12. A. Kantrowitz and J. Grey, Rev. Sci. Inst., 22, 328 (1951).

13. J. C. Polanyi, Acct. Chem. Res., 5, 161 (1972).

14. R. D. Levine and R. B. Bernstein, Disc. Faraday Soc., 55, 100 (1973).

15. B. C. Eu and W. S. Liu, J. Chem. Phys., 63, 592 (1975).

16. M. A. A. Clyne and I. S. McDermid, J. Chem. Soc. Fara. Trans. II, 74, 1644 (1978).

17. J. A. Coxon, Chem. Phys. Lett., 33, 136 (1975).

18. P. H. Brodersen and J. E. Sicre, Zeit. fur Physik, 141, 515 (1955).

19. M. A. A. Clyne, and I. S. McDermid, J. Chem. Soc. Fara. Trans. II, 74, 1376 (1978).

20. B. S. Ault and L. Andrews, J. Am. Chem. Soc., 97, 3824 (1975).

21. S. R. Ungemach and H. F. Schaefer III, J. Am. Chem. Soc., 98, 1658 (1976).

22. G. Herzberg, Molecular Spectra and Molecular Structure Vol. III, (Van Nostrand Reinhold, New York, 1966).

23. F. Engelke, J. C. Whitehead and R. N. Zare, Disc. Faraday Soc., 62, 222 (1977).

24. G. D. Patterson, S. H. Dworetsky and R. S. Hozack, J. Mol. Spec., 55, 175 (1975).

25. R. C. Estler, D. Lubman and R. N. Zare, Disc. Faraday Soc., 62, 317 (1977).

26. M. Broyer and J. C. Lehmann, Phys. Lett., A40, 43 (1972).

27. R. B. Kurzel and J. I. Steinfeld, J. Chem. Phys., 53, 3293 (1970).

28. F. Engelke, J. C. Whitehad and R. N. Zare, Disc. Faraday Soc., 62, 317 (1977).

Table I. Internal Energy (kcal/mole) of the Beam Gases

Beam	Mach Number	Vibration		Rotation	
		Temperature	Energy	Temperature	Energy
I_2	4.22	397°K	.503	86.9°K	.17
ICl	3.63	397	.358	109.2	.22
Br_2	4.06	397	.410	92.1	.18
10 F_2/Ar, 300°K	15.04	300	.034	6.64	.01
10 F_2Ar, 700°K	11.78	700	.449	24.5	.05
7 F_2/He+Ar, 300°K	13.09	300	.034	8.46	.02
7 F_2/He+Ar, 692°K	8.64	692	.445	43.6	.08
1 F_2/He, 300°K	18.27	300	.034	4.53	.01
1 F_2/He, 694°K	10.72	694	.449	29.1	.06

Table II.[8] Energy Levels of the v' = 0 level of the B and A States of the Dihalogens.

	ν_{00}(kcal/mole)	
	B→X	A→X
I_2	45.0	(33.7)
IBr	46.0	35.1
ICl	49.4	39.0
IF	54.2	44.6
IBr	46.0	35.1
Br_2	45.2	39.5
BrCl	47.8	---
BrF	51.8	(49.3)

Figure Captions

Fig. 1. Molecular orbital correlation diagram for a C_{2V} transition state four center reaction of $I_2 + F_2 \rightarrow 2IF$.

Fig. 2. Sample velocity flux distribution for the supersonic beam source, output from program FLUX. The intensity scale is in arbitrary units. The (X) represents the data punched for input to program CELUM, the curve is a fit to these points. For further information on program FLUX, see reference 5.

Fig. 3. Sample velocity flux distribution for the quasi-effusive beam source, also from program FLUX.

Fig. 4. Sample collision energy distribution calculated from the distributions such as in Figures 2 and 3 using program CELUM. The points are those calculated by CELUM, adjusted for the relative velocity/collision energy Jacobian, the curves were drawn through the points for clarity. The probability scale is normalized to the point of maximum flux having a probability equal to 1.0.

Fig. 5. I_2 pressure dependence of the chemiluminescence. The signal scale is in arbitrary units. The pressure scale is the pressure of the chemiluminescence machine main chamber as measured by an ionization gauge.

Fig. 6. F_2 pressure dependence of the chemiluminescence. The signal scale is in arbitrary units. The pressure, $P(F_2)$, is the pressure, in torr, behind the nozzle.

Fig. 7. Energy dependence near threshold for the reaction $I_2 + F_2$. (▲) represent the data points, the curve is a fit to the data given by $\sigma = C(1-(3.4/E))^{.5}$. The intensity scale is in arbitrary units. The collision energy scale is a cross section weighted mean collision energy (see text).

Fig. 8. Energy dependence for the reaction of $I_2 + F_2$. The scales are determined in the same way as for Figure 7. (▲) represent the data points.

Fig. 9. Energy dependence near threshold for the reaction $ICl + F_2$. (▲) represent the data points, the curve is a fit to the data given by $\sigma = C(1-(5.1/E))^{.5}$. The scales are calculated as for Figure 7.

Fig. 10. Energy dependence for the reaction of $Br_2 + F_2$. The dots represents the data points, the curve is a fit to the data by a quadratic equation (see text). The intensity scale is in arbitrary units, the energy scale is described in the text.

Fig. 11. Schematic energy diagram for the reactions $F_2 + I_2$, ICl, Br_2. The reactants are taken to be at zero energy, the energy scale is in kcal/mole. The energy levels for I_2F and ClIF are taken from reference 5. (B) and (A) refer to the $B(^3\Pi_0^+)$ and $A(^3\Pi_1)$ excited electronic states.

Fig. 12. Schematic of the mechanism proposed to account for the observation of chemiluminescent bimolecular halogen-halogen reactions. The majority of the reactants follow branch 1 wherein a stable trihalogen is formed and an F atom leaves.

One out of a thousand collisions follows branch 2 where a secondary, reactive encounter of the F atom with the trihalogen results in the formation of two interhalogens, one being electronically excited.

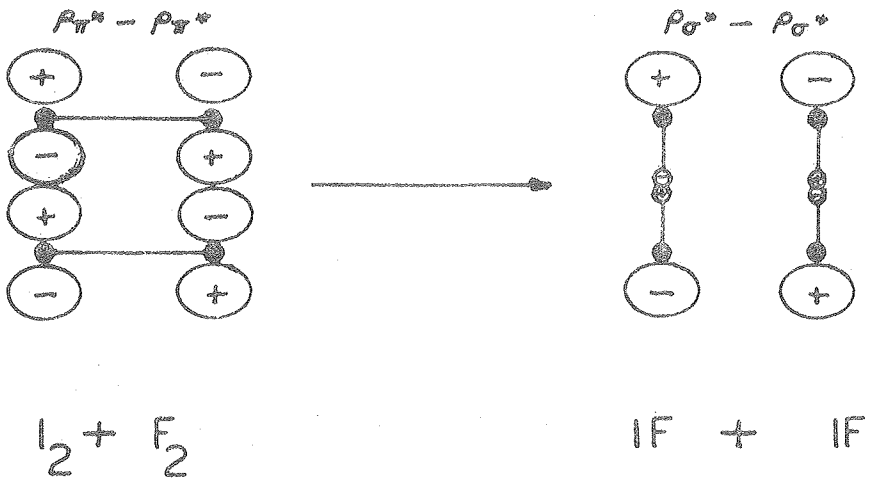

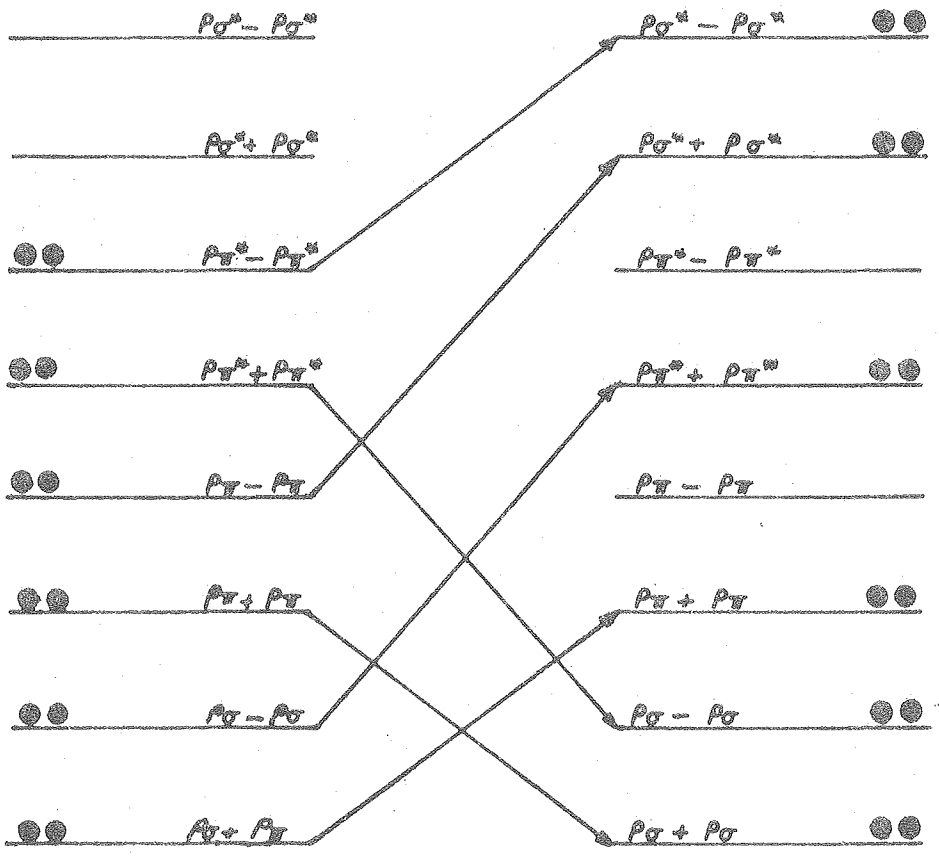

Figure 1

XBL 801-7857

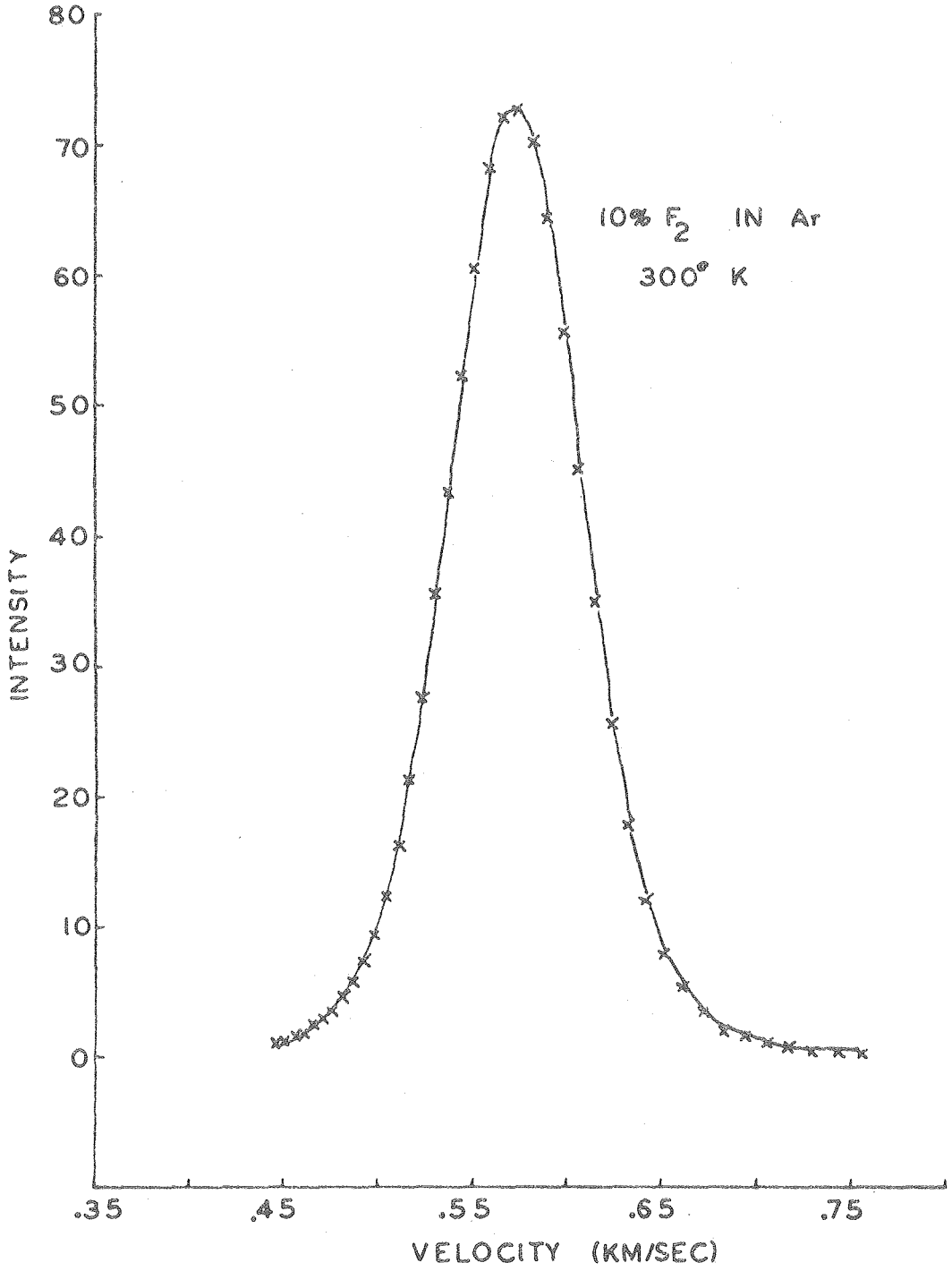

Figure 2

XBL 801-7853

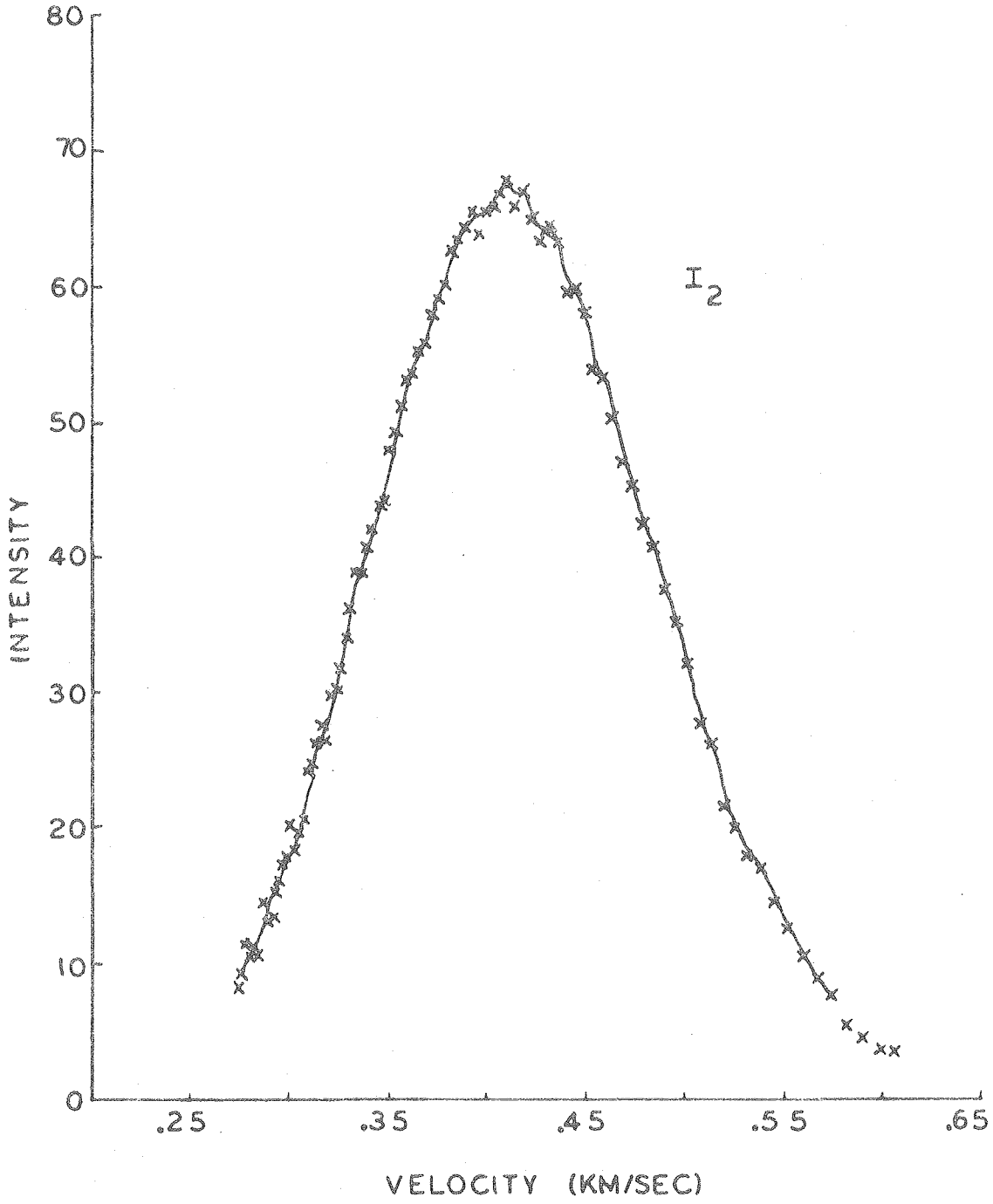

XBL 801-7854

Figure 3

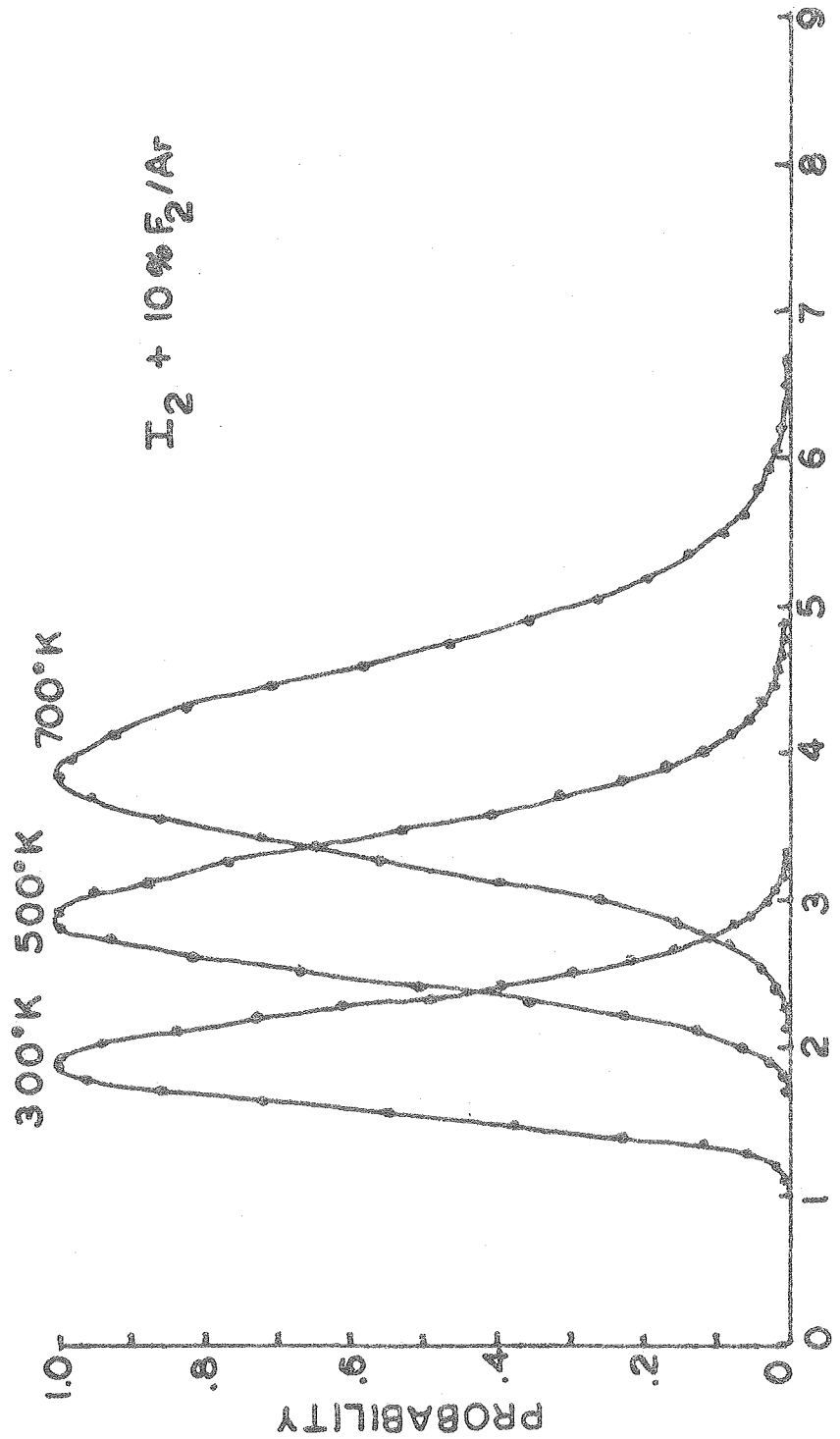

XBL 803-8481

Figure 4

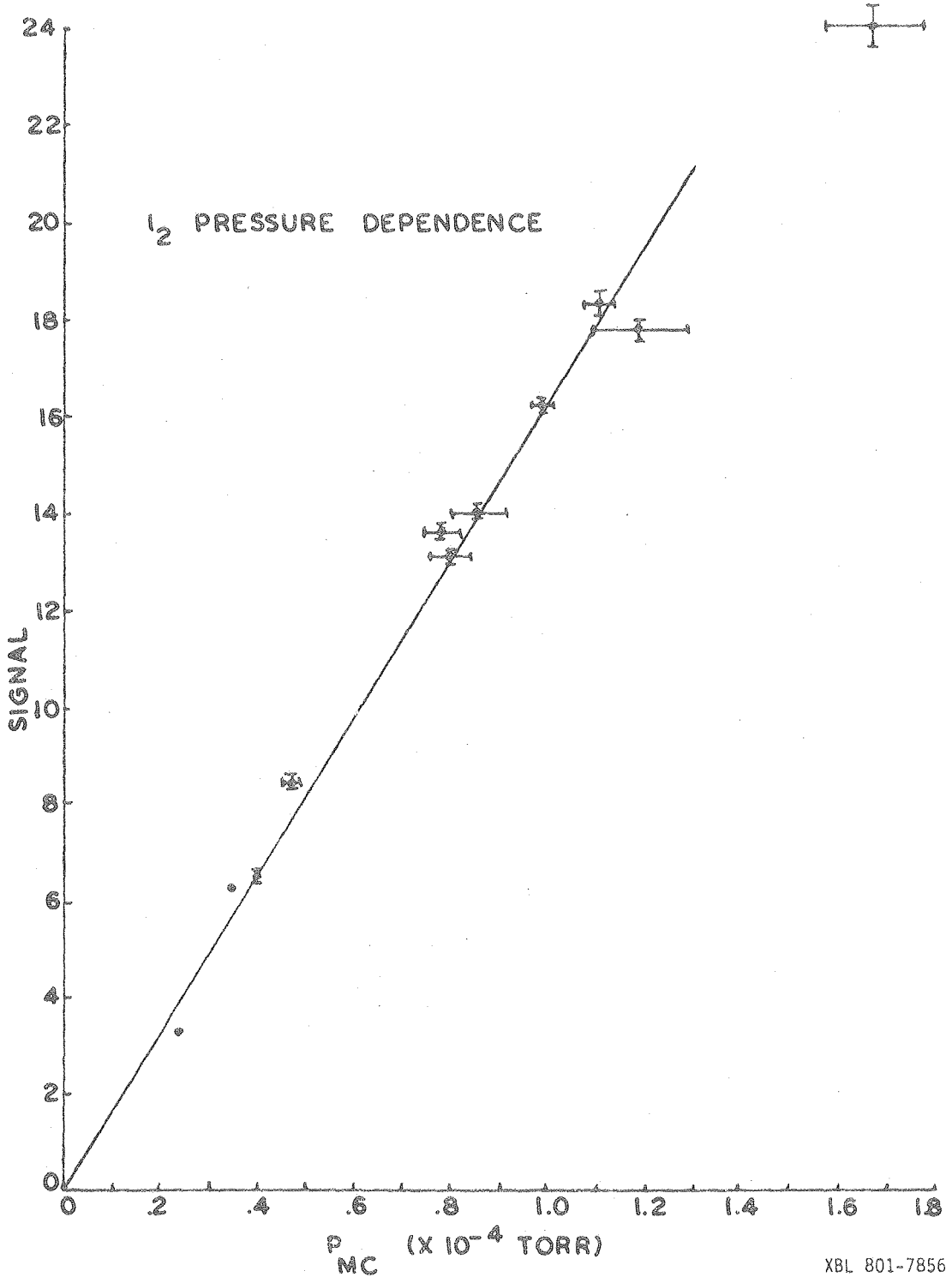
I_2 PRESSURE DEPENDENCE
SIGNAL
0
2
4
6
8
10
12
14
16
18
20
22
24
0
.2
.4
.6
.8
1.0
1.2
1.4
1.6
1.8
P_{MC} (X 10^{-4} TORR)
XBL 801-7856

Figure 5

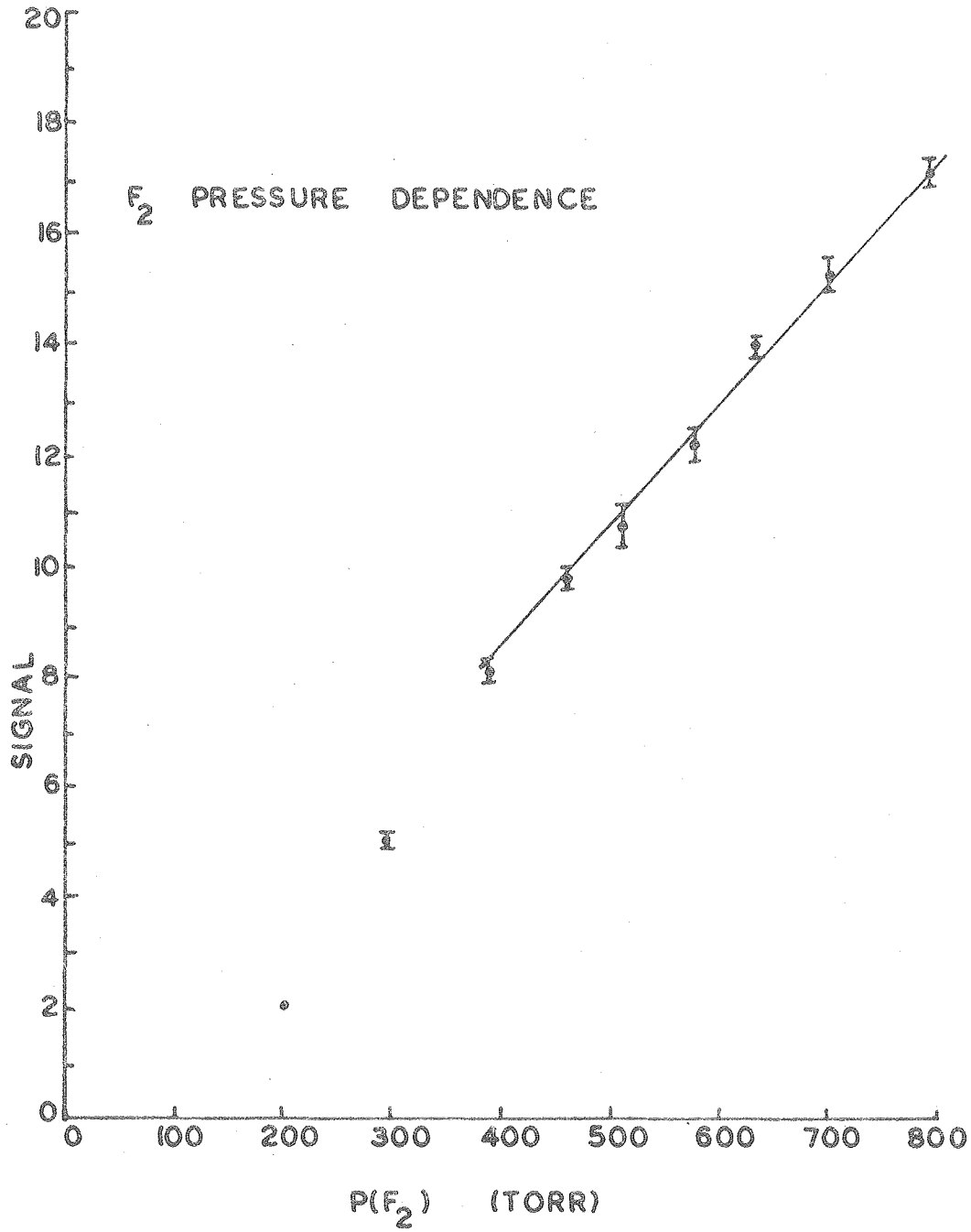

Figure 6

XBL 801-7855

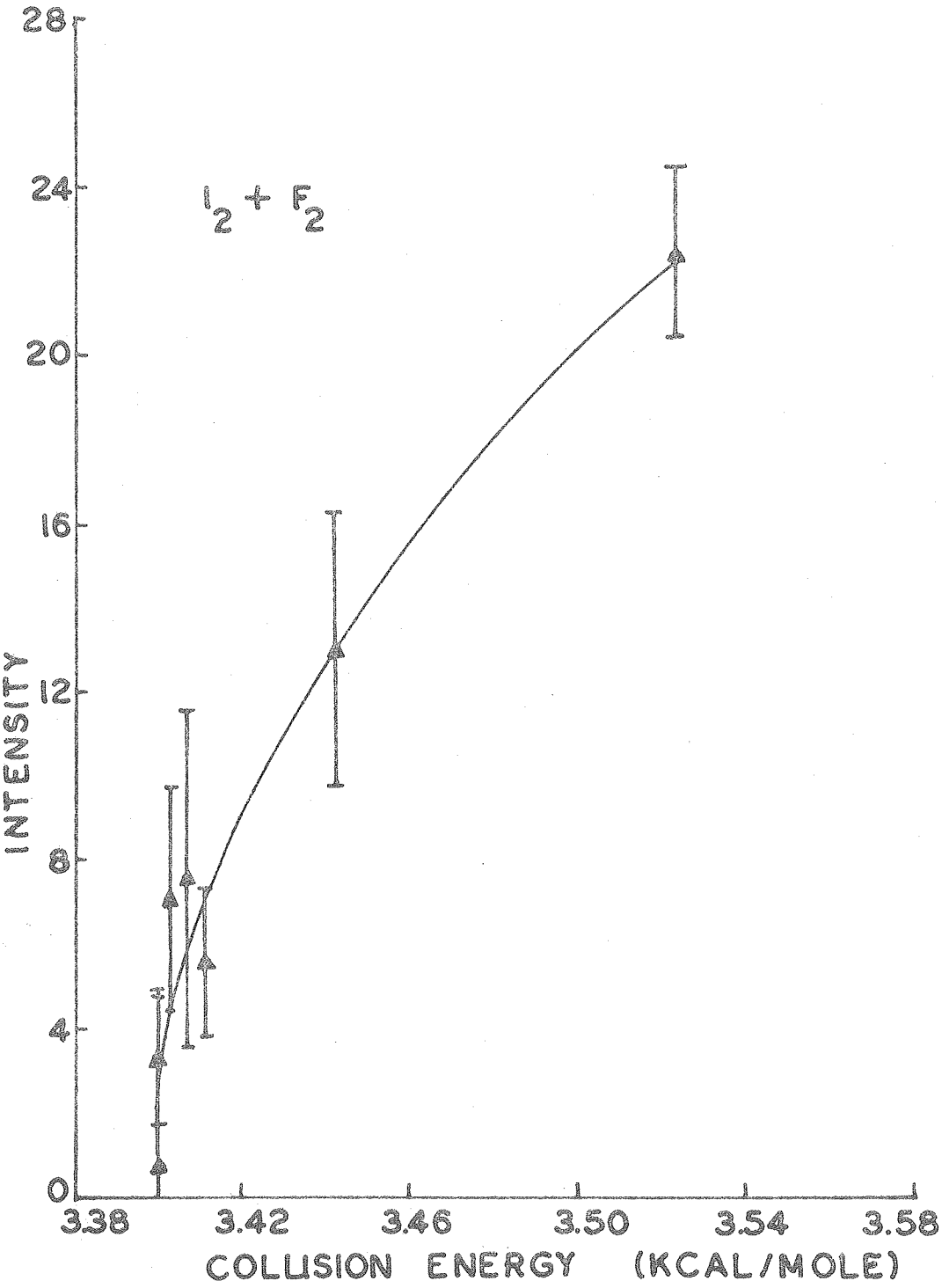

XBL 7912-13567

Figure 7

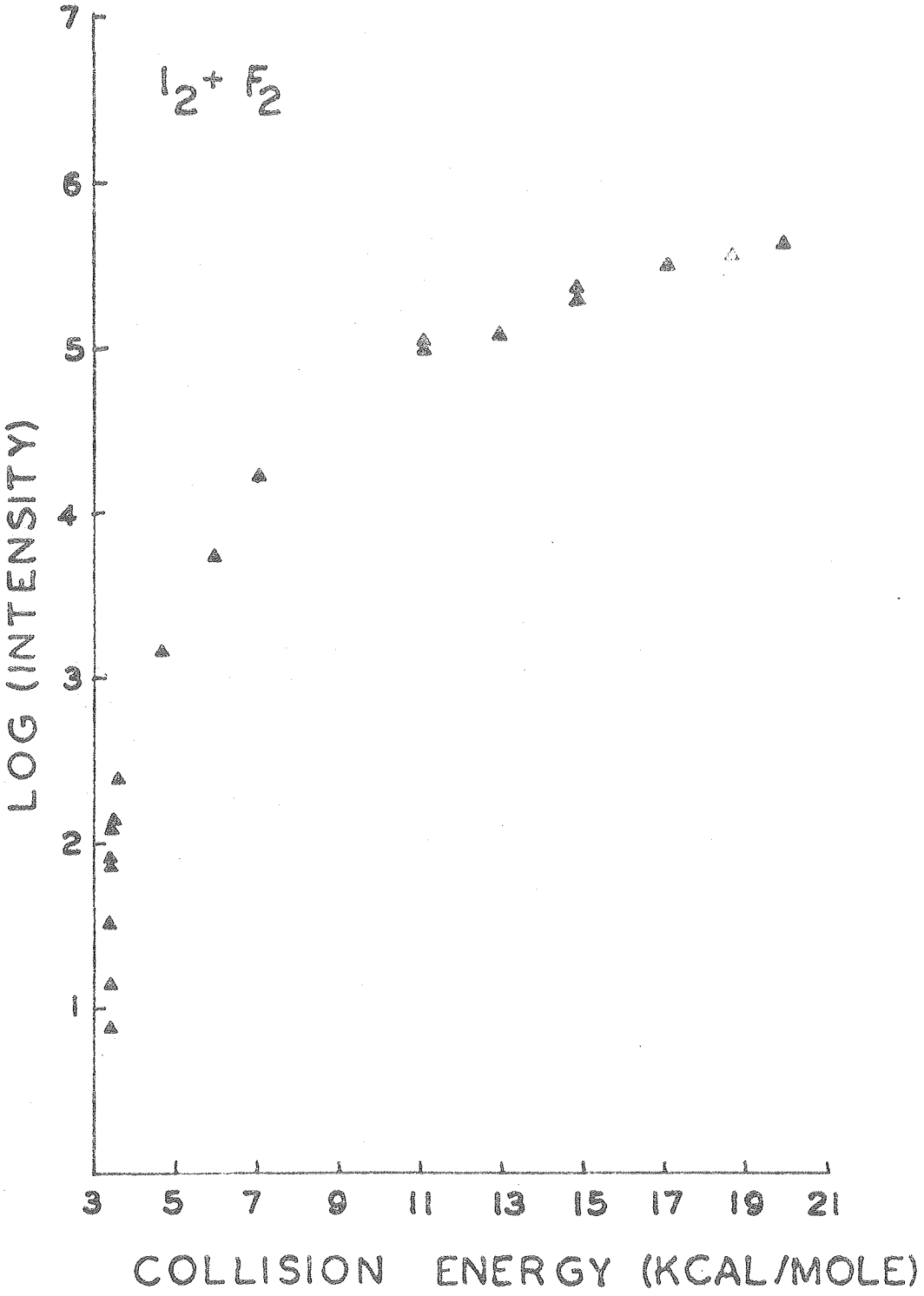

Figure 8

XBL 7912-13566

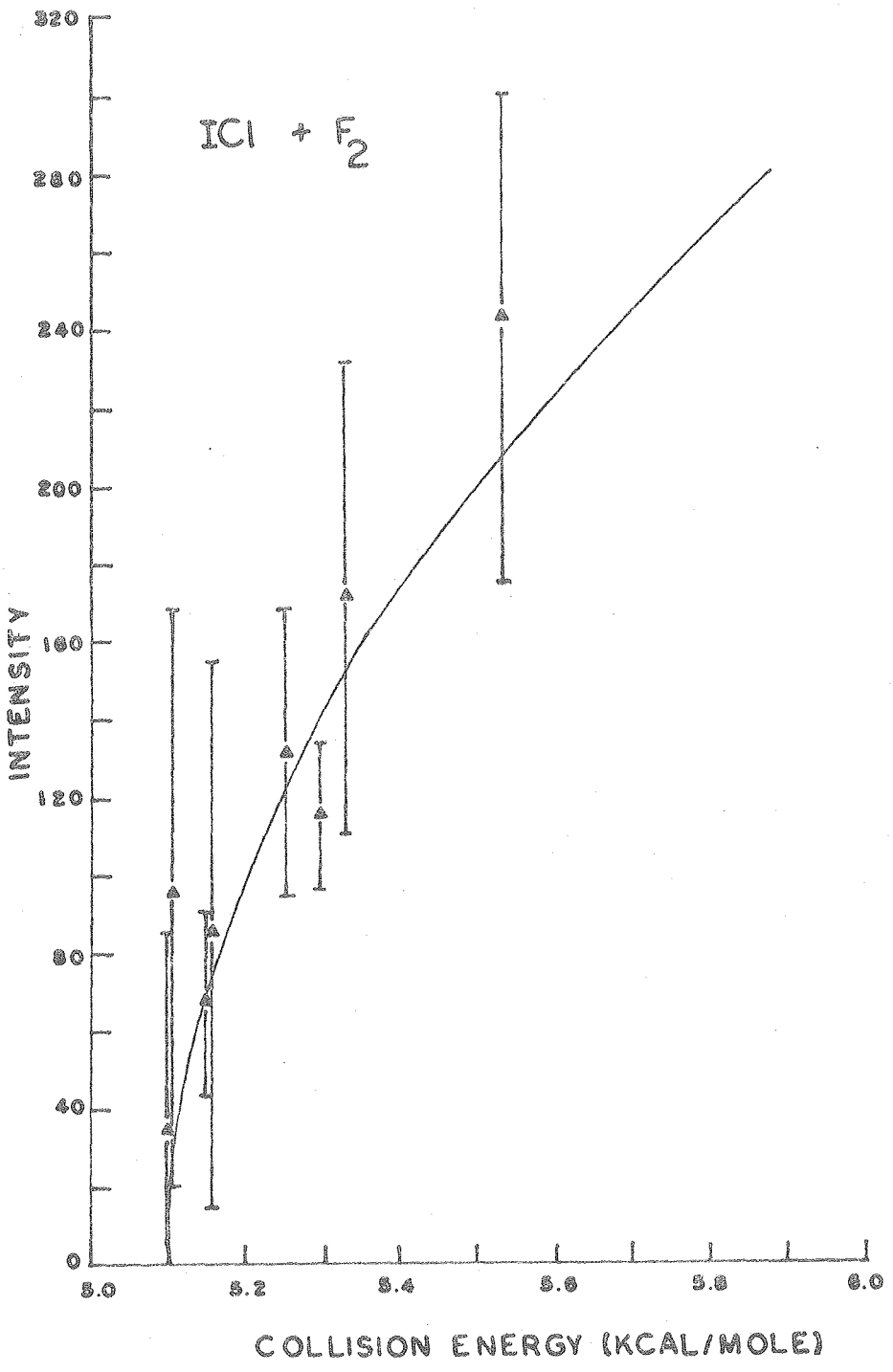

Figure 9

XBL 7912-13569

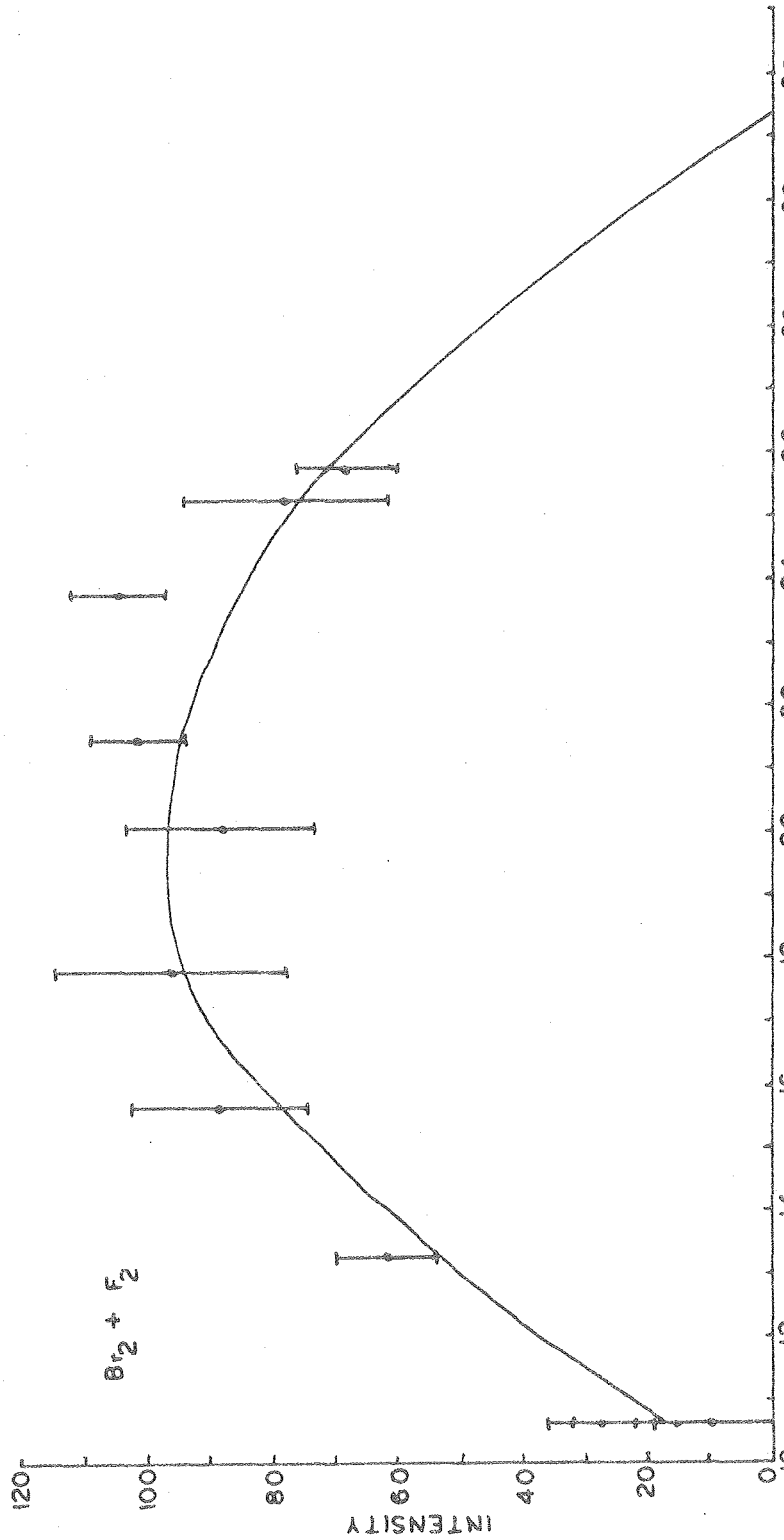

XBL 801-7850

Figure 10

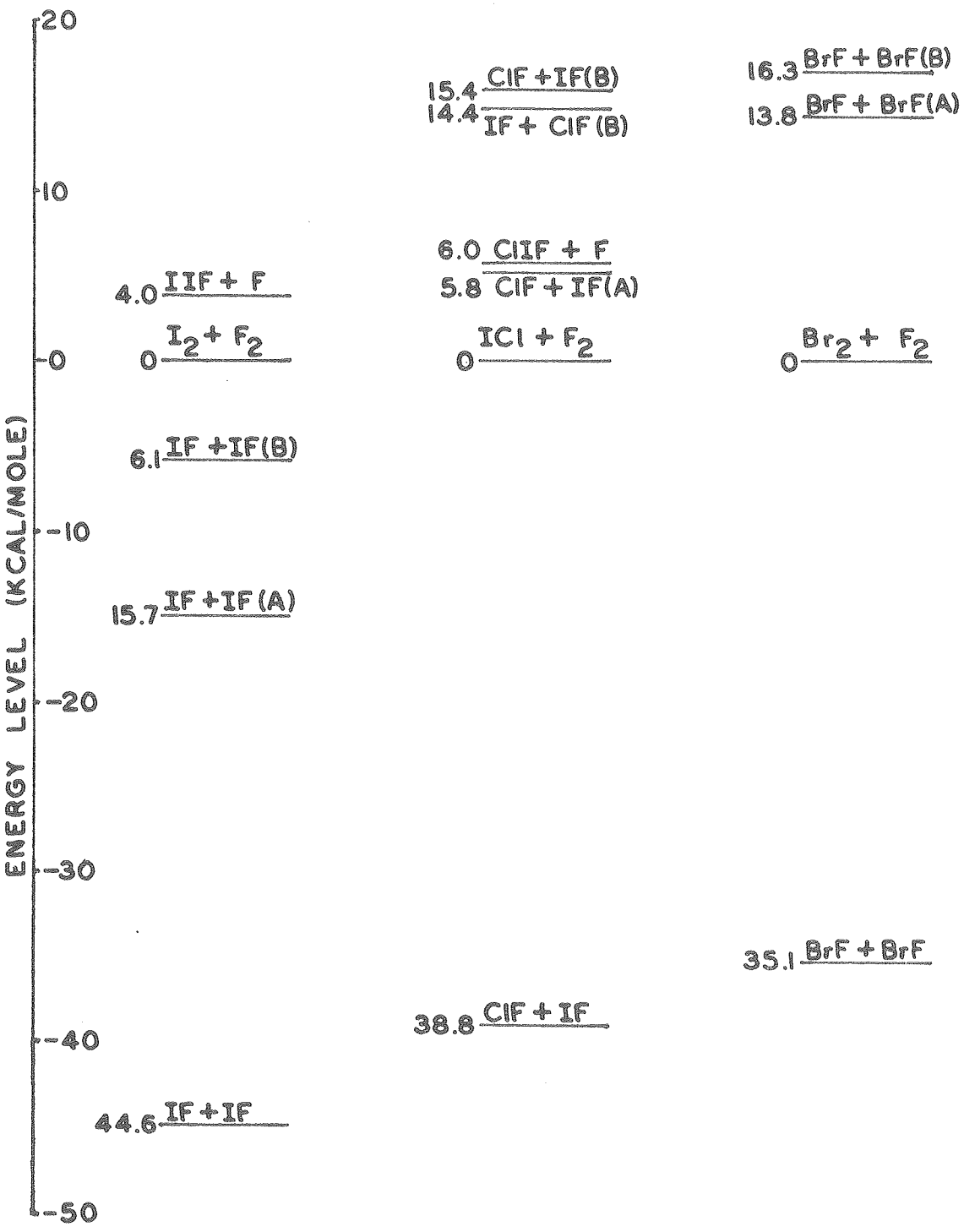

Figure 11

XBL 7912-13570

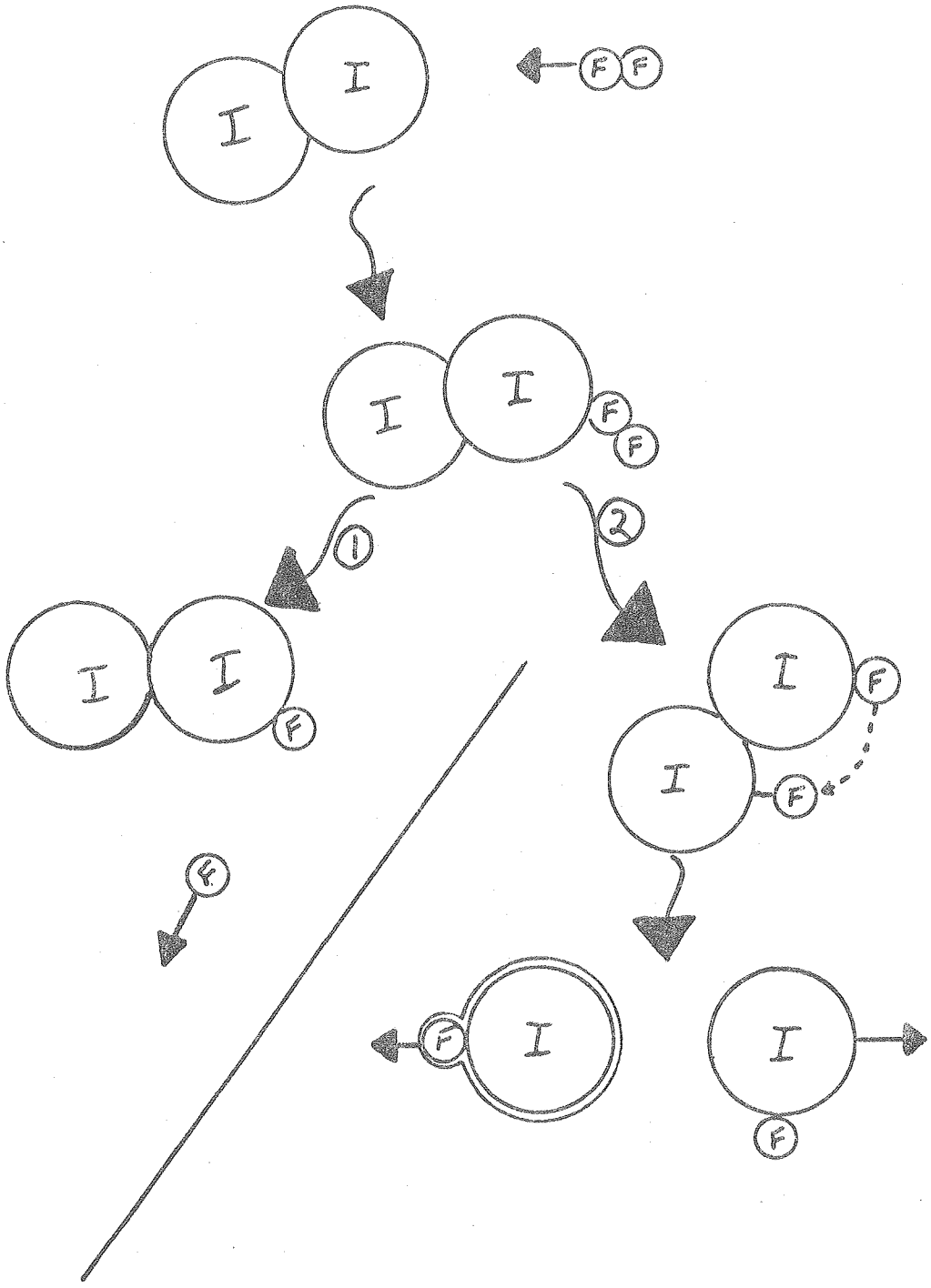

Figure 12

XBL 803-8477

IV.* A STUDY OF THE CHEMILUMINESCENT REACTION OF NO + O_3

A. Introduction

The reaction of NO with O_3 to give NO_2 and O_2 is of great significance in atmospheric chemistry[1] and although it has been studied extensively, some of the features of the reaction are not well understood. The reaction is 49 kcal/mole[2] exoergic and has two pathways:

$$NO + O_3 \rightarrow NO_2^* + O_2 \quad (1)$$

$$\rightarrow NO_2 + O_2 \quad (2)$$

where the NO_2^* is formed in the electronically excited $^2B_2$ or $^2B_1$ state.[3] Reaction 2 forms ground state NO_2 ($^2A_1$) which may be vibrationally excited. Chemiluminescence is seen in the spectral region of 4950Å into the infrared,[3,4] with bands at 6–7μ and 3.8μ identified as $NO_2(A_1)\nu_1$ and ν_3 fundamentals and a combination band. Initial work on the NO_2 vibrational emission suggested that the $NO_2^{\neq}$ was not directly formed in reaction 2 but resulted from NO_2^* relaxation.[4] Subsequent work[5,6] suggests that the $NO_2^{\neq}$ is formed directly, although the three sets of data contain contradictions. While there is sufficient energy to form electronically excited O_2 in either the $^1\Delta_g$ or $^1\Sigma_g^+$ and either state would be symmetry allowed, evidence of their formation has not been found.[7] Both reactions 1 and 2 are bimolecular and the following rate constants have been derived:[8]

$$k_1 = 7.6 \times 10^{11} e^{-4180 \pm 300/RT} \text{ cc/mole sec}$$

$$k_2 = 4.3 \times 10^{11} e^{-2330 \pm 150/RT} \text{ cc/mole sec}$$

although a later paper questioned the pre-exponential value for reaction 1.[1] If the above values are accepted, then the difference between the activation energies and the similarity of the relatively large pre-exponential factors can be attributed to both reactions proceeding through a similar reaction geometry but on different potential surfaces.[8] These rate constants mean that approximately 93% of the reactions form $NO_2(^2A_1)$ while the remaining 7% form $NO_2^*(^2B_2$ or $^2B_1)$ at room temperature.[4]

Another approach to studying the reaction has been through the selective vibrational excitation of either NO or $O_3(\nu_3)$. The effect of vibrational excitation of the NO to $NO^{\neq}(v = 1)$ was studied in a flow system using a CO laser to excite the magnetically tuned $v = 0 \rightarrow v = 1$ transition.[9] NO has a low-lying excited spin-orbit state ($^2\Pi_{3/2}$) 121.1 cm^{-1} above the ground ($^2\Pi_{1/2}$) state,[10] both are populated at room temperature. Because the $NO(v' = 0 \rightarrow v'' = 1)$ transition had to be magnetically tuned to coincide with the CO laser output, only the $^2\Pi_{3/2}$ state vibrational transition could be excited. The vibrational excitation enhanced channel 1 by a factor of 4.7 as well as increasing ground state NO_2 production. Many papers have been published on the effect of $O_3(\nu_3)$ excitation on the

reaction rate with the final conclusion that ν_3 and ν_1 (through rapid equilibration) are the active modes and enhance the chemiluminescent channel by a factor of 5.6 while total reaction rate enhancement was 22.[3,11-14]

Another effect on the reaction rate was first suggested by Redpath and Menzinger[15] who studied the NO + O_3 system in a beam-gas arrangement. Initially, Redpath and Menzinger studied the chemiluminescent branch of the NO + O_3 reaction as a function of collision energy[16] and found a threshold energy of 3.00 kcal/mole for the reaction. Because the analysis of the results from this experiment relied on calculated velocity distributions for the beams, a second study was done using time-of-flight beam velocity analysis.[15] The first experiment used a supersonic beam of NO/H_2 and varied the collision energy by changing the seeding ratio for NO, while the second experiment used NO/H_2 and NO/He and varied both the seeding ratio and nozzle temperature; the beams were shot into an O_3 filled scattering chamber in both studies. In this second study, Redpath et al. found that, at the same collision energy, the chemiluminescence signal was 4-5 times higher at the high temperature (573°K) than at the low temperature (238°K). Four-possible contributors to this effect were suggested: vibrational excitation, rotational excitation, $(NO)_x$ clusters and fine structure ($NO\,^2\Pi_{3/2}/^2\Pi_{1/2}$) excitation. The first two possibilities were discarded as requiring unreasonably large effects of such a population shift, that $\sigma(v = 1) \geq 150\ \sigma(v = 0)$ for example. Possibility 3, although shown to increase the chemi-

luminescence in the reaction of NO + O_3[17] could be discarded because it would show a decrease in chemiluminescence with increasing temperature. The final possibility, that NO($^2\Pi_{3/2}$) had a much higher cross section for NO_2^* production than NO($^2\Pi_{1/2}$), was adopted as the most likely. This initial finding was followed by more extensive work and data analysis by Redpath, Menzinger and Carrington[6] with the same conclusions as before. The same apparatus was used except that both visible and infrared emission was measured as a function of collision energy over the range of 1-12 kcal/mole. In analyzing the data, the O_3 target motion was accounted for and complete rotational relaxation, but no vibrational relaxation, was assumed for the NO beams. The fine structure temperature was treated as a variable because it may be only partially relaxed.[18,19] Redpath et al. concluded that the cross section for NO_2^* production by the excited spin-orbit state, NO($^2\Pi_{3/2}$), was at least four times as large as the cross section associated with NO($^2\Pi_{1/2}$), and NO($^2\Pi_{3/2}$) may be exclusively responsible for the NO_2^* reaction branch. Assuming that NO($^2\Pi_{1/2}$) does not contribute to reaction 1, an energy dependence of the NO($^2\Pi_{3/2}$) cross section was obtained:

$$\sigma_{3/2}(E) = C(E - E_o)^{2.4}$$

where E_o is the threshold energy and is equal to 3.0 kcal/mole. The dependence of $\sigma_{3/2}(E)$ on energy becomes even steeper than $E^{2.4}$ in the highest part of the energy range.

Because significant relaxation of the excited spin-orbit state of NO occurs in a supersonic expansion,[18,19] Redpath and Menzinger's conclusion is somewhat questionable. We therefore decided to study the NO + O_3 reaction using an effusive NO beam, where no relaxation of the NO would occur. There were three parts to our experiment; first, we used a supersonic NO beam and quasi-effusive O_3 beam to determine the translational energy dependence of the reaction over the range of 2-10 kcal/mole. In the second part, the supersonic NO and quasi-effusive O_3 configuration was used to obtain a low resolution spectrum of the chemiluminescence at four collision energies. Finally, we switched to an effusive NO beam and supersonic O_3 beam to measure the chemiluminescence as a function of NO temperature.

B. Experimental

The reaction of NO + O_3 was studied using the machine described in Chapter II. The general setup is shown in Figures 1 and 2 of that chapter and only the specific experimental details relevant to each part of the study will be discussed here.

1) Supersonic NO + Quasi-effusive O_3.

The NO supersonic source[20] consisted of a 1/4 inch diameter stainless steel tube, with a 0.003 inch (.008 cm) diameter nozzle hole in the end, that could be maintained at temperatures between -196°C and 165°C. Both heating and cooling were accomplished (similar to the quasi-effusive source described in Chapter II) via a block that clamped onto the stainless steel tube and was connected to a liquid

nitrogen feed tube as well as having resistance heating wires which were insulated by alumina rods. The temperature was monitored by an iron-constantan thermocouple spot-welded onto the nozzle tip. The nozzle was directed at a 0.023 inch diameter skimmer 0.28 inch away. Pure NO as well as three seeded mixtures, 24 percent NO/Ar, 10 percent NO/He and 1 percent NO/He, were used, and were passed through a silica gel trap (immersed in a dry ice/isopropanol bath) to remove any NO_2 impurity present before entering the nozzle tube. The pressure was monitored on a Wallace-Tiernan pressure gauge and kept at 400 torr for the seeded gases, 250 torr for pure NO, using a vacuum regulator.

The quasi-effusive O_3 source consisted of a quartz tube with a 0.0055 inch (.013 cm) hole in the end, not the source described in Chapter II. The use of quartz instead of metal as the nozzle material eliminated O_3 decomposition problems. The nozzle was aligned using a method similar to the method described for the metal nozzle except the alignment screws acted on the top of the nozzle, outside the machine, rather than in the vacuum. The nozzle was held in place, 0.192 inch (.488 cm) above the collision zone, by using a hose clamp to hold a piece of plastic tubing tight on the nozzle end (outside of the vacuum) such that the end of the plastic tubing butted up against the Cajon fitting holding the nozzle. The nozzle would have been sucked into the machine by the vacuum without the plastic tubing in place. The ozone was run pure, no seeding gases were used, and kept at its vapor pressure (about 13 torr) off the dry ice/isopropanol cooled silica gel trap on which it was kept stored after production on

a home-made ozonizer. The freshly filled trap was pumped prior to use to remove excess O_2. As the ozone was depleted from the trap, the O_3 pressure decreased, requiring the chemiluminescence signal to be corrected for this change. The ozone pressure was monitored using 300 nm light from a high pressure Hg lamp and the equation

$$\log \frac{I}{I_o} = -\sigma\, c\, l$$

where $l = 10$ cm, $\sigma = 5.92 \times 10^{-3}$ torr^{-1} cm^{-1}, and c is the pressure of O_3 in torr. The ozone pressure was checked before and after each series of counts at one NO temperature and was found to change by approximately 0.1 torr every two counting series. The gas line was made entirely of glass for the O_3 source.

The pressure of the main chamber was approximately 5×10^{-5} torr with both beams running. Because O_3 tended to build up to quite a high background in the main chamber, a trap was placed in the machine directly below the ozone source. The trap consisted of a cone directed at the ozone nozzle to act as a differential wall, guiding most of the ozone beam to a fluted sheet of silver (to decompose the ozone) after it had passed through the reaction zone. Once the trap had been installed, there were no further ozone background problems.

The signal collection system was the same as that described in Chapter II for collecting total reaction chemiluminescence. An RCA C31034 photomultiplier was used; the signal was correlated with a chopper on the NO source. Counting times were 100 sec with an average of ten counts at each temperature.

The same procedure was used for each of the NO gas mixtures and pure NO: the total chemiluminescence from the reaction of NO with ozone was measured as a function of NO nozzle temperature from 165°C to -125°C (the NO condensed at approximately -130°C). The signal was corrected for both ozone and NO pressure.

Time-of-flight analysis was performed on the ozone beam and on the NO beam at three temperatures for each seeding mixture and pure NO. The ozone velocity distribution is shown in Figure 1 and a sample collision energy distribution (calculated using CELUM, Chapter V) is shown in Figure 2. In addition, the NO beams were tested, using a mass spectrometer, for NO_2 impurities and $(NO)_x$ cluster formation.[17] No impurities were found and no clusters were found that correlated with the source chopper. The flux of the NO beams was measured using an ionization gauge. The chemiluminescence signal was corrected for NO pressure fluctuations by noting changes in the source tee pressure (approximately 5.6×10^{-5} torr). The flux measurements indicated that the source tee pressure was accurate, linear with respect to beam number density, and had sufficient sensitivity to be used for this purpose.

2) Spectral Distribution of the $NO + O_3$ Reaction

The spectral distribution of the chemiluminescence was measured using the same set-up as in part 1) with the addition of a narrow pass interference filter mounted on the face of the photomultiplier. The filters are made by Bausch and Lomb, have a 17Å pass width (full width at half maximum) with center wavelengths of 450, 500, 550, 600, 650,

700, and 800 nm. A Corning 3-70 cut-off filter was used with the 550, 600 and 650 nm filters and a Corning 3-73 filter was used with the 500 nm filter to cut out the short wavelength windows in the narrow pass filters. The maximum transmissions of the filters were between 20 percent and 45 percent.

The spectral distribution was measured at four collision energies, 10 percent NO/He at room temperature (~4.5 kcal/mole) and 400°K (~6.2 kcal/mole), and 1 percent NO/He at room temperature (~6.5 kcal/mole) and 400°K (~8.6 kcal/mole), by measuring the chemiluminescence signal and correcting for both maximum filter transmission and photomultiplier wavelength response.

3) Supersonic O_3 + Effusive NO

The supersonic O_3 source consisted of a 1/4 inch diameter quartz tube with a 0.0032 inch (.008 cm) diameter hole in the end. The nozzle was held to a brass block by a set of springs and a hose clamp, and the block, in turn, was bolted to the source reducer. This assembly held the nozzle in alignment even when the glass tube was rotated about its axis. The nozzle was directed at a 0.037 inch diameter skimmer 0.22 inch away. The tube was left at room temperature. The ozone was seeded in He (1000 torr) by attaching the He input to the inlet of the silica gel trap and attaching the trap outlet to the ozone pressure monitor, which then attached to the nozzle. This resulted in an ozone pressure of about 12 torr in 1000 torr of He or approximately 1.2 percent O_3/He. The ozone depletion occurred very fast in this configuration so that the ozone

pressure had to be measured after every 600 sec count and the chemiluminescence signal corrected accordingly.

The quasi-effusive source described in Chapter II was used for the effusive NO soure. The nozzle temperature was kept at either 136°K or 400°K for this experiment, so it was necessary to use the heater radiation shield to reduce background light. The nozzle was aligned, as described in Chapter II, and kept at 0.200 inch (.508 cm) above the collision zone. The nozzle hole was 0.015 inch (.038 cm) diameter. Only pure NO gas was used in this experiment and it was passed through the dry ice/isopropanol bath cooled silica gel to remove NO_2. The NO pressure was controlled using a leak valve and experiments were run for pressures between 0.125 and 0.025 torr. The NO pressure was monitored after the leak valve using a thermocouple gage (NRC 531 tube with NRC 801 gage) calibrated against a CVC Type GM-100 McLeod gage.

The main chamber pressure was ~7.4×10^{-5} torr with both beams running. The ozone trap used in part 1) was left in the machine, although gas flow from the supersonic source into the main chamber is not as high as it was from the quasi-effusive source. The signal collection system was the same as for part 1); the chopper remained on the supersonic source. An average of ten 600 sec counts were made for each data point.

For this experiment, the chemiluminescence was measured for a given NO pressure at a high nozzle temperature (400°K), then the nozzle was quickly cooled to 136°K and the signal measured again. The rapid temperature change was designed to minimize the effect of ozone

depletion (which would decrease the O_3/He ratio and increase the collision energy) making comparison of the hot and cold data simpler. This was repeated for lower and lower NO pressure until we were certain that we had a truly effusive (not quasi-effusive) beam (i.e., until the signal was linear with respect to NO pressure, which is not the case in the effusive-supersonic transition region).

Time-of-flight velocity measurements were made for the ozone beam for different ozone partial pressures to check for ozone depletion effects. The velocity distribution for the NO beam was not measured because it was an effusive beam and could be adequately described by a Maxwell-Boltzmann distribution for each temperature. The collision energy distributions for the hot and cold NO beams, crossed with the various ozone beams, are shown in Figures 3 and 4. The difference between the collision energy distributions for different ozone pressures is shown, the effect of this difference will be discussed later.

C. Results and Analysis

1) Supersonic NO + Quasi-Effusive O_3

The purpose of the data obtained in this part of the experiment was to obtain an expression for the reaction 1 cross section as a function of collision energy. While two of the internal degrees of freedom of NO relax significantly in the supersonic expansion, the mininum equilibrium temperatures they could reach are equal to the translational temperatures of the beams.[21] The translational

temperature can be calculated from the Mach number, as described in Chapter III, which is, in turn, calculated from the time-of-flight velocity data by program KELVIN.[22] The collision energy was changed in this experiment by changing both the seeding ratio and temperature of the NO beam. In changing either the seeding ratio or the nozzle temperature, the final beam translational temperature is changed and so the internal energy is changed. Therefore, while ideally we change only the collision energy—in practice we also change the internal energy. Using the Mach numbers from program KELVIN, the temperatures of the NO beams were calculated and, from them, the internal energies were calculated. The temperatures, vibrational, rotational and spin-orbit energies for the NO beams are shown in Table I and were calculated under the assumption that the rotational and spin-orbit temperatures are the same as the translational temperature, but that no vibrational relaxation occurs. The biggest change is in the vibrational degree of freedom where the energy increases from 0 to 0.07 kcal/mole. Unless there is a <u>much</u> stronger dependence on the internal energy than on the translational energy (something which has yet to be described), these small increases in internal energy should have no effect on our collision energy data.

The data for each seeding ratio was analyzed using the same procedure described in Chapter III. For each gas pair, a relative velocity distribution was calculated from the beam velocity distributions, taking angular spread of the beams into account, using

program CELUM (see Chapter V). Using program LUMFIT (Chapter V), the relative velocity distribution is used in conjunction with a functional form of the reaction cross section, $\sigma(E)$, to calculate the signal at each experimental temperature. The calculated signal is compared with the experimental data and the cross section parameters varied until an acceptable fit is made. The final cross section function is used to calculate a cross section weighted mean collision energy for each nozzle temperature.

For both the pure NO + O_3 and 24 percent NO/Ar + O_3 data, a cross section of the form $\sigma(E) = C(1-(E_{thresh}/E))^{.5}$ was used. This cross section form is derived from scattering theory[23] and is useful near reaction threshold. The data, plotted versus the cross section weighted mean collision energy, is shown in Figures 5 and 6 for 100 percent NO and 24 percent NO/Ar, respectively. The data for both gas pairs contains the reaction threshold although the threshold occurs at high temperature for 24 percent NO/Ar and at low temperature for 100 percent NO. The threshold collision energy obtained for both sets of data was approximately the same: 2.0 kcal/mole for 24 percent NO/Ar and 2.2 kcal/mole for 100 percent NO. As in Chapter III, this calculation considers the collision energy only, not the internal energy. The internal energy, as discussed above, is insignificant unless it is much more effective than translational energy. The data shown here presumes that the amount of internal energy is, in fact, negligible.

For the case of pure NO + O_3, the calculated signal curve underestimates the higher energy data by a large amount. As will be seen for the other two seeded mixtures, the dependence of the cross section on the collision energy goes up dramatically as the collision energy increases. This effect was also seen by Redpath et al.[6] and is due, at least in part, to the reaction becoming less specific about either the form of energy input (e.g., vibrational vs. translational), or preferred physical approach as the total energy input increases.[6,24] The quantum efficiency of the photomultiplier varies with wavelength and could also have an effect on the apparent cross section collision energy dependence. As will be seen later, the chemiluminescence spectrum shifts to the blue (where the quantum efficiency is higher) as the collision energy increases. This would make the cross section appear higher at higher energies than it really is. The spectral shift is actually quite small, however, and so should not have much effect.

The data for 10 percent NO/He and 1 percent NO/He + O_3 is shown in Figures 7 and 8, respectively. For these two gas pairs, the following functional form of the cross section was used:

$$\sigma(E) = C \left(\frac{E}{E_T} - 1\right)^n \quad .$$

This cross section, unlike the threshold cross section, was not derived from scattering theory. The 10 percent NO/He data was fit by

$$\sigma(E) = C\left(\frac{E}{3.95} - 1\right)^{1.70}$$

and the 1 percent NO/He data was fit by

$$\sigma(E) = C\left(\frac{E}{4.3} - 1\right)^{1.95} \quad .$$

As the collision energy increases, n increases (because of the increase in reactive collisions due to a decrease in reaction specificity as mentioned above) and E_T increases (which is an artifact in the analysis, the sharp dependence of σ on E makes the extrapolation back to $\sigma = 0$ come appear to be at a higher E_T). Again, the internal energy is small in value and assumed to be neglible.

2) Spectral Distribution of the NO + O_3 Reaction

The spectral distribution of reaction 1 chemiluminescence was measured at four collision energies: 4.5 and 6.2 kcal/mole using 10 percent NO/He, and 6.5 and 8.6 kcal/mole using 1 percent NO/He. The collision energies reported are the most probable energies according to the collision energy distributions calculated using CELUM. The raw data was normalized with respect to NO and ozone pressure, and corrected for the relative transmission of the filters used (including the cut-off filters) as well as for the quantum efficiency of the photomultiplier tube (which decreases, almost linearly, from .18 at 450 nm to .11 at 800 nm). The rest of the optics in the collection system have a flat transmission curve over the spectral range observed. The data, in its final form, is shown in Figure 9.

One effect that was not accounted for is the variation of lifetime over the spectral range. The physical volume viewed by the photomultiplier is limited in size, so a greater fraction of the long-lived states than of the short-lived states will travel out of the viewing area before emitting. The approximate dimensions of the viewing area are 0.092 cm x 0.266 cm x 0.892 cm (along the photomultiplier axis), and a molecule traveling 1×10^5 cm/sec would travel across 0.266 cm in 2.7 μsec. The lifetimes of the vibrational levels in the $^2B_2$ and $^2B_1$ excited electronic states of NO_2 are known to vary a great deal, with values of 55-90 μsec measured for the spectral range 3980-6000Å.[25,26] The lifetime tended to increase with increasing excitation wavelength. While, especially in this lifetime range, there would certainly be an effect from the lifetime variation over the spectral range, we cannot identify which transitions were observed and cannot, therefore, make any corrections. Qualitatively, however, we know that the lifetime increases with increasing wavelength, and so the fraction of light observed will decrease relative to the short wavelength data. While the data points on the long wavelength side of the graph should probably be higher on the intensity scale, any estimate of their true position would just be a guess.

3) Supersonic O_3 + Effusive NO

The purpose of this part of the experiment was to determine what effect changing the internal energy of NO would have on the reaction 1 chemiluminescence. The internal energy of NO was changed by heating

the effusive NO source, but heating the source also changes the number density and velocity of the gas. To be sure that any signal increase we see is strictly due to NO internal energy, the hot and cold NO data must be normalized to the same number of NO-O_3 collisions per second and the increased collision energy effect accounted for.

The number of NO - O_3 collisions occurring per second is given by

$$\int N_{NO}\, N_{O_3}\, v_R\, V\sigma dv_R$$

where the N are the number density of the gases, in the interaction zone that have velocities corresponding to v_R, v_R is the relative NO - O_3 velocity, V is the interaction volume and σ is the collision cross section. If we assume that the collision cross section does not change with collision energy (the reaction cross section does change with collision energy, but this will be accounted for later), then the ratio of the number of NO - O_3 collisions per second occurring for cold NO over hot NO is given by

$$\left(\int N_{NO} N_{O_3} v_R dv_R\right)^{cold} / \left(\int N_{NO} N_{O_3} v_R dv_R\right)^{hot} \quad .$$

This ratio was calculated from the output from program FLUX[22] using a modification of program CELUM (Chapter V). The flux at each NO or O_3 velocity was converted to a number density and normalized to unit area under the velocity distribution peak. The modified

program CELUM then summed up the values of $N_{NO}N_{O_3}$ in an increment Δv_R about each v_R and summed up the total $N_{NO}N_{O_3}$ v_R over all values of v_R for the hot and cold NO beam crossed with both 0.6 percent and 1.2 percent O_3/He. The ratio,

$$(\int N_{NO}N_{O_3} v_R dv_R)^{cold}/(\int N_{NO}N_{O_3} v_R dv_R)^{hot}$$

uses normalized NO number densities, so the change in the number density in the collision zone with temperature must still be accounted for. The number density in the collision zone is given by $I(\theta,r)/v = nA\cos\theta/4\pi r^2$ where n is the number density in the nozzle, A is the area of the nozzle and θ and r are the angle and distance from the nozzle at which the number density is being measured.[27] Because A,θ and r can be assumed to be the same, the change in number density at the collision zone due to cooling the NO is given by

$$n_{NO}^{cold}/n_{NO}^{hot} \text{ , or } (P^{cold}/T^{cold})/(P^{hot}/T^{hot})$$

for an ideal gas. The final factor used in accounting for the increase in collisions is then

$$\frac{P^{C}T^{H}(\int N_{NO}N_{O_3} v_R dV_R)^{cold}}{P^{H}T^{C}(\int N_{NO}N_{O_3} v_R dv_R)^{hot}}$$

which is equal to .95 $P^{C}T^{H}/P^{H}T^{C}$ for 1.2 percent O_3/He and .96 $P^{C}T^{H}/P^{H}T^{C}$ for 0.6 percent O_3/He.

The data was taken at two NO nozzle temperatures, 136°K and 400°K, as measured by a thermocouple on the nozzle tip. The pressure was measured by a calibrated (see Section B) thermocouple pressure gauge in the NO gas line, as described earlier. The data was normalized to an O_3 pressure of 10 torr using a simple ratio (the accompanying change in O_3 velocity is accounted for later). Table II shows the NO nozzle temperature, NO and O_3 pressures, the data at the two temperatures (normalized for O_3 pressure changes and collision frequency) and the ratio of the hot to cold NO data. The ratio is shown plotted versus the cold NO pressure in Figure 10. The points show a lot of scatter, especially the two points corresponding to an NO pressure of 0.0255 and 0.0275 torr. If a straight line is drawn through the less scattered high pressure data and the average of the ~0.026 torr pressure points, an intercept of 8.3 ± 1.1, corresponding to zero NO pressure, is obtained. The correct ratio is clearly open to debate, although a value of 8.3 ± 1.1 will be taken as correct for use in the subsequent discussion.

The ratio of 8.3 ± 1.1 corresponds to the signal measured at high temperature divided by the signal at low temperature, both of which are influenced by collision energy, vibrational energy and possibly rotational and electronic energy as well. If the contributions from these different forms of energy are assumed to be separable, then the signal is proportional to

$$\Sigma X_T^i \sigma_T^i (1 + \Sigma X_v^j \sigma_v^j + \Sigma X_R^k \sigma_R^k + \Sigma X_E^l \sigma_E^l)$$

where X_m^n refers to the mole fraction of molecules having cross section σ_m^n for each n state of the m degree of freedom. The σ_m may have very different energy dependences. If the internal energy cross section sums are treated as one sum, $\Sigma X_I^h \sigma_I^h \equiv S_I$, then the data takes the form

$$8.3 \pm 1.1 = (S_T(400^\circ K)(1 + S_I(400^\circ K)))/(S_T(136^\circ K)(1 + S_I(136^\circ K))) .$$

This can be simplified to three unknown variables by calculating what effect the change in collision energy has on the ratio. Looking back at Figures 3 and 4, the collision energy distributions for both the hot and cold NO data lie in the region of approximately 3.0 - 8.0 kcal/mole. Unfortunately, it is not possible to obtain a reasonably accurate quantitative estimate of how much the collision energy contributed to the signal at the two nozzle temperatures. While the data from part 1 gives us the collision energy dependence of the cross section, it does not provide us with an absolute value. An absolute value could be estimated, as was done in Chapter III, but there the lifetime of the emitting species varies little and is fairly well known. A cross section estimate for part 1 would not be very reliable for use here; the estimates for the emitter lifetime, beam fluxes for part 1 and beam fluxes for part 3 would result in a large compounded error. Therefore, instead of trying to get an absolute value for the collision energy contribution, the functional form of the collision energy dependence will be used to get a value for η where $\eta = S_T(400^\circ K)/S_T(136^\circ K)$. This part of the collision energy range is best

described by the equation used to fit the 10 percent NO/He data earlier, $\sigma \propto \left(\frac{E}{3.95} - 1\right)^{1.70}$, in the range 4.0 - 6.5 kcal/mole although as noted before, the cross section dependence changes with collision energy. Using the relative velocity distribution output by CELUM, a signal was calculated:

$$S_T = \int F(v) \left(\frac{E}{3.95} - 1\right)^{1.70} dv \quad ,$$

where F(v) is distribution of relative velocities for the gas pair, normalized to unit area. The expression in the integral sign is then summed over the relative velocity distribution for both the hot and cold NO beams. This summation was carried out for the relative velocity distributions at the two extremes of the ozone seeding ratio, 1.2 and 0.6 percent. The signals and the ratio, η, obtained by this calculation are given below:

	Signal (arbitrary units)		
Seeding ratio	NO(400°K)	NO(136°K)	η
0.6 percent	251.08	144.04	1.74
1.2 percent	191.95	97.52	1.97

The equation for the data is then simplified to:

$$8.3 \pm 1.1 = (1.86\ S_T(136^\circ K)(1 + S_I(400^\circ K)))/$$

$$(S_T(136^\circ K)(1 + S_I(136^\circ K)))$$

where $\eta = 1.86$, the average for the two seeding ratio extremes. This reduces to:

$$4.46 \pm .59 = \frac{(1 + S_I(400^\circ K))}{(1 + S_I(136^\circ K))}$$

Regardless of how the different forms of internal energy affect the reaction, the ratio $S_I(400^\circ K)/S_I(136^\circ K)$ will be a real number, m. The expression can now be written as (simplifying the notation, $S_I(136^\circ K) \equiv S_I$))

$$4.46 \pm 5.9 = (1 + mS_I)/(1 + S_I)$$

so that $3.46/(m - 4.46) = S_I$. This is not an absolute value for S_I, but it does indicate what m would have to be for the limits of S_I. As S_I approaches infinity, m approaches 4.46 while as S_I gets smaller, m gets larger. The smallest value for m is therefore, $4.46 \pm .59$.

The minimum signal ratio of $4.46 \pm .59$ is due just to the increase in internal energy and so

$$4.56 \pm .59 \leq \Big(S_V(400^\circ K) + S_R(400^\circ K) + S_E(400^\circ K)\Big) / \Big(S_V(136^\circ K) + S_R(136^\circ K) + S_E(136^\circ K)\Big) \quad .$$

If, again assuming the signal from the various modes is completely separable, S_V can be separated out, and bounds can be obtained for the ratio

$$p = \frac{(S_R(400^\circ K) + S_E(400^\circ K))}{(S_R(136^\circ K) + (S_E(136^\circ K))}$$

Using $\frac{N_V}{N_o} = e^{-1094.0v/.695T}$, X_1, the mole fraction of NO in the v = 1 state, is calculated to be 9.4×10^{-6} for T = 136°K and 1.96×10^{-3} for T = 400°K. Coupling X_1 and X_o with the cross section ratio $\sigma(v = 1) = 4.7\sigma(v = 0)$,[9] a value of 1.009 is obtained for the ratio $S_v(400^\circ K)/S_v(136^\circ K)$. This results in the equation:

$$\frac{S_V}{S_R + S_E} = \frac{m - 4.46}{3.46}$$

Using limits on the ratio of $S_V/(S_R + S_E)$, the same bounds of 4.46 ± .59 and infinity for p are obtained.

Next, assuming $S_R = 0$, we can see what this minimum ratio of 4.46 requires for $S_E(400^\circ K)/S_E(136^\circ K)$. Redpath et al.[6] suggested that $0 \leq \sigma_{1/2}/\sigma_{3/2} \leq .25$ for the cross sections of the two NO spin orbit states. Using $N_{3/2}/N_{1/2} = e^{-121.1/.695T}$, values of 0.21 at 136°K and 0.39 at 400°K are obtained for the mole fraction of NO($^2\Pi_{3/2}$). These mole fractions and cross section

ratios give a signal ratio of between 1.33 ($\sigma_{1/2}/\sigma_{3/2} = .25$) and 1.86($\sigma_{1/2} = 0$), which does not agree with the observed minimum ratio of 4.46 ± .59.

Finally, assuming $S_E = 0$, we can see how the rotational cross section must behave to account for this ratio of 4.46. At these temperatures, there is a tremendous spread in the rotational level population and trying to find a cross section rotational level dependence would be fairly complicated. A threshold for the rotational contribution to the signal is not known and it would be necessary to deal with σ_J/σ_0 ratios for the entire distribution. To a first, and admittedly rough, approximation, the average rotational energy at the two temperatures can be used. Using $N_J/N_0 = (2J + 1)e^{-1.7046J\ (J\ +\ 1)/.695T}$ with $E_J = 1.7046J(J + 1)cm^{-1}$, average rotational energies of 0.269 kcal/mole at 136°K and 0.793 kcal/mole at 400°K are obtained. Using $S_R=(E_R)^n$, an $n = 1.4$ is required to produce this kind of a signal ratio.

The above discussion assumes that the signal can be separated into signal due to the various modes of energy. This is almost certainly not rigorously true. One conclusion that can be drawn from our data in any case—the internal energy of NO has a very noticeable effect on the chemiluminescence signal. Because the beam temperature stayed constant for the ozone beam, internal energy contributions from ozone were not considered. More will be said about ozone internal energy in the next section.

D. Discussion

Subsequent to the papers referenced in the introduction to this chapter, work on NO + O_3 by two other groups has been reported.[28,29] In one study,[28] the translational and internal energy effects are separated through the use of a velocity selector on the NO beam. In that way, the collision energy can be increased under static beam temperature conditions and, conversely, the beam temperature may be changed while maintaining constant collision energy. This study covered only high collision energies (9.2 - 36.8 kcal/mole) where a cross section collision energy dependence of $\sigma \propto (E)^{3.75}$ was found with some leveling off in chemiluminescence occurring above 27.6 kcal/mole. A reaction threshold of 2.97 kcal/mole was obtained and enhancement of the chemiluminescence signal with increasing internal energy observed. Although they could not differentiate between increases in rotational, vibrational or electronic energy, if the enhancement is assumed to be due solely to the change in electronic energy then they found $\sigma(^2\Pi_{1/2})/\sigma(^2\Pi_{3/2}) = .27$. This is in very good agreement with Redpath et al.'s results.[6]

The study reported by Anderson et al.[29] differentiated between the effect of the different types of internal energy. Using magnetic focussing of a supersonic NO beam, the population of $^2\Pi_{3/2}$ could be increased relative to $^2\Pi_{1/2}$, but there was also a preferential focussing of low rotational level NO molecules. At 6.5 kcal/mole collision energy, virtually no effect was seen when the focussing magnet was on. The conclusion from this study was that the enhancement upon heating the NO beam was due to rotational effects, not

electronic. The data presented in this chapter will be discussed in comparison with the results of references 6, 26, and 27 to see if our results can provide evidence in support of either rotational or electronic enhancement.

As was mentioned in the previous section, we observed a chemiluminescent reaction collision energy threshold of 2.1 kcal/mole. This threshold has also been measured by Redpath et al.[6] and Stolte et al.,[28] who obtained values of 3.2 and 3.0 kcal/mole, respectively. Although there is good agreement between their values, we believe our value is more accurate (although a possible problem is mentioned in the discussion of the effusive $NO + O_3$ results). Stolte's study was performed only at high collision energies (9.2 - 36.8 kcal/mole) and so the threshold determination is the result of a fit to the high energy data. In fitting our high energy data, we used $\sigma \propto (E/E_T - 1)^n$ and obtained "threshold" energies of 3.95 for the 10 percent NO/He data and 4.30 for the 1 percent NO/He data. In other words, the "threshold" energy is much higher than what we found near threshold and changes with collision energy. Therefore, extrapolation to the reaction threshold from high energy data such as Stolte's would probably have a large degree of uncertainty associated with it.

Redpath et al. determined their threshold value from data taken at the reaction threshold, so the value should be fairly accurate. We believe that the difference between their results and ours is not in the data itself but in the data analysis. Although Redpath determined

the energy dependence of the NO($^2\Pi_{3/2}$) state cross section and our results are for the NO($^2\Pi_{1/2}$) state (see Table I, Section C), there should be no discrepancy here because Redpath assumed that the forms of $\sigma_{3/2}$ and $\sigma_{1/2}$ were the same except for a multiplicative factor. The difference comes in the fact that Redpath fit the data to a cross section function of the form $((E/E_T) - 1)^n$ where n was found to be 2.4, while we fit our threshold data to a cross section form $(1 - (E_T/E))^{.5}$. We can also get a reasonable fit to our threshold data with a functional form like Redpath's and the the threshold comes out higher (2.5 kcal/mole). The function we used is derived from scattering theory and so has physical significance.[23] We feel that this function will be more sensitive in the energy region near threshold and therefore give a more accurate threshold value.

As part of finding the cross section energy dependence, Redpath found the electronic temperature, T_{fs}, to be given by $T_{fs} = T_S + 40^\circ K$ for the H_2 seeded NO beams, where T_s is the translational temperature of the beam. This was obtained by assuming the increase in NO($^2\Pi_{3/2}$) population to be solely responsible for the chemiluminescence enhancement and varying T_{fs}, as well as the $\sigma_{3/2}/\sigma_{1/2}$ ratio, until the data was fit. Redpath et al. used both He and H_2 to seed the NO beams (although the analysis is given for NO/H_2 only), and found that T_{fs} is higher for He while T_s is lower. This conclusion is based on a data fitting procedure which relies on a debatable assumption, but it is supported to a certain extent by independent work. McClelland et al.[30] obtained the vibrational

and rotational temperatures for a seeded supersonic I_2 beam for a variety of diluent gases, including He and H_2. They found that T_{rot} was basically the same for He and H_2 but T_{vib} (H_2) was roughly half T_{vib}(He). $B_e(I_2)$ is .03735 cm^{-1} while $\omega_e(I_2)$ is 214.57 cm^{-1} (reference 10) so, using the energy gap as a measure of relaxation efficiency, the 121.1 cm^{-1} spin-orbit splitting is large enough to expect about a 50°K difference in T_{fs} for He and H_2. It is tempting to use this difference in internal temperature to explain the difference in collision energy thresholds. Unfortunately, Redpath did not quote a threshold for their He data, so we cannot tell for sure if this idea is correct. If the temperature difference does exist, then if our beam had been seeded in H_2 instead of He, there would be very little difference in E_{rot}, ~.04 kcal/mole in E_{s-o}, and perhaps .02 kcal/mole in E_{vib}. Unless there was an incredibly strong dependence on internal energy as compared to translational energy, this would not make up the 1 kcal/mole difference in thresholds. The internal energy present in our beam may have decreased the collision energy threshold by ~.1 kcal/mole, however.

There is more of a discrepancy between our high collision energy results and Redpath's. We can, again, exclude Stolte et al.'s results from this discussion because their data was in an even higher collision energy range and the cross section energy dependence changes with collision energy. Stolte's cross section went as $E^{3.75}$ which does support the idea of a steep but changing cross section energy

dependence. Our data was fit to $\sigma = C(\frac{E}{3.95} - 1)^{1.70}$ for $4.0 \leq E \leq 6.5$ kcal/mole and $\sigma = C(\frac{E}{4.30} - 1)^{1.95}$ for $4.5 \leq E \leq 9.0$ kcal/mole while Redpath's was fit to $\sigma = C(\frac{E}{3.0} - 1)^{2.4}$ for $3.5 \leq E \leq 6.0$ kcal/mole. Redpath's cross section was derived for NO/H_2 at a nozzle temperature of 281°K, assuming the chemiluminescence is due solely to $NO(^2\Pi_{3/2})$ and $T_{fs} = T_S + 40°K$. In increasing the collision energy from 1 - 10 kcal/mole, T_S rose from 30 to 175°K (Figure 3, reference 6). Although these values for T_s seem high and may indicate a poor expansion, the internal energy will have changed significantly over this collision energy range. Although Redpath et al. discounts any effect of rotational energy, it is possible that part of the exponent in Redpath's cross section has to account for signal due to this rotational energy increase. It is not clear whether this fully accounts for the difference in cross section functions in the high collision energy range.

The more important question is: how does our data on the internal temperature effect compare with the data of the other three groups Our data indicates that an increase in rotational and electronic temperature from 136°K to 400°K results in at least 4.46 ± .59 times as much chemiluminescence. In the last section we showed that this increase was not compatible with Redpath's claim that $\sigma_{1/2}/\sigma_{3/2} = n=0 - .25$. As was also mentioned in the previous section, if the rotational energy is solely responsible for the increase in chemiluminescence then the cross section would have to increase as $E_{rot}^{1.4}$ to account for this ratio, where E_{rot} is the average rotational

energy in the NO beam. Anderson et al.[29] found that their data was not consistent, either, with the assumption that the $^2\Pi_{3/2}$ state is much more reactive than the $^2\Pi_{1/2}$ state. They then analyzed their results with the idea that only rotational excitation was responsible for the chemiluminescence increase and found that, for this to be the case, the cross section would have to go as E_{rot}^n where E_{rot} is again the average rotational energy and $n = 1.8 - 2.5$, although there is some uncertainty in their beam rotational temperature. They did not obtain a dependence of the cross section on J. They have performed the same analysis on Redpath's data and found that the increase in chemiluminescence could be explained using only the increase in rotational energy by $n = 1.5 - 2.5$. On the other hand, Stolte and Van den Ende found an increase of 1.5 in chemiluminescence for an internal temperature change from 100°K to 300°K. This temperature change corresponds to a rotational energy change by a factor of 3.02, which would require $n = .4$ to produce the observed ratio. This increase in chemiluminescence can be explained, however, by an increase in $NO(^2\Pi_{3/2})$ population using $\sigma_{1/2} = .27\ \sigma_{3/2}$, which is in agreement with Redpath's results.

It seems then that there is a contradiction in results with Redpath and Stolte claiming the enhancement is due to electronic excitation while Anderson's and our results indicate rotational excitation. This contradiction can be explained by a more careful look at Redpath's results. There are two problems with the data presented in reference 6: the streaming temperatures given in

Figure 3 seem high and the calculation of the cross section ratio, n, does not seem to agree with Figure 6. Because it is not clear why T_s is so high, it is not clear what effect this has on the data. Even without the unlikely T_s given, the chemiluminescence data shown in Figure 6 of reference 6 is consistent with the enhancement being due to rotational excitation (as suggested by Andersen et al.) but not with the $\sigma_{3/2}/\sigma_{1/2}$ ratio given. At 8 kcal/mole, for the NO/H_2 beam, the ratio of the signal at the high nozzle temperature to that at the low nozzle temperature is approximately four, as seen from Figure 6. According to $T_{fs} = T_s + 40^\circ K$ (T_s, the translational temperature of the beam, is given in Fig. 4 of reference 6.), $X_{3/2}(573^\circ K) = .41$, $X_{1/2}(573^\circ K) = .59$ while $X_{3/2}(281^\circ K) = .29$ and $X_{1/2}(281^\circ K) = .71$. Using the same equation as was used to analyze our results and assuming $S_{rot} = 0$,

$$S(573^\circ K)/S(281^\circ K) = (X_{3/2}\sigma_{3/2} + X_{1/2}n\sigma_{3/2})^H/(X_{3/2}\sigma_{3/2} + X_{1/2}n\sigma_{3/2})^C,$$

where $n = \sigma_{1/2}/\sigma_{3/2}$, we get a ratio of 1.19 with $n = .25$ and 1.41 with $n = 0$. This does not agree with the value of 4 from Figure 6. So, it would seem that Anderson's, Redpath's and our data are all consistent with the enhancement being due to rotational excitation with the cross section going as E^n, where $1.0 \leq n \leq 2.5$ and not electronic excitation. Stolte's results would then indicate, as

expected,[24] that the reaction becomes much less energy mode specific as the collision energy increases.

A couple more comments should be made about the results obtained in the effusive NO + O_3 experiment. First, while our results are not consistent with Menzinger's suggestion that the $^2\Pi_{1/2}$ state is zero to one quarter as reactive as the $^2\Pi_{3/2}$, a dependence on the electronic energy cannot be ruled out. It is possible that part of the increase in chemiluminescence is due to the increase in $^2\Pi_{3/2}$ population, we have no way of telling from our experiment. The second comment that should be made is that if NO rotational energy is the cause (either wholly or in part) of the chemiluminescence increase, then rotationally excited ozone should have the same effect. This suggests further experimentation but also points out a flaw in the work presented here. As was mentioned at the end of the previous section, the internal energy of the ozone beam remained almost constant for the effusive NO- supersonic ozone experiment and so was not taken into account. In obtaining the collision energy dependence using supersonic NO, the internal energy of the quasi-effusive O_3 beam, likewise, did not change. But, in the quasi-effusive O_3 beam there should be some degree of rotational excitation while there should be very little in the supersonic O_3 beam. This could change our collision energy dependence somewhat, but just how much is not clear. It would certainly be interesting to repeat the NO + O_3 experiment using a variable temperature ozone source to test the idea that rotational energy is important to the branch 1 reaction.

Finally, the spectra we obtained (Figure 9) are consistent with previously published spectra,[2,3,6,8] although comparisons are difficult to make. Our data was obtained for collision energies of approximately 4, 6 and 9 kcal/mole. while the spectra of references 2, 3 and 8 were taken at thermal energies. The spectra were taken at higher collision energies in reference 6, but only extend to 600 nm whereas the peaks in our data are to the red of that. So, while the behavior of the spectra is what is expected (a shift to the blue with increasing collision energy, also observed in reference 6), little more can be said from this data.

E. Summary

The chemiluminescent reaction of $NO + O_3 \rightarrow NO_2^* + O_2$ was studied using the crossed beam technique. In the first part of the experiment, the collision energy dependence of the chemiluminescence was measured using a supersonic NO beam and quasi-effusive O_3 beam. The cross section was found to have a threshold energy of 2.1 kcal/mole and an energy dependence that increases with collision energy over the range studied (2.0-9.0 kcal/mole). A low resolution spectrum was recorded at four collision energies and the peak was observed shifting to the blue as the collision energy was increased. The final part of the experiment was performed using an effusive NO beam and supersonic ozone beam. The chemiluminescence was measured at two NO beam temperatures.

The signal increased with increasing NO temperature and the ratio of the signals at the two temperatures could not be reduced to one by accounting for the signal increase due to increased collision rate, collision energy and NO vibrational energy. Redpath et al.[6] attributed this effect to the increased NO($^2\Pi_{3/2}$) population at higher temperatures, but our signal ratio still cannot be reduced to one using their claim that $\sigma(^2\Pi_{1/2})/\sigma(^2\Pi_{3/2}) = 0\text{-}.25$. If the effect is due solely to increased NO rotational temperature, then, to explain our results, the reaction cross section would have to vary as $E_{rot}^{1.4}$ where E_{rot} is the average rotational energy. Our experiment cannot differentiate between the effects of rotational and spin-orbit excitation and indicates the need for further experiments. If NO rotational excitation is important, rotational excitation of O_3 should have the same effect. An experiment testing the effect of O_3 rotational energy could help solve the problem.

References

*see M. Kowalczyk, Ph.D. Thesis, Berkeley, (in preparation) for further information on this work.

1. J. W. Birks, B. Shoemaker, T. J. Leck and D. M. Hinton, J. Chem. Phys., 65, 5181 (1976).
2. M.A.A. Clyne, B. A. Thrush and R. P. Wayne, Trans. Faraday Soc., 60, 359 (1964).
3. W. Braun, M. J. Kurylo, A. Kaldor and R. P. Wayne, J. Chem. Phys., 61, 461 (1974).
4. P. N. Clough and B. A. Thrush, Trans. Faraday Soc., 65, 23 (1969).
5. M. F. Golde and F. Kaufman, Chem. Phys. Lett., 29, 480 (1974).
6. A. E. Redpath, M. Menzinger and T. Carrington, Chem. Phys., 27, 409 (1978).
7. M. Gauthier and D. R. Snelling, Chem. Phys. Lett., 20, 178 (1973).
8. P. N. Clough and B. A. Thrush, Trans. Faraday Soc., 63, 915 (1967).
9. J. C. Stephenson and S. M. Freund, J. Chem. Phys., 65, 1893 (1976).
10. G. Herzberg, Molecular Spectra and Molecular Structure Vol. I. (Van Nostrand Reinhold Co., New York, 1950).
11. R. J. Gordon and M. C. Lin, Chem. Phys. Lett, 22, 262 (1973).
12. M. J. Kurylo, W. Braun, A. Kaldor, S. M. Freund and R. P. Wayne, J. Photochem., 3, 71 (1974/75).
13. K-K. Hui, D. I. Rosen, and T. A. Cool, Chem. Phys. Lett., 32, 141 (1975).
14. R. J. Gordon and M. C. Lin, J. Chem. Phys., 64, 1058 (1976).
15. A. E. Redpath and M. Menzinger, J. Chem. Phys., 62, 1987 (1975).

16. A. E. Redpath and M. Menzinger, Can. J. Chem., 49, 3063 (1971).

17. D. Golomb and R. E. Good, J. Chem. Phys., 49, 4176 (1968).

18. H. J. Bauer, H. O. Kneser, and E. Sittig, J. Chem. Phys., 30, 1119 (1959).

19. H. Thuis, S. Stolte, and J. Reuss, Chem. Phys., 43, 351 (1979).

20. Designed by Dennis Trevor, Lawrence Berkeley Laboratory, Berkeley, Ca.

21. H. Pauly and J. P. Toennies, "Beam Experiments at Thermal Energies," Methods of Experimental Physics, Vol. 7A, (Academic Press, New York, 1968).

22. J. J. Valentini, Ph.D. Thesis, U. C. Berkeley, 1976.

23. B. C. Eu and W. S. Liu, J. Chem. Phys., 63, 592 (1975).

24. R. D. Levine and R. B. Bernstein, Molecular Reaction Dynamics, (Oxford University Press, New York, 1974).

25. S. E. Schwartz and H. S. Johnston, J. Chem. Phys., 51, 1286 (1969).

26. P. B. Sackett and J. T. Yardley, Chem. Phys. Lett., 6, 323 (1970).

27. M.A.D. Fluendy and K. P. Lawley, Chemical Applications of Molecular Beam Scattering, (Chapman and Hall, London, 1973).

28. D. Van den Ende and S. Stolte, Chem. Phys., 45, 55 (1980).

29. S. L. Anderson, P. R. Brooks. J. D. Fite and O. V. Nguyen, in preparation.

30. G. M. McClelland, K. L. Saenger, J. J. Valentini, and D. R. Herschbach, J. Phys. Chem., 83, 947 (1979).

Table I. Internal Energies of the NO Beams

Beam	T_{NOZZLE}(°K)	T_{FINAL}(°K)	E_{VIB} (kcal/mole)	E_{ROT} (kcal/mole)	E_{S-O} (kcal/mole)
100 NO	188°K	10.21	0	.019	0
	300°K	23.84	.016	.046	0
	411°K	32.43	.069	.063	.002
24 NO/Ar	300°K	6.91	.016	.012	0
	411°K	12.65	.069	.023	0
10 NO/He	188°K	2.76	0	.011	0
	300°K	4.28	.016	.007	0
	411°K	13.79	.069	.026	0
1 NO/He	171°K	1.18	0	.000	0
	300°K	3.08	.016	.004	0
	411°K	12.34	.069	.023	0

Table II. Normalized data and HOT/COLD data ratio for effusive NO + supersonic O_3

NO Temperatuure (OK)	NO Pressure (torr)	O_3 Pressure (torr)	Raw Data (Counts/600 Sec)	Normalized data* (Counts/600 Sec)	HOT NO Signal / COLD NO Signal
404	.125	7.8	550.4 ± 8.9	1216.3 ± 4.5	
135	.075	8.6	157.6 ± 6.1	183.3 ± 7.1	6.7 ± .2
400	.102	10.4	397.8 ± 13.9	643.8 ± 22.7	
136	.061	10.0	94.9 ± 5.6	90.4 ± 5.3	7.2 ± .5
389	.101	10.2	293.6 ± 6.3	444.9 ± 9.2	
136	.055	11.2	69.8 ± 8.1	62.3 ± 7.2	6.9 ± 1.3
404	.076	8.2	315.8 ± 67.5	596.8 ± 12.2	
135	.041	8.7	69.4 ± 5.6	79.8 ± 6.4	7.6 ± .7
400	.046	9.0	172.8 ± 9.9	322.2 ± 198.5	
136	.028	9.6	35.2 ± 3.7	36.9 ± 3.9	8.7 ± 1.6
400	.046	11.2	169.2 ± 6.1	126.5 ± 8.4	
136	.026	9.0	29.8 ± 3.5	33.1 ± 3.9	7.2 ± 1.2
400	.026	9.1	123.2 ± 7.2	230.4 ± 13.4	
136	.016	10.0	22.8 ± 5.0	11.8 ± 5.0	10.1 ± 3.6

* Normalized to 10 torr O_3 and, in each data pair, to the collison frequency of the cold NO data. The collision frequency normalization used the factor for 1.2 percent O_3/He, 0.96 $P^{C}T^{H}/P^{H}T^{C}$ (see text). The 0.6 percent O_3/He factor is .95 $P^{C}T^{H}/P^{H}T^{C}$.

Figure Captions

Fig. 1. Sample velocity flux distribution for the quasi-effusive ozone beam, output from program FLUX. The intensity scale is in arbitrary units. The (X) represents data punched for input to program CELUM, the curve is a fit to these points. For further information on program FLUX, see reference 22.

Fig. 2. Sample collision energy distribution calculated from the NO velocity spectrum and the distribution shown in Figure 1 using program CELUM. The points are those calculated by CELUM, the curves were drawn for clarity. The intensity scale is normalized to maximum flux having unit probability.

Fig. 3. Collision energy distribution for effusive NO (400°K) and supersonic ozone calculated using CELUM. The dots are the distribution for 0.6 percent O_3/He and the crosses are for 1.2 percent O_3/He. The curves through the points are for clarity. The distribution was calculated assuming a Maxwell-Boltzmann velocity distribution for NO.

Fig. 4. Collision energy distribution for effusive NO(136°K) and supersonic ozone. The dots are, as for Figure 3, for 0.6 percent O_3/He and the crosses for 1.2 percent O_3/He. This calculation also assumed a Maxwell-Boltzmann velocity distribution for NO.

Fig. 5. Energy dependence of $NO + O_3 \rightarrow NO_2^* + O_2$ near threshold for 100 percent NO (supersonic). The dots are the data points, the curve is a fit to the data given by

$\sigma = C(1 - (2.2/E))^{.5}$. The intensity scale is in arbitrary units while the collision energy scale is a cross section weighted mean collision energy.

Fig. 6. Energy dependence of $NO + O_3 \rightarrow NO_2^* + O_2$ near threshold for 24 percent NO/Ar. The curve is a fit to the data points given by $\sigma = C(1 - (2.0/E))^{.5}$. The scales are determined in the same way as for Figure 5.

Fig. 7. Energy dependence of $NO + O_3 \rightarrow NO_2^* + O_2$ for 10 percent NO/He. The curve is a fit to the data given by $\sigma = C((E/3.95)-1)^{1.70}$. The scales are determined in the same way as for Figure 5.

Fig. 8. Energy dependence of $NO + O_3 \rightarrow NO_2^* + O_2$ for 1 percent NO/He. The curve is a fit to the data given by $\sigma = C((E/4.30)-2)^{1.90}$. The scales are determined in the same way as Figure 5.

Fig. 9. Spectral distribution of the NO_2^* chemiluminescence from $NO + O_3 \rightarrow NO_2^* + O_2$ for four collision energies. The lowest two collision energies (4.5 and 6.2 kcal/mole) were measured using 10 percent NO/He, the highest two using 1 percent NO/He. The data points are normalized to a maximum intensity of 1.0 for each collision energy. The curves are drawn for clarity only.

Fig. 10. Ratio of the signal for $NO(400^\circ K) + O_3$ to the signal for $NO(136^\circ K) + O_3$ as a function of NO pressure. The pressure axis, in torr, is the pressure of NO at 136°K. The data

points have been normalized to account for the change in the $NO - O_3$ collision frequency in going from 400°K to 136°K. The value of the ratio at zero NO pressure is 8.3 ± 1.1 as determined by the intercept of the straight lines drawn visually (i.e., not a least squares fit) through the data points.

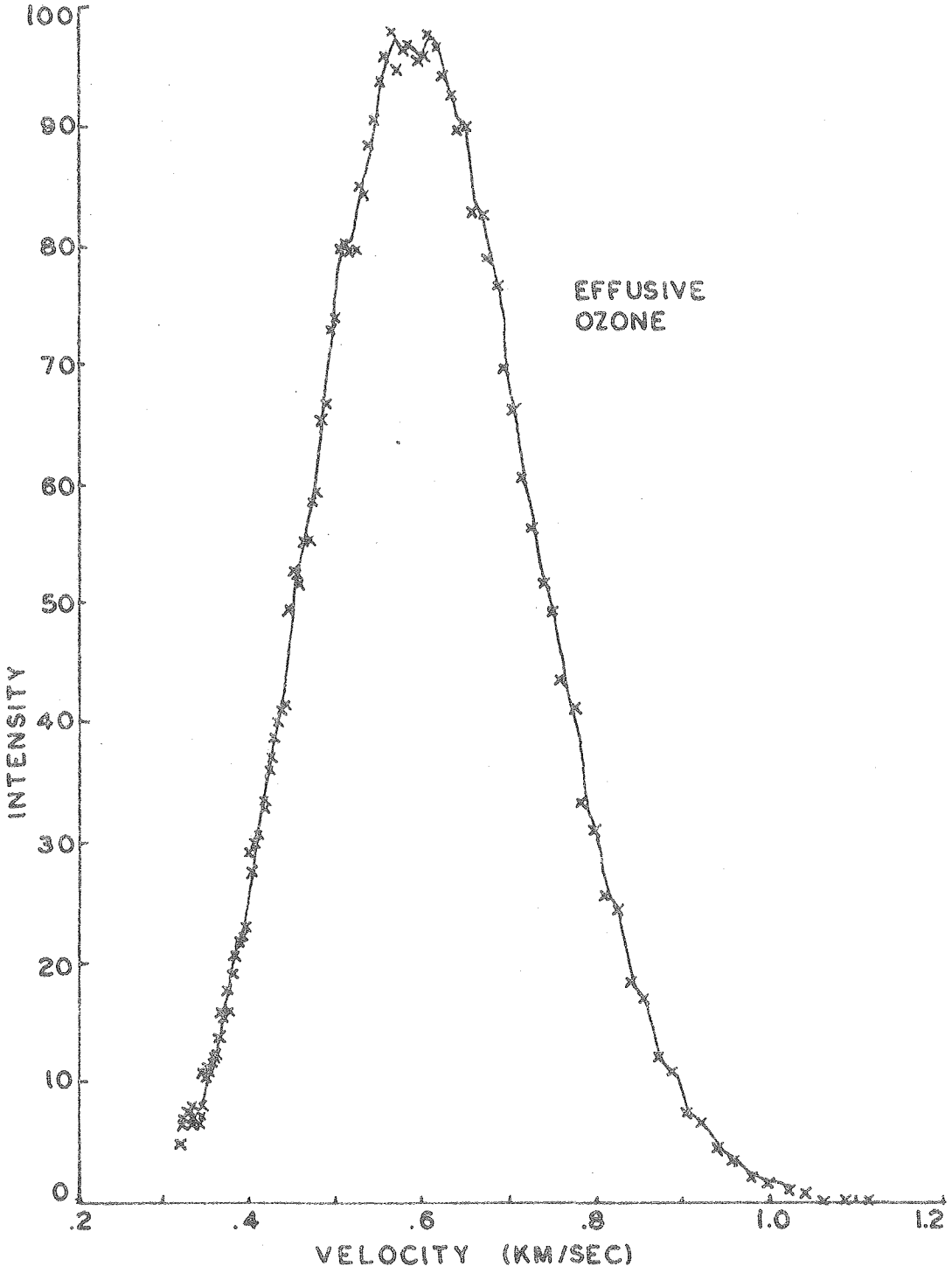

XBL 803-8479

Figure 1

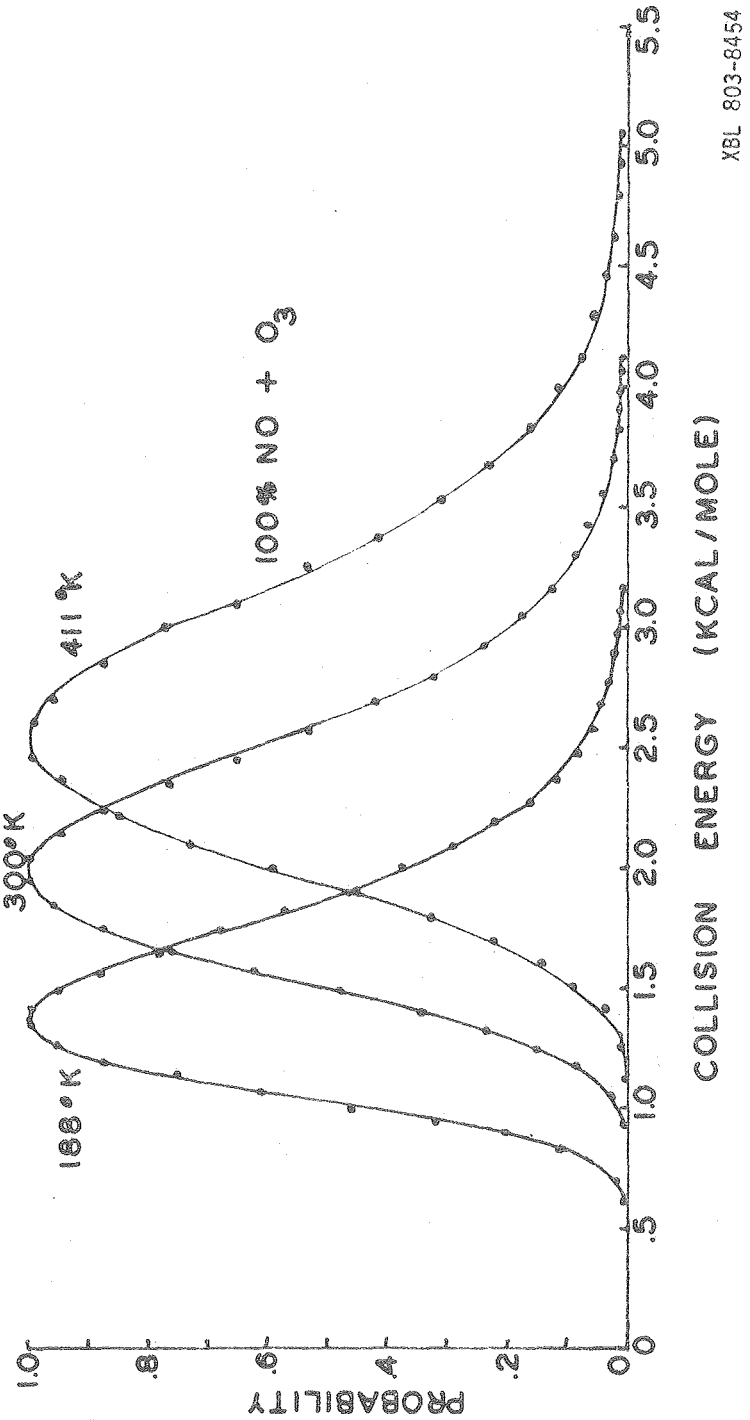
PROBABILITY
1.0
.8
.6
.4
.2
0
.5
1.0
1.5
2.0
2.5
3.0
3.5
4.0
4.5
5.0
5.5
COLLISION ENERGY (KCAL/MOLE)
188°K
300°K
411°K
100% NO + O3
XBL 803-8454

Figure 2

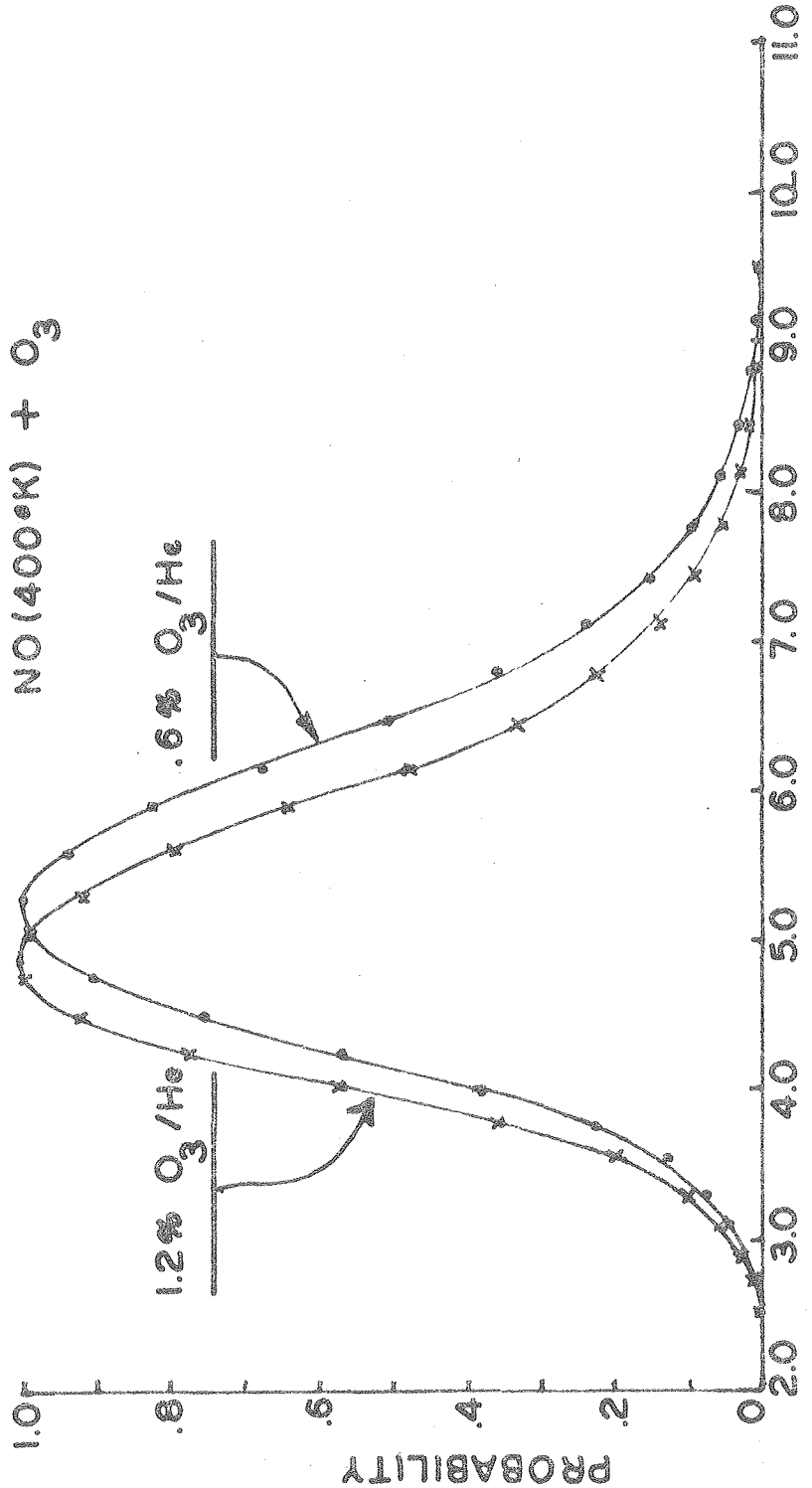

XBL 803-8452

Figure 3

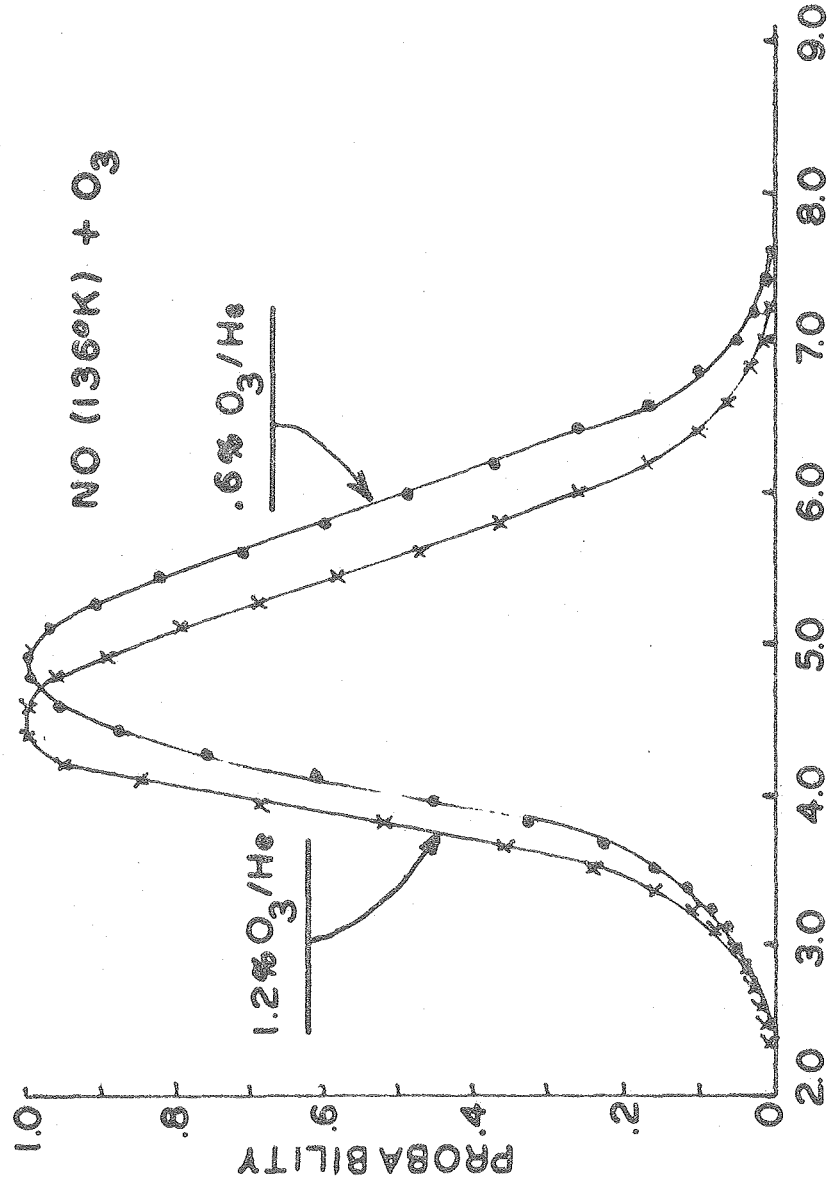

Figure 4

XBL 803-8453

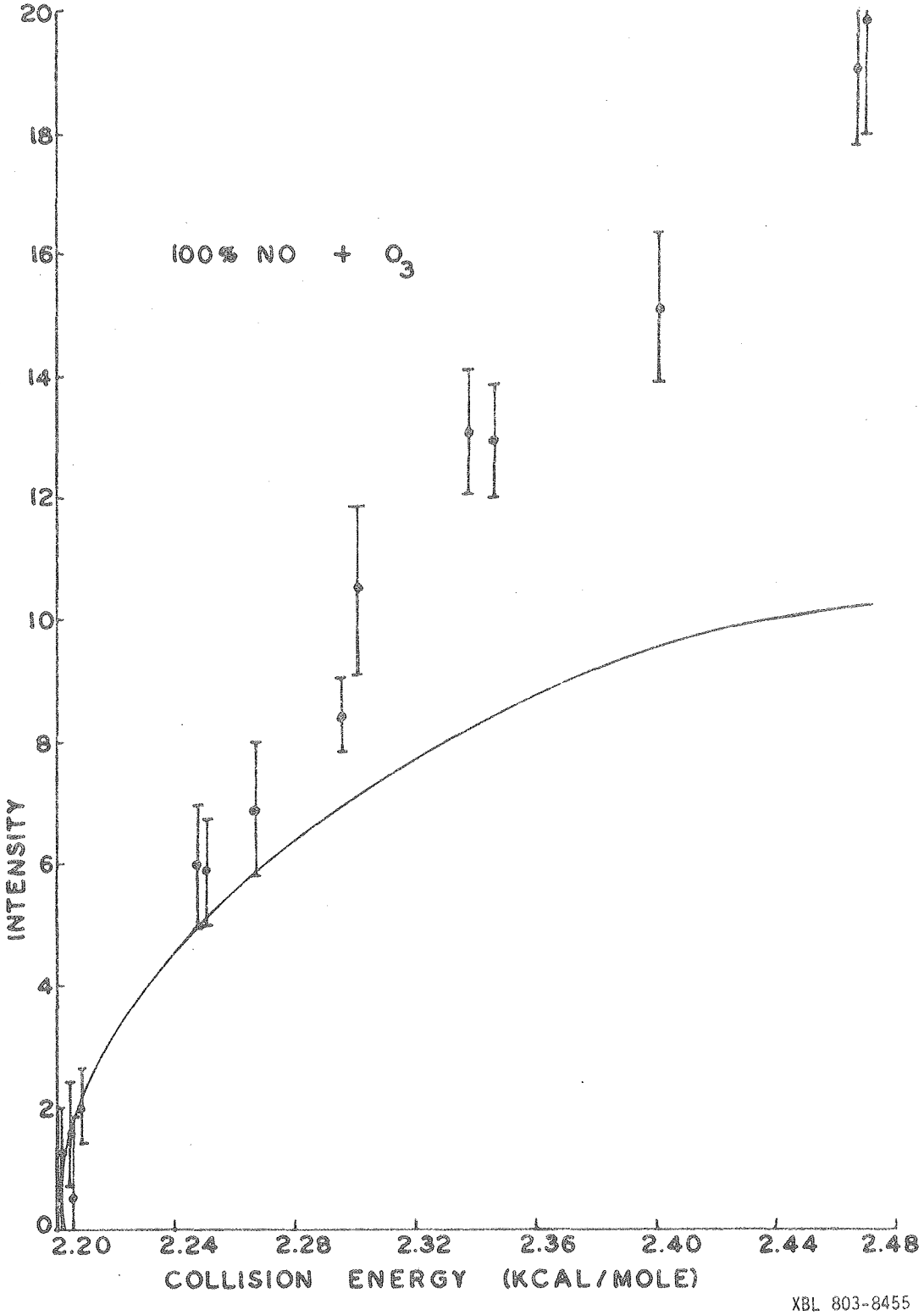
100% NO + O_3
INTENSITY
0
2
4
6
8
10
12
14
16
18
20
2.20
2.24
2.28
2.32
2.36
2.40
2.44
2.48
COLLISION ENERGY (KCAL/MOLE)
XBL 803-8455

Figure 5

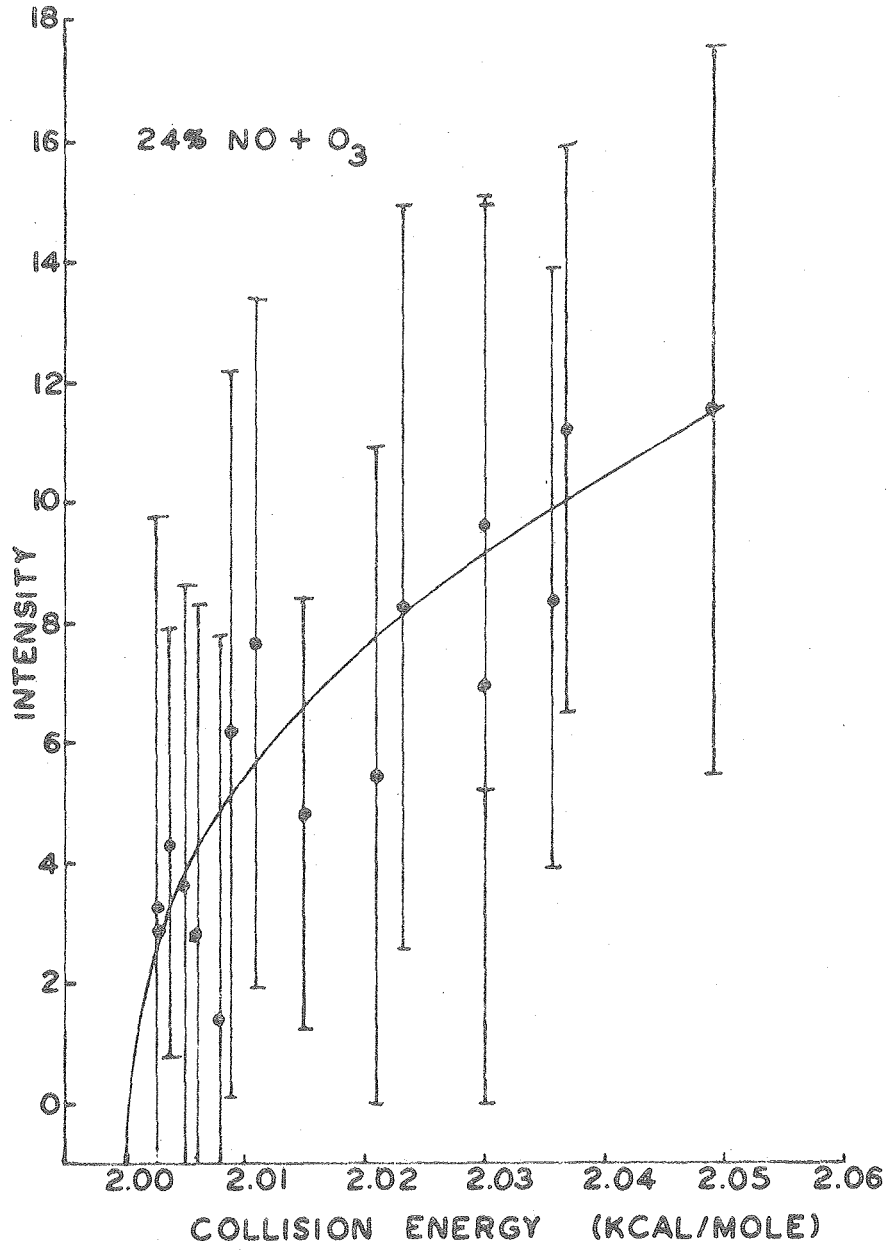

Figure 6

XBL 803-8478

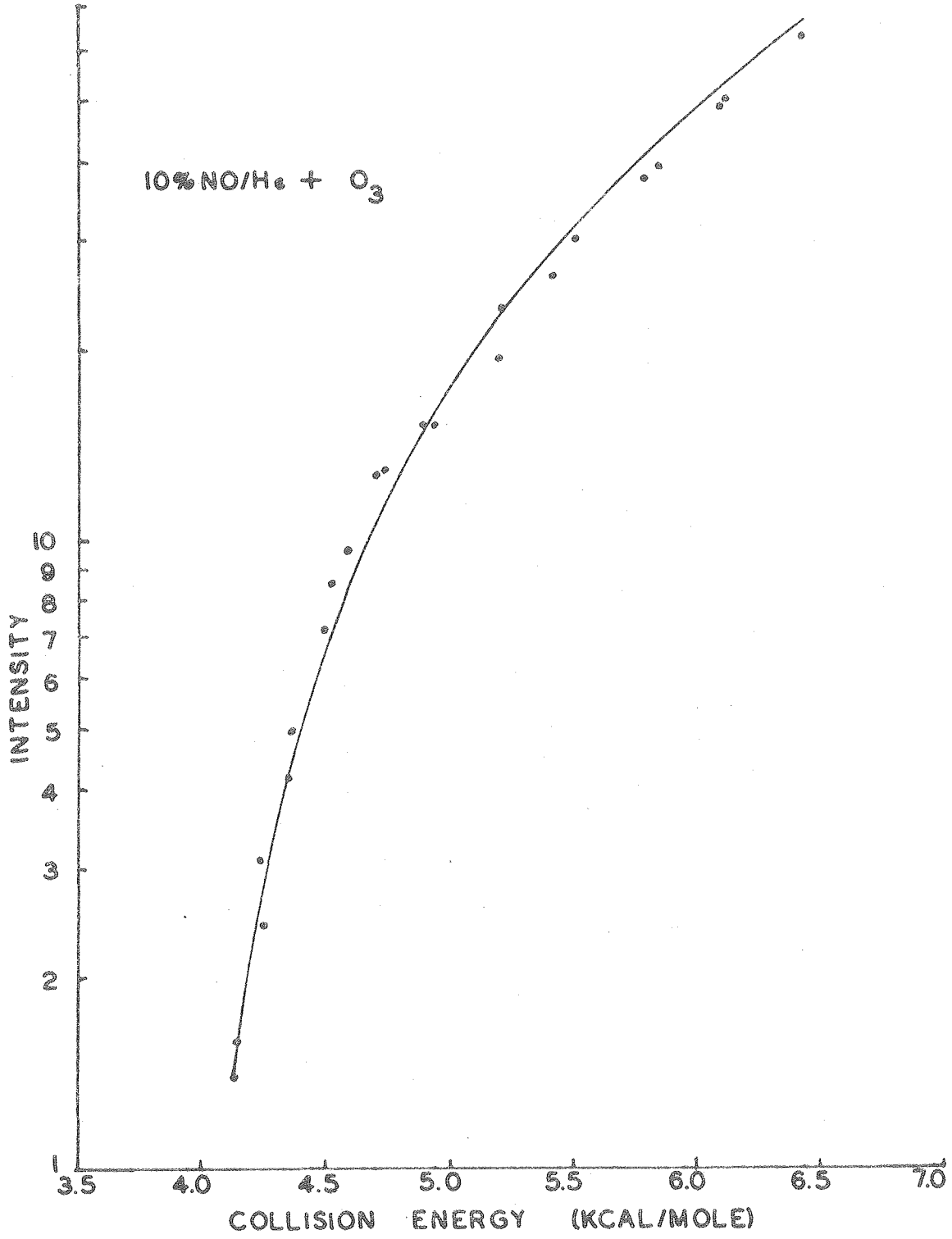

Figure 7

XBL 803-8456

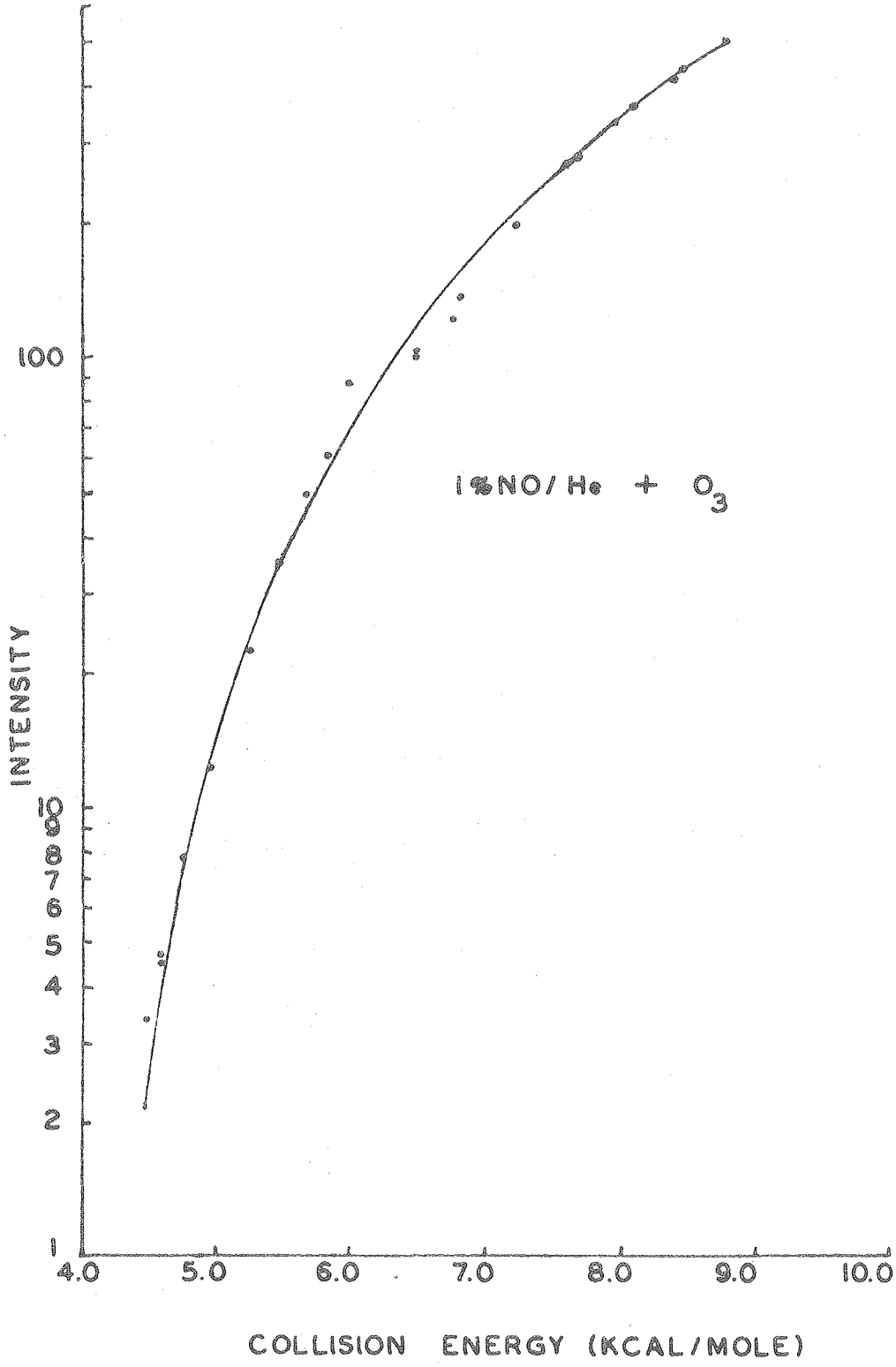

XBL 803-8480

Figure 8

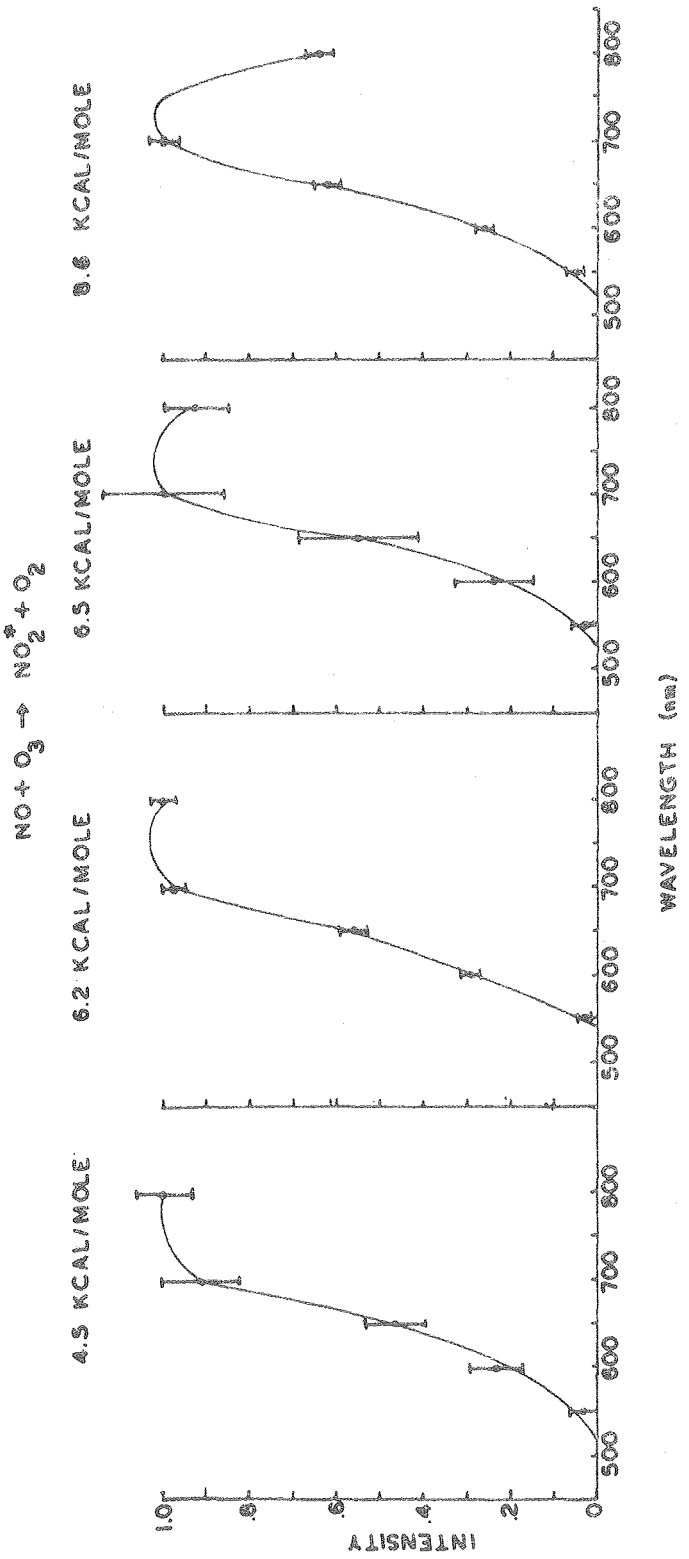

XBL 803-8669

Figure 9

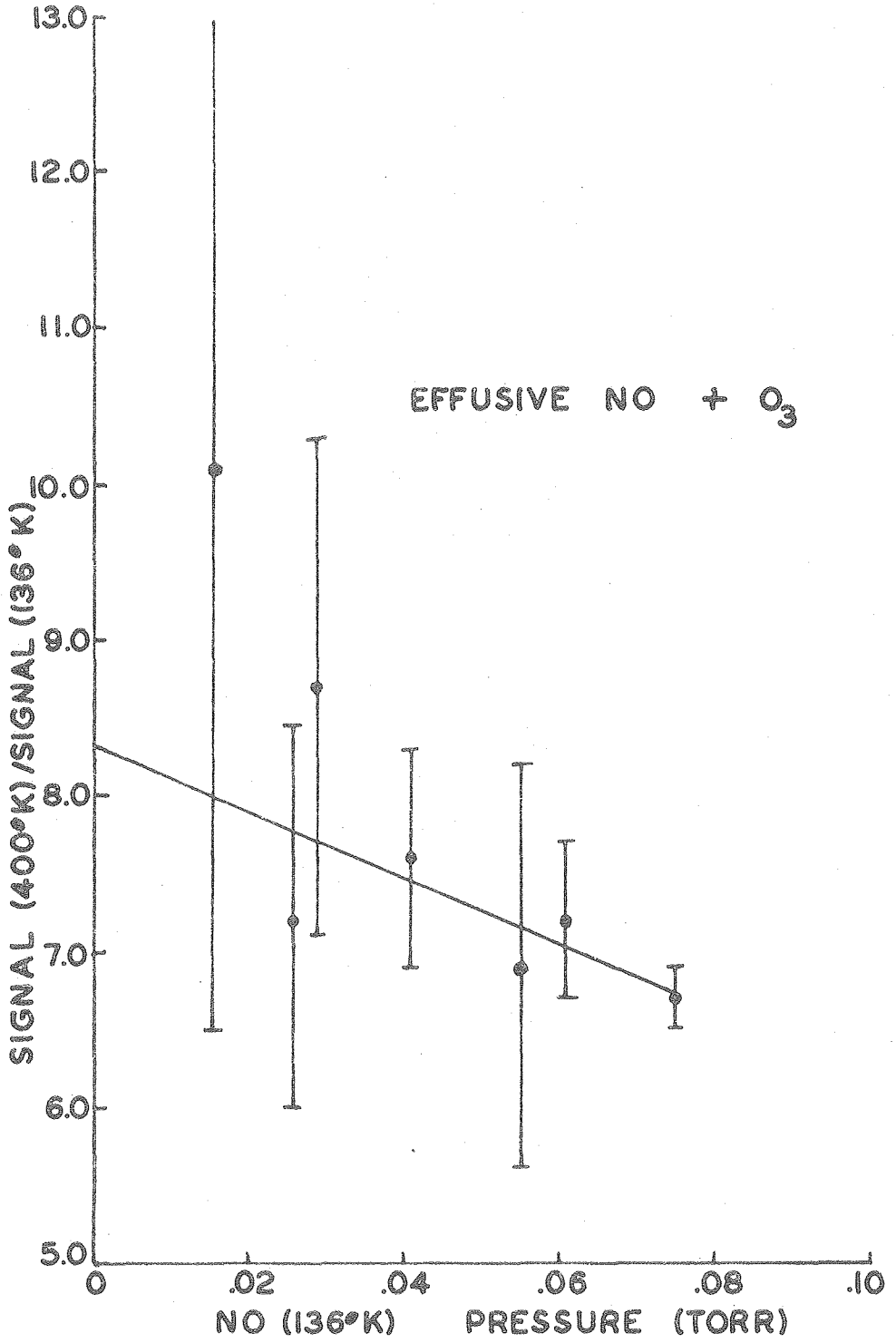

XBL 803-8476

Figure 10

V. COMPUTER PROGRAMS FOR ANALYSIS OF SUPERSONIC BEAM-EFFUSIVE BEAM REACTIVE SCATTERING

A. Introduction

While a number of data analysis programs have been written by other members of this research group,[1,2] the chemiluminescence-laser fluorescence machine is unique not only in the type of data recorded (photons vs. angular distributions), but also in the characteristics of the beam sources used. The beam sources can be taken to another machine in the laboratory and a time-of-flight analysis of the velocity distribution made (the chemiluminescence machine does not have time-of-flight capability). Programs KELVIN[1] and FLUX[1] are meant for converting the time-of-flight data into parameters describing the beam (e.g., Mach number, beam temperature) and converting number density versus velocity into a flux distribution, and can be used for the chemiluminesnce machine beam sources as well as for any other. The difficulty comes in trying to obtain an energy dependence for a reaction when the velocity and angular spread of the beams are not negligible. This problem was solved in two steps. Program CELUM converts the flux distribution obtained for each beam source into a flux distribution as a function of relative velocity for beam source pairs. Program LUMFIT takes the distribution from CELUM and, using a suitable cross section energy dependence, aids in fitting the data points. The end result is a deconvolution of the data as a function of nozzle temperature to data as a function of a cross section weighted mean collision energy.

It should be noted that these programs are meant to fit total chemiluminescence data, not a spectral distribution of data. While each transition could be fit to a cross section as a function of energy, a comparison of transitions would have to consider variations in the lifetime of the excited products as well. LUMFIT should include a correction for increased velocity of the products (resulting in a decrease in the fraction of light collected) with increased collision energy, but this was left out for a couple of reasons. Because we are detecting total chemiluminescence instead of a spectrum, we have no way of knowing how the spectrum changes with collision energy. For stable levels in a single electronic transition, there should be little change in lifetime with vibrational level. In the two reactions reported here, NO + O_3 and halogen-halogen, we are not dealing with stable, single electronic state transitions but highly perturbed levels from NO_2 in the first case and possibly predissociating levels or two transitions (B $\rightarrow$ X and A $\rightarrow$ X) in the second case. There should a negligible effect on our threshold results because a very narrow energy range is covered in the threshold determinations.

B. Program CELUM

The chemiluminescence-laser fluorescence machine has two beam sources, both with fairly broad angular widths and one with a broad velocity distribution as well. In this case, therefore, neither velocity spread nor angular spread can be neglected in determining a

collision energy distribution. In both reactions discussed in this dissertation the reaction cross section has a very strong dependence on the collision energy, so the high energy tail of the effusive sources becomes important. Program CELUM was written to take the output from Program FLUX[1] and first convert it to a flux as a function of relative velocity, then punch cards for input to a second program, LUMFIT, designed to fit the experimental data.

The input for CELUM consists mainly of the output from FLUX, a deck of cards on which is punched a set of flux values. Accompanying the FLUX input to CELUM, then, is the starting velocity associated with the first flux value, the amount the velocity is incremented for each successive flux value, as well as the number of velocities for which there are flux values. This data is read in for both beam sources, and is printed out by CELUM to check for proper data read in. Masses for beam 1 and beam 2 are read in and the reduced mass, G, calculated from these. The reduced mass is required in calculating the relative velocity from the relative velocities. Because the beams are so broad spatially, the nominal collision angle of the beams (90°) and the actual full angular width of molecular collisions are read in (in degrees) so an adjustment can be made in the relative velocity for collisions that occur at angles other than 90°. Finally, the number of collision energies at which a flux should be calculated, the number of velocities for both beams to be used in the calculation, the number of collision angles to be used within the full angular width and the number of flux points to be output for the next program are read in.

The first major calculation in CELUM is the interpolation of the FLUX output. Because the number of beam velocities desired may differ from the number input by FLUX, the flux at each of the desired velocities is interpolated from the FLUX data then converted to a number density. Next, using the equation

$$RV = (V_1^2 + V_2^2 - 2V_1V_2\cos\theta)^{.5} \quad . \tag{1}$$

the relative velocity is calculated from each pair of beam velocities and the flux associated with that velocity

$$PE = F_1 F_2 V_{relative} F(\theta) \tag{2}$$

is calculated where $F(\theta)$ accounts for the distribution of collision angles relative to the nominal 90°, and F_1 and F_2 are the number densities at a given velocity for beams 1 and 2. The flux in each velocity increment is summed, normalized to the highest flux, and printed out along with the average relative velocity (and collision energy) in that increment. Finally, using the input number of output flux points desired, a flux increment and starting flux is calculated and the two velocities (on the high and low end of the relative velocity range) corresponding to a given flux are interpolated from the velocities just calculated. These velocities are then output in the form of punched cards for the next program, LUMFIT, as well as being printed out in CELUM.

The output is organized so that for each pair of gases the title, masses for beam 1 and beam 2 and the FLUX data are printed out first. Next the lowest collision angle (i.e., nominal collision angle minus one-half the angular width) and full angular width are printed out in radians. The number of velocities used for each of the two beams is printed followed by columns for the calculated relative velocity, relative flux (or probability), and the collision energy associated with that velocity. Finally, the numbers to be input to LUMFIT are printed out with the first column being probability, the second relative velocity.

CELUM can be run to calculate velocity distributions for several gases paired with one gas (e.g., I_2 with 1 percent F_2/He, 7 percent F_2/He + Ar and 10 percent F_2/Ar) by putting the beam 1 input first (e.g., I_2) and then putting the complete set of input cards (program line 14 and on down) in for each of the beam 2 gases.

A description of the input variables, a listing and sample output for CELUM follows.

Program CELUM Input Variables

Variable	Description
IL (title)	Heading for output for each pair of gases - up to one card
NV1, NV2	Integer value for number of velocities input for beams 1 and 2 from FLUX.
VZ1, VZ2	Starting velocity for data input from FLUX for beams 1 and 2 in units of 10^4 cm/sec.
DV1, DV2	Velocity increments for input from Flux for beams 1 and 2 in units of 10^4 cm/sec.

F1(I), F2(I)	Input from FLUX for beams 1 and 2.
G1, G2	Masses in a.m.u. for beams 1 and 2, G1 = 0.0 stops execution.
CA	Collision angle in degrees.
FW	Full angular width in degrees over which the calculation is to be made.
NRV	Integer number of relative velocities to be calculated.
NVA, NVB	Integer number of velocities from beams 1 and 2 to be used in calculation.
NT	Integer number of angles at which calculation will be performed. Either an odd integer should be input or CELUM will assume the next highest odd integer.
NF	Integer number of flux points at which the relative velocity will be determined for output to LUMFIT. Angain, either an odd integer should be used or the next highest odd integer will be assumed.

```
SKIP
      PROGRAM CELUM(INPUT,OUTPUT,PUNCH,TAPE5=INPUT,TAPE6=OUTPUT,
     CTAPE7=PUNCH)
      DIMENSION IL(8),F1(200),F2(200),RV(202),T(50),FT(50),VA(2000),
     CVB(2000),FA(2000),FB(2000),FF(500),FFA(500),FFB(500),EEA(500),
     CFFC(500),FFD(500),EED(500),EFA(500),EFD(500),FFR(500)
      RAD=.0174533
C     READ IN NO. OF VELOCITIES FOR BEAM1
      READ(5,103)NV1
C     READ IN STARTING VELOCITY AND DELTA V FOR BEAM 1
      READ(5,102)VZ1,DV1
C     READ IN FLUX OUTPUT BY PRGM FLUX FOR BEAM 1
      READ(5,102)(F1(I),I=1,NV1)
C     READS IN TITLE UP TO 1 CARD
1     READ(5,101)IL
C     READ IN MASS OF BEAM 1 AND BEAM 2
      READ(5,102)G1,G2
      IF(G1.EQ.0.)GOTO100
      G=G1*G2/(G1+G2)/836.8
C     READ IN COLLISION ANGLE AND FULL ANGULAR WIDTH
      READ(5,102)CA,FW
      FW=RAD*FW
      CA=RAD*CA-FW/2.
C     READ IN NO. OF VELOCITIES FOR BEAM 2
      READ(5,103)NV2
C     READ IN STARTING VELOCITY AND DELTA V FOR BEAM 2
      READ(5,102)VZ2,DV2
C     READ IN FLUX OUTPUT BY PRGM FLUX FOR BEAM 2
      READ(5,102)(F2(I),I=1,NV2)
C     READ IN NO. OF RELATIVE VELOCITIES DESIRED, NO. OF VEL. TO BE USED
C     FROM BEAMS 1 AND 2 (A AND B), NO. OF COLLISION ANGLES TO BE USED
C     AND NO. OF FLUX POINTS FOR NEXT PROGRAM
      READ(5,103)NRV,NVA,NVB,NT,NF
      NF=2*(NF/2)+1
      NT=2*(NT/2)+1
      WRITE(6,104)
      WRITE(6,105)IL
      WRITE(6,106)G1,G2
      WRITE(6,107)
C     THE FOLLOWING ROUTINE PRINTS OUT THE VELOCITIES FROM FLUX
      N=MINO(NV1,NV2)
      DO11,I=1,N
11    WRITE(6,108)VZ1+(I-1)*DV1,F1(I),VZ2+(I-1)*DV2,F2(I)
      IF(NV1.EQ.NV2)GOTO4
      M=MAXO(NV1,NV2)
      N=N+1
      Z=0.0
      DO2,I=N,M
      IF(NV1.GT.NV2)GOTO3
      WRITE(6,108)Z,Z,VZ2+(I-1)*DV2,F2(I)
      GOTO2
3     WRITE(6,108)VZ1+(I-1)*DV1,F1(I),Z,Z
2     CONTINUE
4     WRITE(6,109)CA,FW
      WRITE(6,110)NVA,NVB,NT
      NVA=NVA+1
      NVB=NVB+1
C     THE FOLLOWING DETERMINES DELTA RV, DELTA ANGLE
      RVZ=SQRT(VZ1*VZ1+VZ2*(VZ2-2.*VZ1*COS(CA)))
      VM1=VZ1+(NV1-1)*DV1
      VM2=VZ2+(NV2-1)*DV2
```

```
      RVM=SQRT(VM1*VM1+VM2*(VM2-2.*VM1*COS(CA+FW)))                    62
      DRV=(RVM-RVZ)/NRV                                                63
      DT=FW/(NT+1)                                                     64
C     THE FOLLOWING CALCS COS THETA                                    65
      N=NT/2+1                                                         66
      FFF=1.0/FLOAT(N)                                                 67
      F=0.                                                             68
      DO5,I=1,N                                                        69
      CA=CA+DT                                                         70
      T(I)=COS(CA)*2.                                                  71
      T(NT-I+1)=-T(I)                                                  72
      F=F+FFF                                                          73
      FT(I)=F                                                          74
5     FT(NT-I+1)=F                                                     75
C     THE FOLLOWING CALCS VA(BEAM1) AND VB(BEAM2)                      76
      V=VZ1                                                            77
      DVA=(NV1-1)*DV1/(NVA-1)                                          78
      DO30,I=1,NVA                                                     79
      VA(I)=V                                                          80
      F=(V-VZ1)/DV1                                                    81
      N=INT(F)+1                                                       82
      IF(N.EQ.NV1)GOTO31                                               83
      F=F-N+1                                                          84
      FA(I)=F1(N)+(F1(N+1)-F1(N))*F                                    85
      GO TO 30                                                         86
31    FA(I)=F1(NV1)                                                    87
30    V=V+DVA                                                          88
      V=VZ2                                                            89
      DVB=(NV2-1)*DV2/(NVB-1)                                          90
      DO32,I=1,NVB                                                     91
      VB(I)=V                                                          92
      F=(V-VZ2)/DV2                                                    93
      N=INT(F)+1                                                       94
      IF(N.EQ.NV2)GOTO33                                               95
      F=F-N+1                                                          96
      FB(I)=F2(N)+(F2(N+1)-F2(N))*F                                    97
      GOTO32                                                           98
33    FB(I)=F2(NV2)                                                    99
32    V=V+DVB                                                         100
      NN=NRV+1                                                        101
C     ZERO FLUX ARRAY                                                 102
      DO39,I=1,NN                                                     103
39    RV(I)=0.                                                        104
C     FLUX AS A FUNC OF RELATIVE VEL. WILL BE CALC NOW                105
      DO40,I=1,NVA                                                    106
      VA2=VA(I)*VA(I)                                                 107
      DO41,J=1,NVB                                                    108
      VB2=VB(J)*VB(J)                                                 109
      VAB=VA(I)*VB(J)                                                 110
      FAB=(FA(I)*FB(J))/(VA(I)*VB(J))                                 111
      DO42,K=1,NT                                                     112
      V12=VA2+VB2-VAB*T(K)                                            113
      PE=FAB*FT(K)*SQRT(V12)                                          114
      RVN=SQRT(V12)                                                   115
      N=INT((RVN-RVZ)/DRV)+1                                          116
      RV(N)=RV(N)+PE                                                  117
42    CONTINUE                                                        118
41    CONTINUE                                                        119
40    CONTINUE                                                        120
      EE=0.                                                           121
      DO 43,I=1,NRV                                                   122
43    IF(EE.LT.RV(I))EE=RV(I)                                         123
```

```
      WRITE(6,111)                                                          124
      DO 44,I=1,NRV                                                         125
44    WRITE(6,112)RVZ+(I-1)*DRV,RV(I)/EE,G*((RVZ+(I-1)*DRV)**2.)            126
C     NOW TO CALCULATE REL. VELOC. AT EACH FLUX FOR NEXT PROGRAM            127
C     FIND RVMAX TO DIVIDE FLUX INTO HIGH AND LOW ENERGY PARTS              128
      DO 200,I=1,NRV                                                        129
200   IF(RV(I).EQ.EE)RVMAX=RVZ+(I-1)*DRV                                    130
      DF=1./NF                                                              131
      WRITE(6,113)                                                          132
      K=NF-1                                                                133
      DO 300,I=1,K                                                          134
      FF(I)=DF+(I-1)*DF                                                     135
      DO 400,J=1,NRV                                                        136
      IF ((RVZ+(J-1)*DRV).GE.RVMAX)GO TO 420                                137
C     LOW VELOCITY INTERPOLATION                                            138
      IF(FF(I).LT.RV(J)/EE)GO TO 400                                        139
      FFA(I)=RV(J)/EE                                                       140
      FFB(I)=RV(J+1)/EE                                                     141
      EEA(I)=RVZ + (J-1)*DRV                                                142
      GO TO 400                                                             143
C     HIGH VELOCITY INTERPOLATION                                           144
420   IF(FF(I).GT.RV(J)/EE)GO TO 400                                        145
      FFD(I)=RV(J)/EE                                                       146
      FFC(I)=RV(J+1)/EE                                                     147
      EED(I)=RVZ+J*DRV                                                      148
400   CONTINUE                                                              149
      DFA=(FF(I)-FFA(I))/(FFB(I)-FFA(I))                                    150
      EFA(I)=EEA(I)+DFA*DRV                                                 151
      DFC=(FF(I)-FFC(I))/(FFD(I)-FFC(I))                                    152
C     INVERT ORDER OF HIGH VELOCITY PART FOR OUTPUT                         153
      EFD(NF-I+1)=EED(I)-DFC*DRV                                            154
      FFR(NF-I+1)=FF(I)                                                     155
300   WRITE(6,114)FF(I),EFA(I)                                              156
      EFD(1)=RVMAX                                                          157
      FFR(1)=1.00000                                                        158
      DO 500,I=1,NF                                                         159
500   WRITE(6,114),FFR(I),EFD(I)                                            160
      K=NF-1                                                                161
      WRITE(7,115)(EFA(I),I=1,K)                                            162
      WRITE(7,115)(EFD(I),I=1,NF)                                           163
      GO TO 1                                                               164
100   CONTINUE                                                              165
101   FORMAT(8A10)                                                          166
102   FORMAT(8F10.0)                                                        167
103   FORMAT(16I5)                                                          168
104   FORMAT(1H1,12HDISTRIBUTION,12H OF RELATIVE,11H VELOCITIES)            169
105   FORMAT(1HO,8A10)                                                      170
106   FORMAT(1HO,6HMASS1=,F8.4,9H   MASS2=,F8.4)                            171
107   FORMAT(1H ,14HBEAM1 VELOCITY,3X,4HFLUX,4X,14HBEAM2 VELOCITY,          172
     C3X,4HFLUX)                                                            173
108   FORMAT(1H ,6X,F8.3,2X,F7.3,8X,F8.3,2X,F7.3)                           174
109   FORMAT(1HO,6HANGLE=,F6.2,6HWIDTH=,F6.2)                               175
110   FORMAT(1H ,17HBEAM1 VELOCITIES=,I4,17HBEAM2 VELOCITIES=,I4,           176
     C7HANGLES=,I3)                                                         177
111   FORMAT(1HO,3X,8HVELOCITY,5X,11HPROBABILITY,6X,16HCOLLISION ENERGY)    178
112   FORMAT(1H ,F8.4,6X,F8.5,6X,F8.4)                                      179
113   FORMAT(1HO,3X,11HPROBABILITY,5X,8HVELOCITY)                           180
114   FORMAT(1H ,F8.5,6X,F8.4)                                              181
115   FORMAT(8F10.4)                                                        182
      END                                                                   183
```

DISTRIBUTION OF RELATIVE VELOCITIES

FLUX VS. COLL. ENERGY FOR I2 PLUS F2 IN AR, T=302K

MASS1=254.0000 MASS2= 38.0000

BEAM1 VELOCITY	FLUX	BEAM2 VELOCITY	FLUX
2.700	0.	4.000	0.
2.750	0.	4.050	0.
2.800	22.980	4.100	0.
2.850	22.970	4.150	0.
2.900	28.410	4.200	0.
2.950	30.960	4.250	0.
3.000	35.380	4.300	0.
3.050	37.580	4.350	0.
3.100	42.920	4.400	0.
3.150	51.140	4.450	0.
3.200	54.200	4.500	6.520
3.250	60.700	4.550	7.870
3.300	67.380	4.600	9.210
3.350	77.040	4.650	11.920
3.400	80.600	4.700	14.610
3.450	86.580	4.750	16.580
3.500	90.690	4.800	20.400
3.550	99.650	4.850	25.640
3.600	106.310	4.900	31.440
3.650	109.370	4.950	38.970
3.700	113.070	5.000	47.620
3.750	118.870	5.050	59.730
3.800	121.880	5.100	74.900
3.850	127.850	5.150	93.750
3.900	129.930	5.200	115.920
3.950	131.550	5.250	141.380
4.000	132.040	5.300	171.700
4.050	133.470	5.350	201.410
4.100	136.610	5.400	232.470
4.150	134.850	5.450	265.060
4.200	135.210	5.500	295.190
4.250	131.030	5.550	323.620
4.300	128.770	5.600	346.390
4.350	129.640	5.650	359.190
4.400	123.080	5.700	364.890
4.450	120.820	5.750	363.820
4.500	118.300	5.800	356.040
4.550	110.000	5.850	341.900
4.600	107.950	5.900	321.710
4.650	101.930	5.950	295.560
4.700	95.640	6.000	266.020
4.750	91.890	6.050	235.060
4.800	86.570	6.100	204.850
4.850	83.010	6.150	176.040
4.900	77.730	6.200	148.950
4.950	72.990	6.250	124.250
5.000	68.330	6.300	102.600
5.050	61.630	6.350	84.040
5.100	55.320	6.400	68.610
5.150	52.730	6.450	55.680
5.200	45.060	6.500	44.990
5.250	41.430	6.550	36.780
5.300	38.750	6.600	30.700
5.350	35.880	6.650	25.520
5.400	34.250	6.700	20.750
5.450	30.960	6.750	16.620

5.500	27.720	6.800	13.160
5.550	24.830	6.850	10.710
5.600	21.680	6.900	9.580
5.650	19.290	6.950	8.900
5.700	17.560	7.000	7.660
5.750	15.970	7.050	6.440
0.	0.	7.100	5.510
0.	0.	7.150	4.830
0.	0.	7.200	4.230
0.	0.	7.250	3.630
0.	0.	7.300	3.130
0.	0.	7.350	2.840
0.	0.	7.400	2.640
0.	0.	7.450	2.450
0.	0.	7.500	2.200
0.	0.	7.550	1.810
0.	0.	7.600	0.
0.	0.	7.650	0.
0.	0.	7.700	0.
0.	0.	7.750	0.
0.	0.	7.800	0.
0.	0.	7.850	0.
0.	0.	7.900	0.
0.	0.	7.950	0.

ANGLE= 1.34WIDTH= .47
BEAM1 VELOCITIES= 100BEAM2 VELOCITIES= 100ANGLES= 29

VELOCITY	PROBABILITY	COLLISION ENERGY
4.2717	0.	.7208
4.4032	0.	.7659
4.5346	0.	.8123
4.6661	.00000	.8600
4.7976	.00005	.9092
4.9290	.00029	.9597
5.0605	.00106	1.0116
5.1919	.00314	1.0648
5.3234	.00780	1.1194
5.4549	.01772	1.1754
5.5863	.03692	1.2327
5.7178	.07200	1.2914
5.8492	.12839	1.3515
5.9807	.21301	1.4129
6.1122	.32688	1.4757
6.2436	.46520	1.5399
6.3751	.61448	1.6054
6.5065	.75588	1.6723
6.6380	.88137	1.7406
6.7695	.96409	1.8102
6.9009	1.00000	1.8812
7.0324	.99342	1.9535
7.1638	.93544	2.0272
7.2953	.85302	2.1023
7.4268	.74296	2.1788
7.5582	.62335	2.2566
7.6897	.50221	2.3358
7.8211	.39297	2.4163
7.9526	.29740	2.4982
8.0841	.21422	2.5815
8.2155	.15001	2.6661
8.3470	.10153	2.7521
8.4784	.06561	2.8395

8.6099	.04076	2.9283
8.7414	.02409	3.0184
8.8728	.01371	3.1098
9.0043	.00751	3.2027
9.1357	.00404	3.2969
9.2672	.00211	3.3924
9.3987	.00109	3.4893
9.5301	.00055	3.5876
9.6616	.00027	3.6873
9.7930	.00012	3.7883
9.9245	.00005	3.8907
10.0560	.00002	3.9945
10.1874	.00000	4.0996
10.3189	.00000	4.2061
10.4503	.00000	4.3139
10.5818	0.	4.4231
10.7133	0.	4.5337

PROBABILITY	VELOCITY
.00990	5.3512
.01980	5.4691
.02970	5.5369
.03960	5.5964
.04950	5.6335
.05941	5.6706
.06931	5.7077
.07921	5.7346
.08911	5.7577
.09901	5.7807
.10891	5.8038
.11881	5.8269
.12871	5.8497
.13861	5.8651
.14851	5.8805
.15842	5.8959
.16832	5.9113
.17822	5.9266
.18812	5.9420
.19802	5.9574
.20792	5.9728
.21782	5.9863
.22772	5.9977
.23762	6.0091
.24752	6.0205
.25743	6.0320
.26733	6.0434
.27723	6.0548
.28713	6.0663
.29703	6.0777
.30693	6.0891
.31683	6.1006
.32673	6.1120
.33663	6.1214
.34653	6.1308
.35644	6.1402
.36634	6.1497
.37624	6.1591
.38614	6.1685
.39604	6.1779
.40594	6.1873
.41584	6.1967
.42574	6.2061

.43564	6.2155
.44554	6.2249
.45545	6.2343
.46535	6.2437
.47525	6.2525
.48515	6.2612
.49505	6.2699
.50495	6.2786
.51485	6.2873
.52475	6.2961
.53465	6.3048
.54455	6.3135
.55446	6.3222
.56436	6.3309
.57426	6.3397
.58416	6.3484
.59406	6.3571
.60396	6.3658
.61386	6.3745
.62376	6.3837
.63366	6.3929
.64356	6.4021
.65347	6.4113
.66337	6.4205
.67327	6.4297
.68317	6.4389
.69307	6.4481
.70297	6.4574
.71287	6.4666
.72277	6.4758
.73267	6.4850
.74257	6.4942
.75248	6.5034
.76238	6.5133
.77228	6.5237
.78218	6.5341
.79208	6.5445
.80198	6.5548
.81188	6.5652
.82178	6.5756
.83168	6.5860
.84158	6.5963
.85149	6.6067
.86139	6.6171
.87129	6.6274
.88119	6.6378
.89109	6.6534
.90099	6.6692
.91089	6.6849
.92079	6.7007
.93069	6.7164
.94059	6.7321
.95050	6.7479
.96040	6.7636
.97030	6.7922
.98020	6.8284
.99010	6.8647
1.00000	6.9009
.99010	7.0399
.98020	7.0624
.97030	7.0848
.96040	7.1072

.95050	7.1297
.94059	7.1521
.93069	7.1714
.92079	7.1872
.91089	7.2030
.90099	7.2188
.89109	7.2346
.88119	7.2504
.87129	7.2662
.86139	7.2820
.85149	7.2971
.84158	7.3090
.83168	7.3208
.82178	7.3326
.81188	7.3444
.80198	7.3563
.79208	7.3681
.78218	7.3799
.77228	7.3917
.76238	7.4036
.75248	7.4154
.74257	7.4272
.73267	7.4381
.72277	7.4489
.71287	7.4598
.70297	7.4707
.69307	7.4816
.68317	7.4925
.67327	7.5034
.66337	7.5142
.65347	7.5251
.64356	7.5360
.63366	7.5469
.62376	7.5578
.61386	7.5685
.60396	7.5793
.59406	7.5900
.58416	7.6007
.57426	7.6115
.56436	7.6222
.55446	7.6330
.54455	7.6437
.53465	7.6545
.52475	7.6652
.51485	7.6760
.50495	7.6867
.49505	7.6983
.48515	7.7102
.47525	7.7221
.46535	7.7340
.45545	7.7460
.44554	7.7579
.43564	7.7698
.42574	7.7817
.41584	7.7936
.40594	7.8055
.39604	7.8174
.38614	7.8305
.37624	7.8441
.36634	7.8578
.35644	7.8714
.34653	7.8850

.33663	7.8986
.32673	7.9122
.31683	7.9259
.30693	7.9395
.29703	7.9532
.28713	7.9688
.27723	7.9845
.26733	8.0001
.25743	8.0158
.24752	8.0314
.23762	8.0471
.22772	8.0627
.21782	8.0784
.20792	8.0970
.19802	8.1172
.18812	8.1375
.17822	8.1578
.16832	8.1780
.15842	8.1983
.14851	8.2196
.13861	8.2464
.12871	8.2733
.11881	8.3001
.10891	8.3270
.09901	8.3562
.08911	8.3924
.07921	8.4287
.06931	8.4649
.05941	8.5112
.04950	8.5636
.03960	8.6190
.02970	8.6971
.01980	8.7957
.00990	8.9535

C. Program LUMFIT

While the data taken for the reactions described earlier was recorded as a function of collision energy, the raw data is actually a function of nozzle temperature seeding ratio. If the data were produced by two spatially well-defined supersonic sources, the collision energy distribution would be sufficiently narrow that the collisions between the two beams could be considered energetically monochromatic. When this is true, the most probable velocity from the time-of-flight spectra for the beams at given temperatures and seeding ratios can be directly converted to the collision energy. In the case of a supersonic source crossing an effusive source, the distribution is not monoenergetic and a more complicated calculation must be made to convert the nozzle temperature, at which the data was recorded, to a mean collision energy. The method chosen here was to assume an energy dependence for the reaction cross section and, using the relative velocity distribution from CELUM, fit the calculated signal to the experimental data at each temperature for each seeded gas. After determining the correct cross section energy dependence, a cross section weighted mean of the energy distribution at each temperature can be calculated.

The input for LUMFIT primarily consists of the CELUM output and identifying information like number of flux points for which there are velocities from CELUM and the temperatures at which the distributions were measured. The experimental data and the temperatures at which they were recorded are also input. Lines 80 is of the form:
signal = σx flux and looks like

$$SS = ((1. - C/(VEL(K))^2)^E)F(K)/SF$$

where SS is the signal, VEL(K) is the relative velocity with flux F(K), SF is the factor that normalizes the flux distribution to unit area and C is the square of the relative velocity corresponding to the threshold energy. C and E are adjustable parameters. The equation for the cross section:

$$\sigma = (1 - (C/(VEL(K))^2)^{.5} \qquad (2)$$

is derived from scattering theory[3] and is applicable near threshold. A cross section equation like

$$\sigma = ((VEL(K))^2/C)-1)^E \qquad (3)$$

where $E > 1$ was necessary to fit data above threshold that has a much steeper dependence than $E = .5$. This cross section form has no physical meaning and was used just to convert nozzle temperature to collision energy. A cross section formula of any sort can be used in line 80. The signal calculation leaves out the beam number densities, these are assumed constant (any data for which the density is not constant may be adjusted before being input).

To save storage space, LUMFIT treats each experimental point one at a time. Because the experimental temperatures usually fall between, rather than on, the temperatures at which time-of-flight data

was taken, the relative velocity distribution must be interpolated from CELUM data. If 500 flux points are used in the CELUM calculation and there are 10 experimental points, a lot of storage space is used up. Therefore, LUMFIT first identifies the two CELUM temperatures the experimental temperature is between, then interpolates to find the relative velocity at that temperature that corresponds to each flux value. If no interpolation is required (as mentioned above) the distribution directly from CELUM is used in the next step. When the interpolation is complete, LUMFIT converts this distribution, which is normalized to a peak probability of one, to a distribution that is normalized to an area of one and divides the distribution into equal velocity increments. LUMFIT then calculates SS for each flux and sums all the SS calculated at an experimental temperature. The above calculation is then repeated for the next temperature. Line 86 allows the user to normalize the calculated and experimental data to obtain agreement at one temperature.

The output is organized so that first the title is printed, followed by the reference temperatures in °K (temperatures at which the CELUM data was taken). Next the adjustable parameters, the exponent and threshold energy, from which C is calculated, in kcal/mole, are printed, followed by the reduced mass in a.m.u. A series of columns are output next - the first and second are the experimental temperatures and signal, then the calculated signal, and finally, the square of the difference between the calculated and observed signal. The last three lines provide the sum of the

difference squared, the scale factor from line 86 used to normalize the calculated points, and lastly the sum of flux from the last velocity distribution used.

A few final notes should be made. The temperatures are all in degrees Kelvin and should be input in order with the lowest temperature first. The experimental data, of course, must be input in the same order as the associated temperatures. This program does not automatically fit the data, the parameters must be changed by hand. This is disadvantageous in so far as the best fit may not be obtained, but it is advantageous in that it is very difficult to guess, apriori, what the cross section dependence will be, especially far from threshold. The manual method eliminates the nasty problem of convergence and, with such a small number of points to fit, probably requires less time in the long run. The cross section weighted mean energy must be back-calculated as follows for

$$\sigma = \left(\left((VEL(K))^2/C\right) - 1\right)^E$$

$$= \left(\left(1/2\mu(VEL(K))^2/1/2\mu C\right) - 1\right)^E$$

$$= \left(\left(E_{VEL(K)}/E_T\right) - 1\right)^E$$

then

$$SS = \left(\left(\text{mean energy}/E_{thresh}\right) - 1\right)^E \text{ SFAC}$$

where SFAC is the scale factor output at the end of the program. Therefore

$$(\text{mean energy} - 1)^E = \frac{SS}{SFAC} (E_{thresh})^E \quad .$$

Because the cross section formula is changeable, the energy calculation was left for a programmable calculator.

A description of the input variables, a listing and sample output for LUMFIT follow.

Program LUMFIT Input Variables

Variable	Description
IL (title)	Heading for output-up to one card.
NIT	Integer number of experimental temperatures.
NF	Integer number of flux points from CELUM.
NT	Integer number of reference temperatures from CELUM.
RT(I)	Reference temperatures in °K for CELUM data, in order of increasing temperature.
T(I)	Experimental temperatures in °K for the data points, in order of increasing temperature. Note-the T(I) must be within the range of the RT(I).
CELUM (I,J)	Input from CELUM, I is the index referring the data to RT(I).
EP(I)	Experimental data, in same order as T(I).
E	Fitting parameter, in this case the exponent for the cross section.
C	Fitting parameter, in this case the threshold energy for the cross section. The threshold velocity, C, used in the cross section is calculated from this in the program.
G	Reduced mass in a.m.u.

DELV	Velocity increment (in 10^4 cm/sec) to be used in dividing up the velocity distribution prior to signal calculation. DELV the same for all the experimental temperatures.

```
SKIP                                                                    1
      PROGRAM LUMFIT(INPUT,OUTPUT,TAPE5=INPUT,TAPE6=OUTPUT)             2
      DIMENSION IL(8),RT(10),T(50),CELUM(10,1001),EP(50),               3
     CTCELUM(1001),S(50),FF(1001),D(50),VEL(500),F(500)                 4
C     READ IN TITLE                                                     5
      READ(5,101)IL                                                     6
C     READ IN NO. OF EXPERMNTL TEMPS, NO. OF FLUX POINTS, NO. OF REF    7
C     TEMPS FROM CELUM AND TOF                                          8
C     NF MUST BE SAME FOR ALL T AND SAME AS IN CELUM                    9
      READ(5,102)NIT,NF,NT                                              10
C     ALL TEMPS SHOULD BE INPUT IN ORDER FROM LOW TO HIGH               11
C     READ IN REF.TEMPS                                                 12
      READ(5,103)(RT(I),I=1,NT)                                         13
C     READ IN EXPERMNTL TEMPS                                           14
C     TMUST LIES BETWEEN RT(1) AND RT(NT)                               15
      READ(5,103)(T(I),I=1,NIT)                                         16
      NF=2*(NF/2)+1                                                     17
      NE=2*(NF-1)+1                                                     18
C     READ IN DATA OUTPUT BY CELUM                                      19
      DO 10 I=1,NT                                                      20
      K=NF-1                                                            21
      READ(5,103)(CELUM(I,J),J=1,K)                                     22
      K=K+1                                                             23
10    READ(5,103)(CELUM(I,J),J=K,NE)                                    24
C     READ IN EXPERMTAL LIGHT POINTS                                    25
      READ(5,103)(EP(I),I=1,NIT)                                        26
C     READ IN FITTING PARAMS AND REDUCED MASS(G)                        27
      READ(5,103)E,C,G                                                  28
C     READ IN DELTA VELOCITY FOR USE IN CALC. SIGNAL                    29
      READ(5,103)DELV                                                   30
      WRITE(6,104)                                                      31
      WRITE(6,105)IL                                                    32
      WRITE(6,106)(RT(I),I=1,NT)                                        33
      WRITE(6,107)                                                      34
      WRITE(6,108)E,C,G                                                 35
      C=836.8*C/G                                                       36
C     ZERO SIGNAL ARRAY                                                 37
      DO 40 I=1,NIT                                                     38
40    S(I)=0.                                                           39
C     CALCULATE FLUX AT EACH ENERGY                                     40
      DF=1./NF                                                          41
      DO 45 I=1,NF                                                      42
45    FF(I)=DF+(I-1)*DF                                                 43
      DO 46 I=1,NF-1                                                    44
46    FF(NF+I)=FF(NF-I)                                                 45
      DS=0.                                                             46
C     INTERPOLATE CELUM DATA FOR EXPERMNTL TEMPS                        47
C     CALCULATE AND SUM SIGNAL                                          48
C     NUMBER DENSITY OF BEAMS ASSUMED CONSTANT                          49
      RT(NT+1)=3000.                                                    50
      DO 30 I=1,NIT                                                     51
      DO 20 J=1,NT                                                      52
      IF((T(I).LT.RT(J)).OR.(T(I).GE.RT(J+1)))GO TO 20                  53
      IF(T(I).EQ.RT(J))GO TO 15                                         54
      DO 25 K=1,NE                                                      55
25    TCELUM(K)=CELUM(J,K)+((T(I)-RT(J))/(RT(J+1)-RT(J)))*              56
     C(CELUM(J+1,K)-CELUM(J,K))                                         57
      GO TO 17                                                          58
15    DO 16 K=1,NE                                                      59
16    TCELUM(K)=CELUM(J,K)                                              60
C     CALC FLUX AND VELOCITY FROM DELTA VEL, NORMALIZE TO UNIT AREA     61
```

```
C       FOR DISTRIBUTION PEAK                                                   62
17      NAV=(TCELUM(NE)-TCELUM(1))/DELV                                         63
        VEL(NAV+1)=TCELUM(NE)                                                   64
        TCM=TCELUM(NF)                                                          65
        SF=0.                                                                   66
        DO 640,K=1,NAV                                                          67
        VEL(K)=TCELUM(1)+(K-1)*DELV                                             68
        DO 630,L=1,NE                                                           69
        IF((VEL(K).LT.TCELUM(L)).OR.(VEL(K).GE.TCELUM(L+1)))GO TO 630           70
        IF(VEL(K).GT.TCM)GO TO 610                                              71
        F(K)=FF(L)+((VEL(K)-TCELUM(L))/(TCELUM(L+1)-TCELUM(L)))*DF              72
        GO TO 620                                                               73
610     F(K)=FF(L)-((VEL(K)-TCELUM(L))/(TCELUM(L+1)-TCELUM(L)))*DF              74
620     SF=SF+F(K)                                                              75
630     CONTINUE                                                                76
640     CONTINUE                                                                77
        DO 650,K=1,NAV                                                          78
        IF((VEL(K)*VEL(K)).LT.C)GO TO 24                                        79
        SS=((1.-C/(VEL(K)*VEL(K)))**E)*F(K)/SF                                  80
        GO TO 650                                                               81
24      SS=0.                                                                   82
650     S(I)=S(I)+SS                                                            83
20      CONTINUE                                                                84
30      CONTINUE                                                                85
        P=EP(NIT)/S(NIT)                                                        86
C       SUM UP SQUARE OF DIFFERENCES BETWN CALC AND OBSRVED                     87
        DO 70,I=1,NIT                                                           88
        S(I)=S(I)*P                                                             89
        D(I)=(EP(I)-S(I))*(EP(I)-S(I))                                          90
70      DS=DS+D(I)                                                              91
        WRITE(6,109)                                                            92
        DO 80,I=1,NIT                                                           93
80      WRITE(6,110)T(I),EP(I),S(I),D(I)                                        94
        WRITE(6,111)DS                                                          95
        WRITE(6,112)P                                                           96
        WRITE(6,115)SF                                                          97
101     FORMAT(8A10)                                                            98
102     FORMAT(16I5)                                                            99
103     FORMAT(8F10.4)                                                         100
104     FORMAT(1H1,41HCALCULATION OF SIGNAL VS COLLISION ENERGY)               101
105     FORMAT(1HO,8A10)                                                       102
106     FORMAT(1HO,24HREFERENCE TEMPERATURES?  ,F10.2,3X,F10.2,3X,F10.2)       103
107     FORMAT(1HO,18HFITTING PARAMETERS)                                      104
108     FORMAT(1HO,10HEXPONENT=  ,F10.5,                                       105
       C2X,11HTHRESHOLD=  ,F10.2,2X,14HREDUCED MASS=  ,F10.2)                  106
109     FORMAT(1HO,11HTEMPERATURE,3X,15HOBSERVED SIGNAL,3X,                    107
       C17HCALCULATED SIGNAL,3X,14H(CALC-OBSV)**2)                             108
110     FORMAT(1H ,F8.2,6X,F8.2,10X,F8.2,12X,F8.2)                             109
111     FORMAT(1HO,22HSUM OF DIFF. SQUARED=  ,F8.2)                            110
112     FORMAT(1HO,14HSCALE FACTOR=  ,F8.6)                                    111
115     FORMAT(1HO,12HTOTAL FLUX=  ,F8.5)                                      112
        END                                                                    113
```

CALCULATION OF SIGNAL VS COLLISION ENERGY

I2 PLUS 10 PRCNT F2 IN AR

REFERENCE TEMPERATURES? 302.00 500.00 700.00

FITTING PARAMETERS

EXPONENT= .50000 THRESHOLD= 3.40 REDUCED MASS= 33.05

TEMPERATURE	OBSERVED SIGNAL	CALCULATED SIGNAL	(CALC-OBSV)**2
318.50	-26.50	.03	703.76
333.50	10.20	.11	101.72
370.00	7.40	.99	41.06
385.00	14.60	1.97	159.55
413.00	2.07	5.52	11.91
436.00	33.50	10.62	523.54
446.00	7.56	14.56	49.03
480.00	71.60	33.32	1465.33
502.00	76.30	53.74	509.09
517.00	56.00	68.67	160.56
563.00	130.20	130.73	.28
617.00	224.90	224.90	.00

SUM OF DIFF. SQUARED= 3725.84

SCALE FACTOR= 1201.613

TOTAL FLUX= 18.45715

References

1. J. J. Valentini, Ph.D. Thesis, University of California, Berkeley, 1976.
2. R. J. Buss, Ph.D. Thesis, University of California, Berkeley, 1979.
3. B. C. Eu and W. S. Liu, J. Chem. Phys., 63, 592 (1975).